NUMERICAL INVESTIGATION OF ROTOR WAKE-STATOR INTERACTION

A THESIS SUBMITTED TO
THE GRADUATE SCHOOL OF NATURAL AND APPLIED SCIENCES
OF
MIDDLE EAST TECHNICAL UNIVERSITY

BY

DERYA GÜRAK

IN PARTIAL FULFILLMENT OF THE REQUIREMENTS
FOR
THE DEGREE OF MASTER OF SCIENCE
IN
AEROSPACE ENGINEERING

SEPTEMBER 2004

Approval of the Graduate School of Natural and Applied Sciences

Prof. Dr. Canan Özgen
Director

I certify that this thesis satisfies all the requirements as a thesis for the degree of Master of Science.

Prof. Dr. Nafiz Alemdaroğlu
Head of Department

This is to certify that we have read this thesis and that in our opinion it is fully adequate, in scope and quality, as a thesis for the degree of Master of Science.

Prof. Dr. Mehmet Şerif Kavsaoğlu Co-Supervisor	Prof. Dr. İbrahim. Sinan Akmandor Supervisor

Examining Committee Members

Prof. Dr. Ünver Kaynak (Chairman)

Prof. Dr. İbrahim Sinan Akmandor

Prof. Dr. Mehmet Şerif Kavsaoğlu

Prof. Dr. İsmail Hakkı Tuncer

Assoc. Prof. Dr. Sinan Eyi

I hereby declare that all information in this document has been obtained and presented in accordance with academic rules and ethical conduct. I also declare that, as required by these rules and conduct, I have fully cited and referenced all material and results that are not original to this work.

Name, Last name :

Derya Gürak

Signature :

ABSTRACT

NUMERICAL INVESTIGATION OF ROTOR WAKE-STATOR INTERACTION

GÜRAK, Derya
M.Sc., Department of Aerospace Engineering
Supervisor: Prof. Dr. İbrahim Sinan AKMANDOR
Co-Supervisor: Prof. Dr. Mehmet Şerif KAVSAOĞLU

September 2004, 162 pages

In this thesis, numerical solutions of a 2D stator compressor cascade at a given inlet Mach number (0.7) and four values of incidence (49°, 51°, 53° and 55°) are obtained. Reynolds averaged, thin layer, compressible Navier Stokes equations are solved. Different grid types have been generated. Finite differencing approach and LU - ADI splitting technique are used. Three block parallel Euler and Navier Stokes solutions are compared with the experimental results. Baldwin-Lomax turbulence model is used in the turbulent predictions and boundary layer comparisons and numerical results are in good agreement with the experiment.

On the last part of the study, a rotor wake in the inlet flow has been introduced in the steady and unsteady analyses. The influence of this wake and the wake location in the inlet flow, to the total force and pressure is presented. The results have been showed that there is a relationship between the wake position and the incidence value of the case.

Keywords: CFD, Navier-Stokes, Euler, Multiblock, Compressor Stator, Rotor Wake

ÖZ

ROTOR İZİ İLE STATOR ETKİLEŞİMİNİN SAYISAL İNCELENMESİ

GÜRAK, Derya
Yüksek Lisans, Havacılık ve Uzay Mühendisliği Bölümü
Tez Yöneticisi: Prof. Dr. İbrahim Sinan AKMANDOR
Ortak Tez Yöneticisi: Prof. Dr. Mehmet Şerif KAVSAOĞLU

Eylül 2004, 162 sayfa

Bu tezde, 2 boyutlu stator kompresör kaskadının verilen giriş Mach sayısı (0.7) ve dört farklı açı (49°, 51°, 53° and 55°) için sayısal çözümü elde edilmiştir. Reynolds ortalamalı, ince tabaka, sıkıştırılabilir Navier Stokes denklemleri çözülmüştür. Farklı çözüm ağları üretilmiştir. Sınırlı türevleme uygulaması ve LU - ADI ayrıştırma tekniği kullanılmıştır. Üç bölgeli paralel Euler ve Navier Stokes çözümleri deneysel sonuçlarla karşılaştırılmıştır. Baldwin-Lomax türbülans modeli türbülans tahminlerinde kullanılmış ve sınır tabaka karşılaştırmalarında sayısal sonuçlarla deneysel verilerin iyi bir uyum içinde oldukları gözlenmiştir.

Çalışmanın son aşamasında, durağan ve durağan olmayan analizlerin giriş akımına rotor izi tanımlanmıştır. Giriş akımındaki rotor izi ve yerinin etkisi toplam kuvvet olarak gösterilmiştir. Sonuçlardan anlaşıldığı üzere rotor izinin pozisyonu ve akımın giriş açısı arasında

bir ilişki bulunmaktadır.

Anahtar Kelimeler: Sayısal Akışkanlar Dinamiği, Navier-Stokes, Euler, Çoklu bölgeleme, Kompresör Statoru, Rotor İzi.

To my parents,

who have always enlightened me with their caring, vision,
wisdom and love.

ACKNOWLEDGMENTS

I would like to express my sincere thanks and appreciation to my supervisors Prof. Dr. İbrahim Sinan Akmandor and Prof. Dr. Mehmet Şerif Kavsaoğlu for being a continuous source of support, encouragement and friendship while this work was being completed. Many of the results in this work have resulted from their innovative ideas and concepts. I am deeply grateful for the time and effort they have taken to teach me and provide direction for my research.

The greatest thanks go to my parents and my family for their love, support and encouragement during this thesis study.

Finally, very special thanks to my special friends and my colleagues at TAI Dr. Erhan Solakoğlu, Özen Güvendik, Cem Talip Öndeş, Ethem Hakan Orhan and all others for giving me the strength to complete this work.

TABLE OF CONTENTS

LIST OF TABLES

TABLES

LIST OF FIGURES

FIGURES

LIST OF SYMBOLS AND ABBREVIATIONS

ADI	Alternating Direction Implicit
CFD	Computational Fluid Dynamics
CFL	Courant-Friedrich-Lewy Number
CPU	Central Processing Unit
DDADI	Diagonally Dominant ADI
FDM	Finite Difference Method
FEM	Finite Element Method
FVM	Finite Volume Method
LU	Lower-Upper Diagonal
MIMD	Multiple Instruction, Multiple Data
MPI	Message Passing Interface
N-S	Navier Stokes
TLNS	Thin Layer Navier Stokes

c	Chord
e	Total energy per unit volume
E, F and G	Inviscid fluxes
E_v, F_v and G_v	Viscous fluxes
J	Jacobian
k_T	Turbulent conductivity
M_∞	Freestream Mach number
n	Normal distance
p, P	Pressure
Pi_0	Inlet total pressure
Pr	Prandtl number
P_T	Total pressure
q	Dependent variables vector
q_x, q_y and q_z	Heat conduction terms
R	Universal gas constant

Re	Reynolds number
S_c	Curvilinear distance between leading and trailing edges of the airfoil
Ti_0	Inlet total temperature
u, v, w	Fluid velocities in the x, y and z coordinate directions
U, V and W	Contravariant velocity components
z	Distance from the blade
β	Inlet angle
γ	Ratio of specific heats
δ	Boundary Layer thickness
δ_1	Displacement thickness
δ_2	Momentum thickness
ρ	Fluid density
ξ, η and ζ	Computational domain coordinates
$\in_i$ and $\in_e$	Implicit and explicit smoothing factors

τ_{xx}, ...	The shear stresses
$\vec{\vec{m}}$	Tensor m
$\vec{v}$	Vector v
$\overline{a}$	Time averaged variable a
$\hat{c}$	Transformed flux c

CHAPTER I

INTRODUCTION

1.1. Literature Survey:

The fluid flows within turbomachinery tend to be extremely complex. Understanding such flows is crucial to efforts to improve current turbomachinery designs, and the computational approach can be used to great advantage in this regard.

The aerodynamic interference effects between two airfoils are also of great practical interest in many aeronautical applications. Prominent examples are the interference effects between the leading or trailing-edge devices and the main airfoil on high-lift systems, the interference effects on canard-wing and wing-tail configurations, and the blade row interactions that occur in axial jet engines. Besides, at transonic flow conditions, many unsteady phenomena are associated with shock wave interaction with a separated boundary layer. The resulting pressure fluctuations cause periodic flows in supersonic cascades, and many other undesirable unsteady effects. Such periodic shock motions have been detected over fifty years ago, but the cause of self-sustained shock oscillations on wings or airfoils is still not fully understood [1], [2].

Several calculations of cascade flow have already been reported in the literature. These studies include two and three dimensional calculations using both the Euler and Navier Stokes equations. Ref. [3] presents a finite-difference, unsteady, thin-layer N-S approach to calculating the flow within an axial turbine stage. The relative motion between the stator and rotor airfoils is made possible with the use of patched grids that move relative to each other.

Ref. [4] presents rotor-stator interaction results obtained using Euler solutions. The various natural boundary conditions such as inlet, discharge, blade surface and periodicity boundary conditions that are required for rotor-stator calculations are presented. However, viscous effects have not been addressed in Ref. [4].

The performance of compressors and the sophistication of analysis tools have reached a level such that less well understood flow mechanisms are gaining in importance to designers. The impact on compressor performance of many of these mechanisms, such as blade row interactions, is not typically addressed in current design systems. Therefore, an initial simulation of interaction of a rotor wake in the stator inlet flow has been performed in this study.

1.2. Purpose:

The main purpose of this thesis is to investigate rotor-stator interaction, to increase cascade stall margin and finally with the help of these to increase total propulsive efficiency by introducing a rotor-wake and a periodic wake motion to the compressor stators in the turbomachines where there is highly effective parameters with each other.

1.3. Scope:

In Chapter 2 of this thesis, the governing Navier-Stokes equations are given in conservative form for the finite different formulation. The finite difference discretization, numerical solution techniques and flow solver are also presented in Chapter 2.

Test problem is described in Chapter 3. Also blade geometry, experimental conditions are presented in this chapter.

In Chapter 4, steady analyses of the test problem are given. These analyses divided into three parts. First analysis is performed for Euler solution. Second analysis is performed for Navier Stokes solution. Finally in the steady analysis Navier Stokes solution with nonuniform inlet velocity profile is presented.

In Chapter 5, unsteady analyses of the test problem are given. In the unsteady analyses Navier Stokes solution with nonuniform inlet velocity profile is presented.

The boundary condition files, subroutines and input files developed for this thesis are described in Appendices A and B.

In Appendix C, CPU time comparisons and computational requirements are given.

CHAPTER II

THEORETICAL BACKGROUND

This chapter is devoted to the especially governing equations and solution algorithm of PML3D flow solver [5].

Modified PML3D program is used for the computations of this thesis. PML3D is a parallel, multi block, structured, Euler / Navier Stokes solver. This code is described in Ref. [5]. Modifications applied to the solver for this thesis are also described in Appendix A.

2.1. Governing Equations:

The governing equations are the Navier-Stokes (N-S) equations. The Reynolds-averaged N-S equations are derived by averaging the viscous conservation laws over a time interval T. The time interval T is chosen large enough with respect to the time scale of the turbulent fluctuations, but has to remain small with respect to the time scales of other time- dependent effects. We consider the Reynolds Averaged N-S equations as the basic model, expressing the conservation laws for mass, momentum and energy written in conservation form

$$\frac{\partial}{\partial t}\begin{vmatrix}\rho \\ \rho\vec{V} \\ \rho e\end{vmatrix} + \vec{\nabla}\begin{vmatrix}\rho\vec{V} \\ \rho\vec{V}\times\vec{V} + p\vec{\vec{I}} - \vec{\vec{\tau}} \\ \rho\vec{V}H - \vec{\vec{\sigma}}\cdot\vec{V} - k\vec{\nabla}T\end{vmatrix} = \begin{vmatrix}0 \\ \rho\vec{f}_e \\ W_f + q_H\end{vmatrix} \tag{2.1.1}$$

or in condensed form

$$\frac{\partial U}{\partial t} + \vec{\nabla}\cdot\vec{F} = Q \tag{2.1.2}$$

The time dependent N-S equations are hyperbolic-parabolic in space -time while the stationary N-S equations are of mixed type in space, that is elliptic-parabolic for subsonic flows and hyperbolic-parabolic for supersonic flows. The physical interpretation of these properties are of great importance for the choice of a numerical scheme, since a hyperbolic system is dominated by wave propagation (or convection) effects, an elliptic system describes diffusion phenomena, while a parabolic system is associated with damped propagation effects. For high Reynolds number flows, the system of conservation equation is convection dominated in most of the flow region. The N-S equations are often written in vector form as in Equation (2.1.3). For convenience, the equations are cast in Cartesian coordinate form.

$$\frac{\partial q}{\partial t} + \frac{\partial E}{\partial x} + \frac{\partial F}{\partial y} + \frac{\partial G}{\partial z} + H = \frac{1}{\mathrm{Re}}\left(\frac{\partial E_v}{\partial x} + \frac{\partial F_v}{\partial y} + \frac{\partial G_v}{\partial z}\right) \tag{2.1.3}$$

These five equations are statements of the conservation of mass and energy and conservation of momentum in the x, y and z directions. This form of the equations assumes that the fluid may be compressible and that heat generation and body forces (except for those which might be included in the source term, *H*) can be ignored. This vector equation states that the time rate of change in the dependent variables *q* is equal to the spatial change in the inviscid fluxes, *E*, *F* and *G*, and viscous fluxes, E_v, F_v and G_v. A source term, *H,* is included to account for the centrifugal and Coriolis force terms, which appear if the coordinate frame is rotating. In the present study, the source term was not taken into account. The presence of the Reynolds number, $Re = \bar{\rho}\bar{u}\bar{L}/\bar{\mu}$, implies that the governing equations have been non-dimensionalized; with $\bar{\rho}$ and $\bar{u}$ often chosen as the freestream density and velocity, $\bar{L}$ chosen as the reference length of the body and $\bar{\mu}$ evaluated at the freestream static temperature. The vector of dependent variables, the inviscid and viscous flux terms are shown below.

$$
q = \begin{bmatrix} \rho \\ \rho u \\ \rho v \\ \rho w \\ e \end{bmatrix} \qquad E = \begin{bmatrix} \rho u \\ \rho u^2 + p \\ \rho uv \\ \rho uw \\ (e+p)u \end{bmatrix} \qquad F = \begin{bmatrix} \rho v \\ \rho uv \\ \rho v^2 + p \\ \rho vw \\ (e+p)\ v \end{bmatrix}
$$

$$
G = \begin{bmatrix} \rho w \\ \rho uw \\ \rho vw \\ \rho w^2 + p \\ (e+p)\ w \end{bmatrix} \qquad E_v = \begin{bmatrix} 0 \\ \tau_{xx} \\ \tau_{xy} \\ \tau_{xz} \\ u\tau_{xx} + v\tau_{xy} + w\tau_{xz} - q_x \end{bmatrix} \tag{2.1.4}
$$

$$
F_v = \begin{bmatrix} 0 \\ \tau_{yx} \\ \tau_{yy} \\ \tau_{yz} \\ u\tau_{yx} + v\tau_{yy} + w\tau_{yz} - q_y \end{bmatrix} \quad G_v = \begin{bmatrix} 0 \\ \tau_{zx} \\ \tau_{zy} \\ \tau_{zz} \\ u\tau_{zx} + v\tau_{zy} + w\tau_{zz} - q_z \end{bmatrix}
$$

Here ρ is the fluid density; u, v and w are the fluid velocities in the x, y and z coordinate directions, and e is the total energy per unit volume. The viscous flux terms are functions of the local fluid velocities, the shear stresses, τ_{xx}, ..., and heat conduction terms, q_x, q_y and q_z.

The pressure, p, which appears in the inviscid flux terms, is related to the dependent variables through an appropriate equation of state. The local pressure is expressed in terms of the dependent variables by applying the ideal gas law.

$$p = (\gamma - 1)\ \left[e - \tfrac{1}{2}\ \rho\left(u^2 + v^2 + w^2\right)\right] \tag{2.1.5}$$

The stresses are related to the velocity gradient of the fluid, assuming a Newtonian fluid for which the viscous stress is proportional to the rate of shearing strain (i.e. angular deformation rate). For turbulent flow, a Reynolds-averaged form of the equations is used where the dependent variables represent the mean flow contribution. The Boussinesq assumption is applied, permitting the apparent turbulent stresses to be related to the product of the mean flow strain rate and an apparent turbulent viscosity. Therefore, the shear and normal stress tensors have the following form;

$$\tau_{ij} = \left(\mu + \mu_T\right)\ \left[\left(\frac{\partial u_i}{\partial x_j} + \frac{\partial u_j}{\partial x_i}\right) - \tfrac{2}{3}\,\delta_{ij}\,\frac{\partial u_k}{\partial x_k}\right]$$

$$\sigma_{ij} = -p\delta_{ij} + \left(\mu + \mu_T\right)\ \left[\left(\frac{\partial u_i}{\partial x_j} + \frac{\partial u_j}{\partial x_i}\right) - \tfrac{2}{3}\,\delta_{ij}\,\frac{\partial u_k}{\partial x_k}\right] \tag{2.1.6}$$

The heat conduction terms, when Reynolds-averaging and the Boussinesq assumption are applied, are proportional to the local mean flow temperature gradient;

$$q_i = \frac{-1}{(\gamma - 1) Pr M_\infty^2}\left(k + k_T\right)\frac{\partial T}{\partial x_i} \tag{2.1.7}$$

Here, γ represents the ratio of specific heats, Pr is the Prandtl number and M_∞ is the freestream Mach number.

To determine the effective turbulent conductivity, k_T, Reynolds analogy is applied and the turbulent conductivity is related to the turbulent viscosity as follows;

$$k_T = \frac{Pr}{Pr_T}\mu_T \tag{2.1.8}$$

Here, and in the equation above, the conductivity and viscosity are non-dimensionalized by their representative (laminar) values evaluated at the freestream static temperature.

In many CFD applications, it is desirable to solve the governing equations in a domain, which has surfaces that conform to the body rather than in a Cartesian coordinate domain. A transformation is applied to the original set of equation to obtain a "generalized geometry" form of the governing equations. The transformed equations are shown below,

$$\frac{\partial \hat{q}}{\partial \tau} + \frac{\partial \hat{E}}{\partial \xi} + \frac{\partial \hat{F}}{\partial \eta} + \frac{\partial \hat{G}}{\partial \zeta} = \frac{1}{\mathrm{Re}}\left(\frac{\partial \hat{E}_v}{\partial \xi} + \frac{\partial \hat{F}_v}{\partial \eta} + \frac{\partial \hat{G}_v}{\partial \zeta} \right) \tag{2.1.9}$$

Typically, the physical domain is oriented in such a way that the coordinate directions in the computational domain, ξ, η and ζ, may correspond to directions relative to the body. In the applications discussed here, ξ corresponds to the direction along the body, η corresponds to the circumferential direction and ζ corresponds to the outward direction from the body surface. Also, τ represents time. Note that the source term, *H,* is not included to the Equation (2.1.9).

The transformed fluxes are functions of the original Cartesian flux terms and have a similar form. After rearranging, the vector of dependent variables and inviscid and viscous flux terms take the following form,

$$\hat{q} = \tfrac{1}{J}\begin{bmatrix} \rho \\ \rho u \\ \rho v \\ \rho v \\ \rho w \\ e \end{bmatrix} \quad \hat{E} = \tfrac{1}{J}\begin{bmatrix} \rho U \\ \rho u U + \xi_x p \\ \rho v U + \xi_y p \\ \rho w U + \xi_z p \\ (e+p)\ U - \xi_t p \end{bmatrix} \quad \hat{F} = \tfrac{1}{J}\begin{bmatrix} \rho V \\ \rho u V + \eta_x p \\ \rho v V + \eta_y p \\ \rho w V + \eta_z p \\ (e+p)\ V - \eta_t p \end{bmatrix}$$

$$\hat{G} = \tfrac{1}{J}\begin{bmatrix} \rho W \\ \rho u W + \zeta_x p \\ \rho v W + \zeta_y p \\ \rho w W + \zeta_z p \\ (e+p)\ W - \zeta_t p \end{bmatrix} \qquad \hat{E}_v = \tfrac{1}{J}\begin{bmatrix} 0 \\ \xi_x \tau_{xx} + \xi_y \tau_{xy} + \xi_z \tau_{xz} \\ \xi_x \tau_{xy} + \xi_y \tau_{yy} + \xi_z \tau_{zy} \\ \xi_x \tau_{xz} + \xi_y \tau_{yz} + \xi_z \tau_{zz} \\ \xi_x A + \xi_y B + \xi_z C \end{bmatrix} \qquad (2.1.10)$$

$$\hat{F}_v = \tfrac{1}{J}\begin{bmatrix} 0 \\ \eta_x \tau_{xx} + \eta_y \tau_{xy} + \eta_z \tau_{xz} \\ \eta_x \tau_{xy} + \eta_y \tau_{yy} + \eta_z \tau_{zy} \\ \eta_x \tau_{xz} + \eta_y \tau_{yz} + \eta_z \tau_{zz} \\ \eta_x A + \eta_y B + \eta_z C \end{bmatrix} \qquad \hat{G}_v = \tfrac{1}{J}\begin{bmatrix} 0 \\ \zeta_x \tau_{xx} + \zeta_y \tau_{xy} + \zeta_z \tau_{xz} \\ \zeta_x \tau_{xy} + \zeta_y \tau_{yy} + \zeta_z \tau_{zy} \\ \zeta_x \tau_{xz} + \zeta_y \tau_{yz} + \zeta_z \tau_{zz} \\ \zeta_x A + \zeta_y B + \zeta_z C \end{bmatrix}$$

where

$$\begin{aligned} A &= u\tau_{xx} + v\tau_{xy} + w\tau_{xz} - q_x \\ B &= u\tau_{yx} + v\tau_{yy} + w\tau_{yz} - q_y \\ C &= u\tau_{zx} + v\tau_{zy} + w\tau_{zz} - q_z \end{aligned}$$

(2.1.11)

The velocities in the ξ, η and ζ coordinates

$$
\begin{aligned}
U &= \xi_t + \xi_x u + \xi_y v + \xi_z w \\
V &= \eta_t + \eta_x u + \eta_y v + \eta_z w \\
W &= \zeta_t + \zeta_x u + \zeta_y v + \zeta_z w
\end{aligned}
\tag{2.1.12}
$$

represent the contravariant velocity components.

The Cartesian velocity components (*u, v, w*) are retained as the dependent variables and are non-dimensionalized with respect to a_∞ (the freestream speed of sound). In addition to the original Cartesian variables, additional terms $(J, \xi_x, \eta_y, \zeta_z, ...)$ appear in the equations. These terms referred to as the metric terms, result from the transformation and contain the purely geometric information that relates the physical space to the computational space. The metric terms are defined as

$$
\begin{aligned}
\xi_x &= J\left(y_\eta z_\zeta - y_\zeta z_\eta\right) & \eta_x &= J\left(z_\xi y_\zeta - y_\xi z_\zeta\right) \\
\xi_y &= J\left(z_\eta x_\zeta - x_\eta z_\zeta\right) & \eta_y &= J\left(x_\xi z_\zeta - x_\zeta z_\xi\right) \\
\xi_z &= J\left(x_\eta y_\zeta - y_\eta x_\zeta\right) & \eta_z &= J\left(y_\xi x_\zeta - x_\xi y_\zeta\right)
\end{aligned}
$$

$$
\begin{aligned}
\zeta_x &= J\left(y_\xi z_\eta - z_\xi y_\eta\right) & \xi_t &= -x_\tau \xi_x - y_\tau \xi_y - z_\tau \xi_z \\
\zeta_y &= J\left(z_\xi x_\eta - x_\xi z_\eta\right) & \eta_t &= -x_\tau \eta_x - y_\tau \eta_y - z_\tau \eta_z \\
\zeta_z &= J\left(x_\xi y_\eta - y_\xi x_\eta\right) & \zeta_t &= -x_\tau \zeta_x - y_\tau \zeta_y - z_\tau \zeta_z
\end{aligned}
$$

and

$$
J^{-1} = \frac{\partial(x, y, z)}{\partial(\xi, \eta, \zeta)} = x_\xi y_\eta z_\zeta + x_\zeta y_\xi z_\eta + x_\eta y_\zeta z_\xi - x_\xi y_\zeta z_\eta - x_\eta y_\xi z_\zeta - x_\zeta y_\eta z_\xi
\tag{2.1.13}
$$

The metrics are evaluated using second-order, central difference formulas for interior points and three-point, one-sided formulas at the boundaries. In general, a simplified form of the governing equations is applied. This set of equations is often referred to as the *"Thin Layer"* N-S equations. In a fashion similar to the boundary layer length scale analysis, only viscous terms, which involve derivatives along a single coordinate direction (typically normal to the body surface), are retained and the other viscous terms are dropped. At this point only a single vector of terms remains.

$$\frac{\partial \hat{q}}{\partial \tau} + \frac{\partial \hat{E}}{\partial \xi} + \frac{\partial \hat{F}}{\partial \eta} + \frac{\partial \hat{G}}{\partial \zeta} = \frac{1}{\mathrm{Re}} \frac{\partial \hat{S}}{\partial \zeta} \tag{2.1.14}$$

where

$$\hat{S} = J^{-1} \begin{bmatrix} 0 \\ \mu A u_\zeta + \left(\mu/3\right) C \zeta_x \\ \mu A v_\zeta + \left(\mu/3\right) C \zeta_y \\ \mu A w_\zeta + \left(\mu/3\right) C \zeta_z \\ \left\{ A\left[0.5\mu\left(V^2\right)_\zeta + \kappa Pr^{-1}(\gamma-1)^{-1}\left(a^2\right)_\zeta\right] + \left(\mu/3\right) BC \right\} \end{bmatrix} \tag{2.1.15}$$

with $A = \zeta_x^2 + \zeta_y^2 + \zeta_z^2 \quad B = \zeta_x u + \zeta_y v + \zeta_z w \qquad C = \zeta_x u_\zeta + \zeta_y v_\zeta + \zeta_z w_\zeta$

$$\mathrm{V}^2 = u^2 + v^2 + w^2 \qquad\qquad \kappa = \frac{1}{\gamma R M_\infty^2}$$

The equations are now in a form, which is amenable to solution by direct implicit numerical techniques such as the Beam and Warming algorithm [6].

2.2. Solution Algorithm:

The numerical scheme used for the solution of the Thin Layer N-S equations is generally based on a fully implicit, approximately factored, finite difference algorithm in delta form [7]. Implicit methods with the delta form are widely used for solving steady state problems since the steady state solutions are indifferent to the left-hand side operators.

The solution of the three-dimensional equations is implemented by an approximate factorization that allows the system of equations to be solved in three coupled one-dimensional steps. The most commonly used method is the Beam and Warming one [8]. The LU-ADI factorization [9] is one of those schemes that simplify inversion works for the left-hand side operators of the Beam and Warming's. Each ADI operator is decomposed to the product of the lower and upper bi-diagonal matrices by using the flux vector splitting technique [10].

To maintain the stability, the diagonally dominant LU factorization is adopted. The explicit part is left to be the same as the Beam and Warming's where central differencing is used.

As indicated in Equation (2.1.14), this solution technique involves solving the time-dependent N-S equations. The procedure is started by assuming a uniform, free-stream solution for all grid points in the computational domain. The calculation then marches in time until a steady state solution is obtained subject to the imposed boundary conditions.

Beam and Warming method applied to Equation (2.1.14) leads to the following approximate factorization form,

$$\left(I + h\delta_{\xi}\hat{A}^{n} - \in_{i} J^{-1}\nabla_{\xi}\Delta_{\xi}J\right)\times\left(I + h\delta_{\eta}\hat{B}^{n} - \in_{i} J^{-1}\nabla_{\eta}\Delta_{\eta}J\right)$$

$$\times\left(I + h\delta_{\zeta}\hat{C}^{n} - h\mathrm{Re}^{-1}\,\delta_{\zeta}\hat{M}^{n} - \in_{i} J^{-1}\nabla_{\zeta}\Delta_{\zeta}J\right)\times\left(\hat{Q}^{n+1} - \hat{Q}^{n}\right)$$

$$= -h\left(\delta_{\xi}\hat{E}^{n} + \delta_{\eta}\hat{F}^{n} + \delta_{\zeta}\hat{G}^{n} - \mathrm{Re}^{-1}\,\delta_{\zeta}\hat{S}^{n}\right)$$

$$- \in_{e} J^{-1}\left[(\nabla_{\xi}\Delta_{\xi})^{2} + (\nabla_{\eta}\Delta_{\eta})^{2} + (\nabla_{\zeta}\Delta_{\zeta})^{2}\right]JQ^{n} \qquad (2.2.1)$$

where $h = \Delta t$, δ is the central finite difference operator, and Δ and ∇ are forward and backward difference operators, respectively. For the convective terms in the right hand side, fourth order differencing is used. Maintenance of the freestream is achieved by subtracting the freestream fluxes from the governing equations.

For the ξ direction, the Beam and Warming's ADI operator can be written in the diagonal form as follows,

$$I + h\delta_{\xi}\hat{A} + J^{-1} \in_{i} \delta_{\xi}^{2}J = T_{\xi}\left[I + h\delta_{\xi}\hat{D}_{A} + J^{-1} \in_{i} \delta_{\xi}^{2}J\right]T_{\xi}^{-1} \qquad (2.2.2)$$

where $\hat{A} = T_{\xi}\hat{D}_{A}T_{\xi}^{-1}$. The flux vector splitting technique is used to decompose the central differencing to two one sided differencing.

$$\hat{A} = T_{\xi}\left[I + \nabla_{\xi}D_{A}^{+} + \Delta_{\xi}D_{A}^{-}\right]T_{\xi}^{-1} \qquad (2.2.3)$$

with

$$D_A^{\pm} = \tfrac{h}{2}\left(\hat{D}_A \pm \left|\hat{D}_A\right|\right) \pm \bar{J}^{-1} \in_i J$$,

where $\bar{J}^{-1}$ is taken to be the Jacobian at the central point corresponding to Equation (2.2.2). Equation (2.2.3) can be rewritten as,

$$\hat{A} = T_{\xi}\left[L_A + M_A + N_A\right]T_{\xi}^{-1} \qquad (2.2.4)$$

where for three point upwinding,

$$L_A = -\frac{8}{6}D^{+}_{A_{j-1}} + \frac{1}{6}D^{+}_{A_{j-2}},$$

$$M_A = I + \tfrac{7}{6}\left(D^{+}_{A\,j} - D^{-}_{A\,j}\right),$$

$$N_A = \frac{8}{6}D^{-}_{A_{j+1}} - \frac{1}{6}D^{-}_{A_{j+2}},$$

The diagonally dominant factorization used here can be described as,

$$L_A + M_A + N_A = \left(L_A + M_A\right)\ M_A^{-1}\left(M_A + N_A\right) + 0\left(h^2\right) \qquad (2.2.5)$$

since $M_A = 0(1)$ and L_A, $N_A = 0(h)$. Thus the LU factorization for an ADI operator can be obtained as

$$I + h\ \ \delta_{\xi}\hat{A} + J^{-1} \in_i \delta_{\xi}^2 J = T_{\xi}\left(L_A + M_A\right)M_A^{-1}\left(M_A + N_A\right)T_{\xi}^{-1} \qquad (2.2.6)$$

By this, the block tri-diagonal system is decomposed to the product of the lower and upper scalar bi-diagonal ones, $L_A + M_A$ and $M_A^{-1}\left(M_A + N_A\right)$.

In order to maintain the stability of the thin layer viscous terms, the splitted Jacobian matrices $\hat{C}^{\pm}$ are modified as follows,

$$\hat{C}_{\nu}^{\pm} = T_{\zeta} \ \left(\hat{D}_{C}^{\pm} \pm \nu \ \ I\right) \ T_{\zeta}^{-1} \tag{2.2.7}$$

where

$$\nu = 2\mu r_{\zeta}^{2} \Big/ Re\rho\Delta\zeta$$

At the end, the Beam and Warming Scheme can be described as follows by using the similar procedure for the other operators,

$$T_{\xi} \times \ \left(L_A + M_A\right) \ \times M_A^{-1} \times \ \left(M_A + N_A\right) \times \left(T_{\xi}^{-1} T_{\eta}\right) \times \left(L_B + M_B\right) \times \ M_B^{-1} \times \left(M_B + N_B\right) \times$$

$$\left(T_{\eta}^{-1} T_{\zeta}\right) \times \left(L_C + M_C\right) \ \times M_C^{-1} \times \left(M_C + N_C\right) \times \ T_{\zeta}^{-1} \times \Delta\hat{U}^{n} = RHS \ \ of \, eqn.(2.2.1)$$

(2.2.8)

As far as accuracy is concerned, the basic algorithm is first order accurate in time and second order accurate in space. Convergence, stability and smoothness of the solution depend on the implicit and explicit smoothing factors, $\in_i$ and $\in_e$, and Courant-Friedrich-Lewy (CFL) number [11]. Physically, the CFL number indicates the relation between one spatial step-size Δx movement in one time step Δt. Numerically, CFL number is defined as:

$$CFL = \frac{\Delta t \cdot \sigma_{\max}}{\min(\Delta\xi, \Delta\eta, \Delta\zeta)} \tag{2.2.9}$$

Here $\sigma_{\max}$ is the maximum eigenvalue. Starting from the definition of speed of sound, $\sigma_{\max}$ is defined as follows

$$c^2 = \frac{\gamma p}{\rho} = \gamma(\gamma - 1)\left(\frac{e}{\rho} - \frac{u^2 + v^2 + w^2}{2}\right) \tag{2.2.10}$$

$$\begin{aligned} \sigma_A &= U + c\sqrt{\xi_x^2 + \xi_y^2 + \xi_z^2} \\ \sigma_B &= V + c\sqrt{\eta_x^2 + \eta_y^2 + \eta_z^2} \\ \sigma_C &= W + c\sqrt{\zeta_x^2 + \zeta_y^2 + \zeta_z^2} \end{aligned} \tag{2.2.11}$$

where *U, V* and *W* were defined in equation (2.1.12).

$$\sigma_{\max} = \max(\sigma_A, \sigma_B, \sigma_C) \tag{2.2.12}$$

In order to simulate turbulence effects, the viscous coefficient is computed as the sum of laminar viscosity and turbulence viscosity. The turbulent eddy viscosity is then calculated by using the two-layer algebraic turbulence model proposed by Baldwin and Lomax [12].

CHAPTER III

TEST PROBLEM

3.1. Description of Test Case:

The test case E/CA-3 High Subsonic Compressor Cascade 115 [13] concerns the experimental investigation of a 2D stator compressor cascade at two inlet Mach numbers (0.7 and 0.85) and four values of incidence β (49°, 51°, 53°, and 55°).

Boundary layer measurements are obtained on five locations along the suction side.

The use of a special suction system on the lateral walls leads to a 2D flow. Therefore 2D Euler and Navier Stokes solutions are employed in the numerical analysis.

This “115” stator blade cascade is designed to achieve a flow deviation angle larger than 50 degrees in a two-dimensional flow. The corresponding diffusion is high and the blade shapes are tailored to minimize the suction side over-expansion and to ensure a recompression without flow separation at the design conditions.

The experimental results cover a sufficiently large range of conditions to allow correct validation of the boundary layer calculation method [13].

3.2. Blade Geometry:

The blade geometry is given in Fig. 3.1. In this figure all the lengths are in millimeters.

The leading and trailing edge radius of the blade is equal to 0.2 mm where the span of the blade is equal to 120 mm. The distance between the leading edge and the trailing edge is approximately 94.9 mm. Blade spacing is 28 mm.

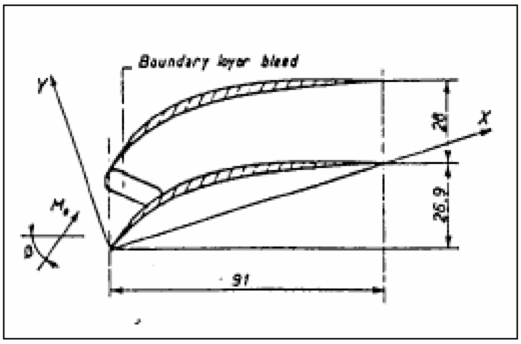

X	Ys	Yp
0	0.150	0.150
5	4.401	2.986
10	7.692	5.528
15	10.072	7.430
20	11.895	8.763
25	13.146	9.591
30	13.858	10.058
35	14.108	10.228
40	13.996	10.128
45	13.568	9.810
50	12.861	9.324
55	11.940	8.716
60	10.864	7.947
65	9.674	7.030
70	8.388	6.016
75	6.997	4.954
80	5.502	3.845
85	3.924	2.686
90	2.253	1.477
95	0.508	0.198

Fig. 3.1 Compressor Cascade115 Stator Blade, the geometric data

3.3. Experimental Conditions:

Test conditions are as follows;

T_{io}: 295 K

P_{io}: $0.8 * 10^5$ Pa

M_o: 0.7 ; 0.85

β: 49° ; 51° ; 53° ; 55°

Re: $1.0 * 10^6$ (c=101.5 mm)

Mean efficiency values are given in Fig. 3.2.

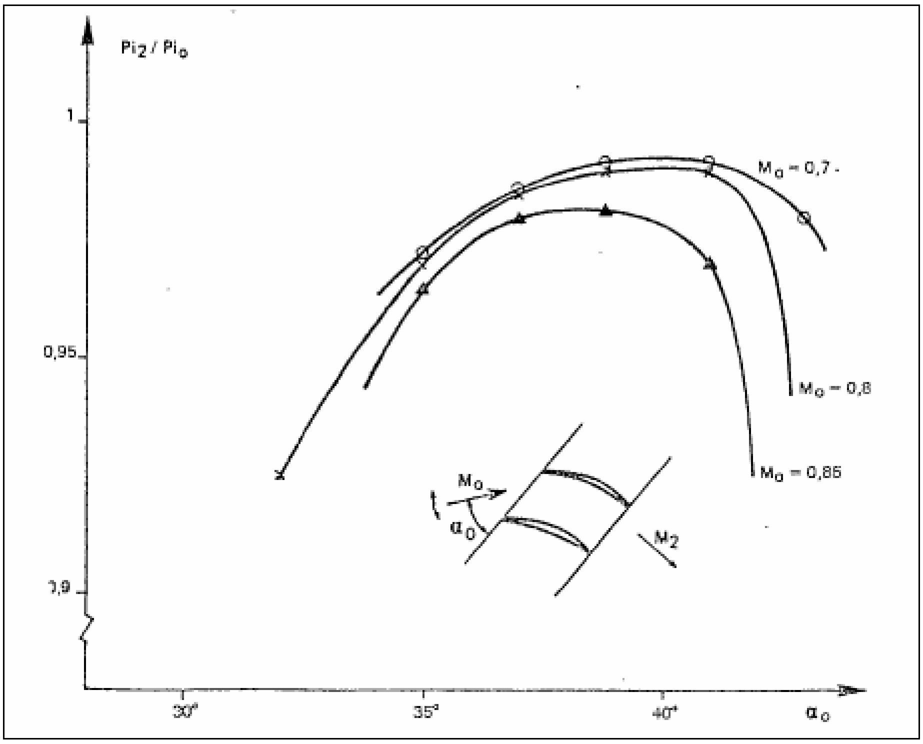

Fig. 3.2 Mean Efficiency Evolution

α_0 and β_0 are related with the following equation:

$$\alpha_0 = 90° - \beta_0 \tag{3.3.1}$$

The integral boundary layer parameters deduced from boundary layer measurements are given in Ref. [13].

The boundary layer total pressure distributions are also given in Ref. [13].

3.4. Evaluation Methods and Data Uncertainty:

The velocity profiles and the main characteristic thicknesses of the boundary layer are computed with the inlet total pressure and the local total pressure. The normal pressure gradient is assumed to be zero. There is no thermal effect.

Data uncertainty is:

$$\frac{\Delta(P / Pi_0)}{P / Pi_0} = \pm 0.3\% \tag{3.4.1}$$

$$\Delta z = \pm 0.03mm \tag{3.4.2}$$

CHAPTER IV

STEADY ANALYSES

In the steady analyses two dimensional

Euler with uniform inlet velocity,

Navier Stokes with uniform inlet velocity,

Navier Stokes with variable inlet velocity profile solutions are presented for the test case described in Chapter 3.

4.1. Euler Solution with Uniform Inlet Velocity Profile:

4.1.1. Grid:

For the 2D Euler Solution two different types of grids are generated. The first grid type called H-grid is shown in Figs. 4.1 and 4.2 and this is a single block grid. The grid dimensions are 140*3*70 in ξ, η, and ζ directions (J,K,L). The normal distance between the surface and the first grid point above the surface is, $\Delta n / c = 0.003076$. The cascade is from J=20 to J=120. The grid is nondimensionalized with chord, *c*, which is the length of the line connecting the leading and trailing edges of the airfoil. c should not be confused with S_c which is the curvilinear distance between these two points.

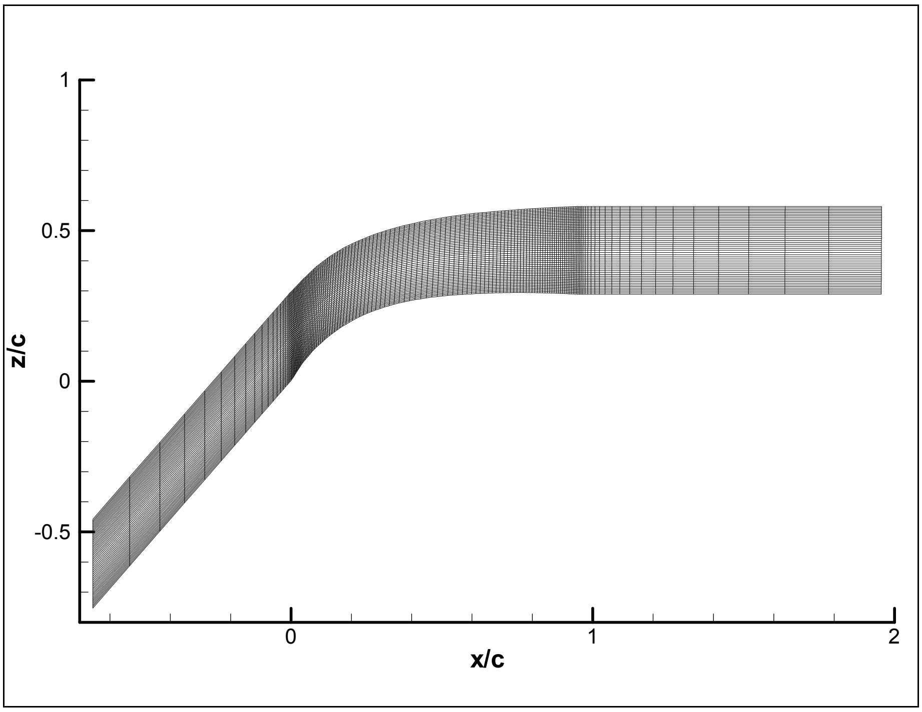

Fig. 4.1 H-grid

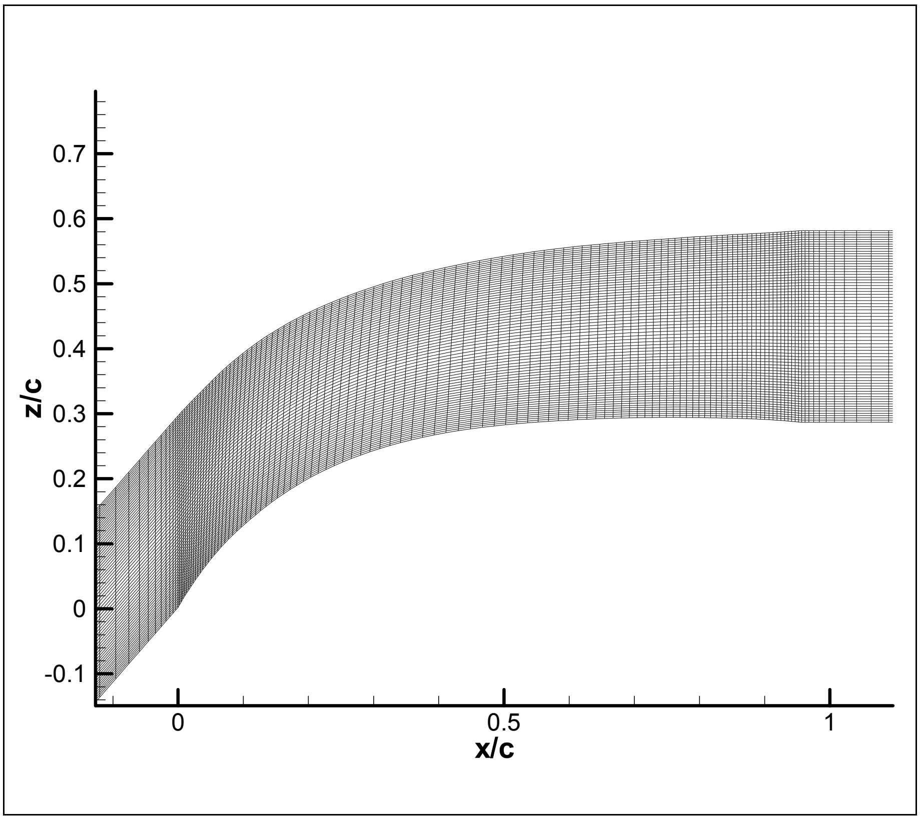

Fig. 4.2 H-grid, enlarged around the cascade

Leading and trailing edge definitions of the H-grid is shown in Fig. 4.3.

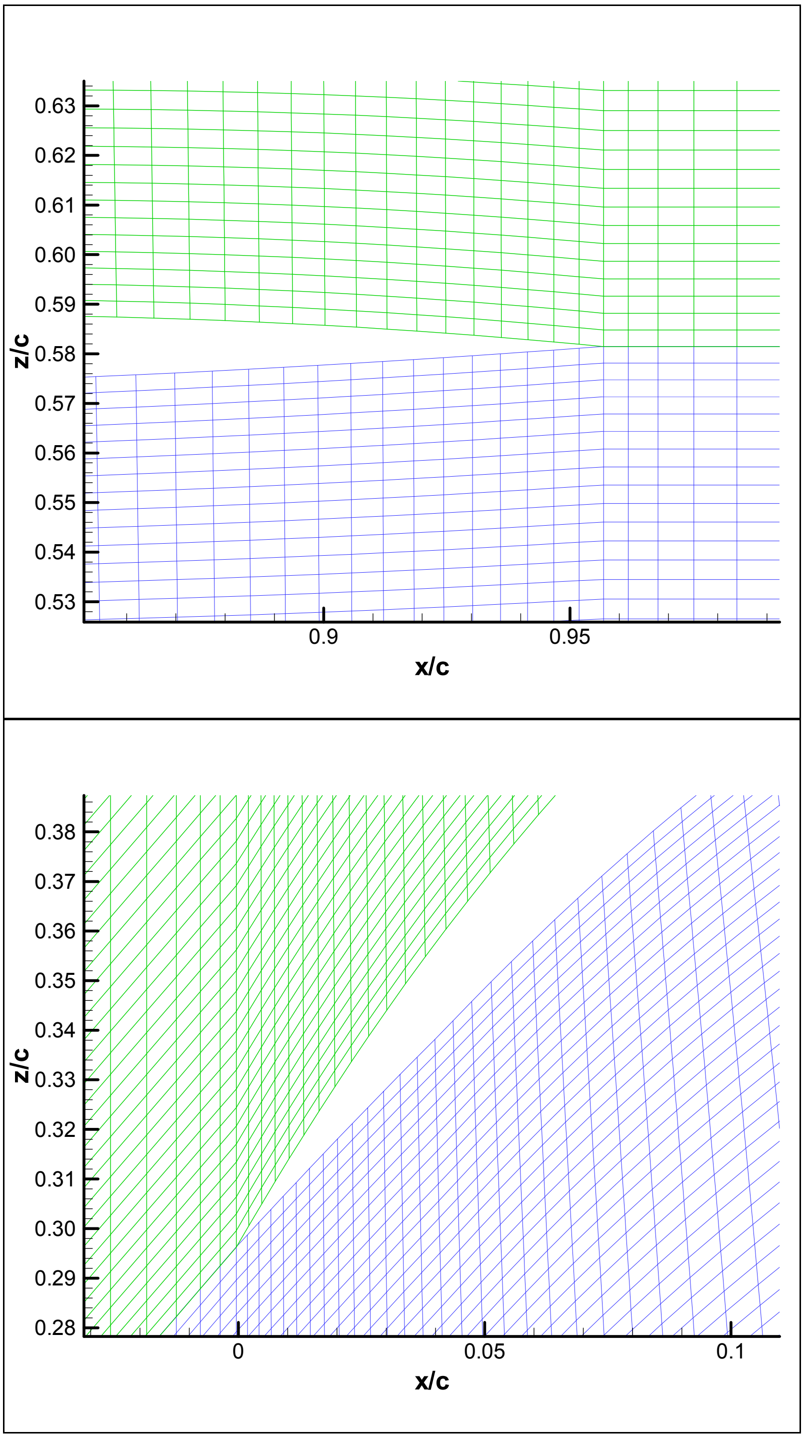

Fig. 4.3 Airfoil trailing and leading edge definition with the H-grid.

The second grid type developed for the Euler solution is H-O-H multi block type grid. It is made of three blocks. The front block, the center block and the rear block. The center block is an O-type grid and its dimensions are 249*3*29 in ξ, η, and ζ directions (J,K,L). The normal distance between the surface and the first grid point above the surface is, $\Delta n / c = 0.001997$. L=1 corresponds to the airfoil surface. This grid is made of two layers inner layer is a hyperbolic grid which provides good orthogonality. The outer layer is an algebraic grid which provides correspondence between the top and bottom surface points for the application of periodic boundary conditions. The front and rear block dimensions are 25*3*21 each in ξ, η, and ζ directions (J,K,L). The grid is shown in Fig. 4.4 through Fig. 4.7.

The grid is nondimensionalized again with chord, *c*.

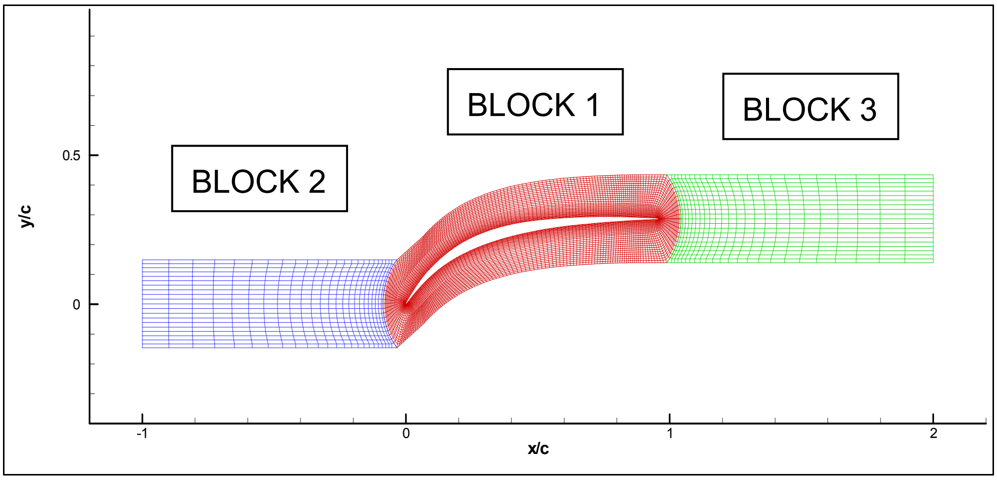

Fig. 4.4 H-O-H Grid

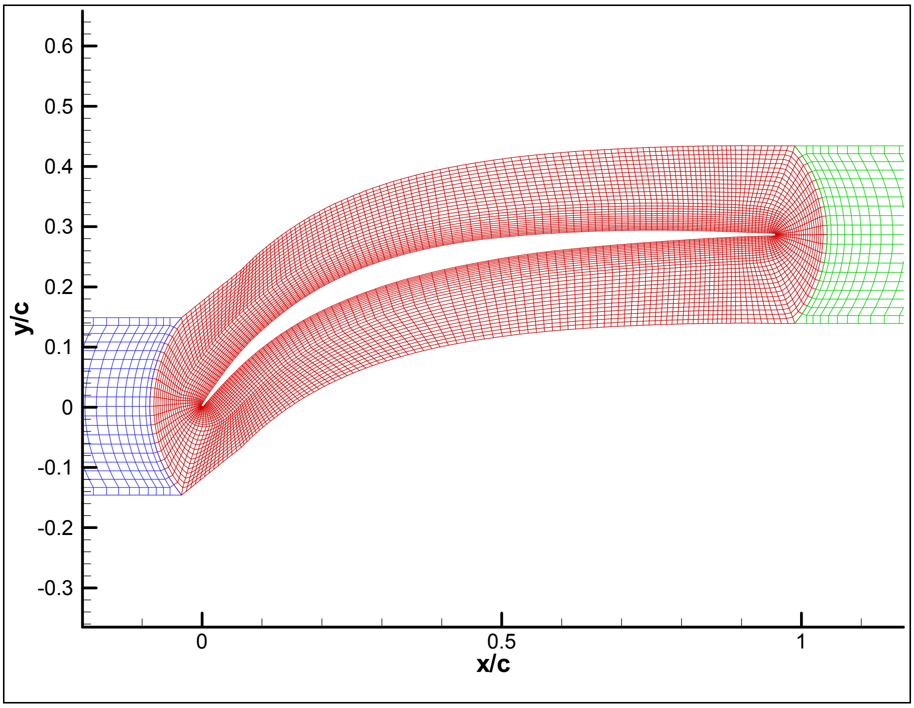

Fig. 4.5 H-O-H Grid, enlarged around the cascade

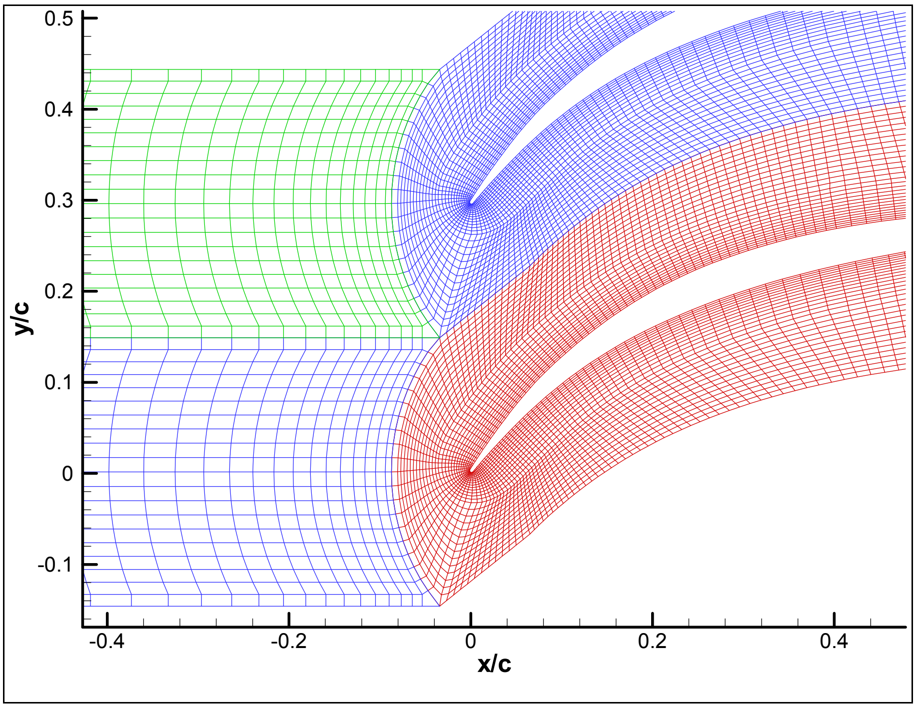

Fig. 4.6 H-O-H Grid, a view showing the periodicity

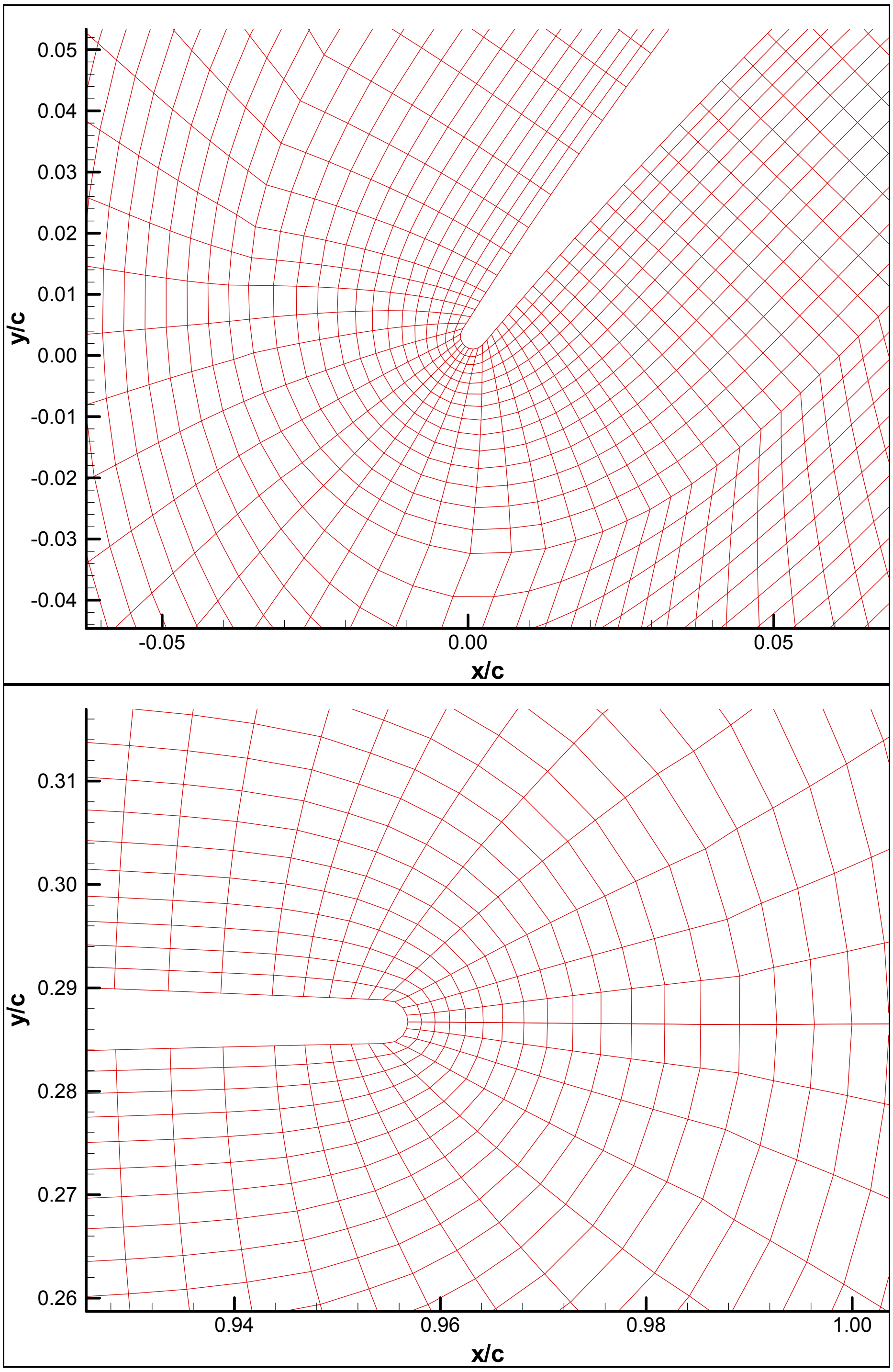

Fig. 4.7 Airfoil leading and trailing edge definition with the H-O-H grid

4.1.2. Boundary Conditions:

Applied boundary conditions are depending on the grid type. For the H-grid and H-O-H grid the boundary conditions are different and explained below.

4.1.2.1. H-Grid Boundary Conditions:

J=1 is the flow in plane the inflow parameters are specified. J=JMAX=140 is the flow out plane pressure fixed extrapolation type boundary conditions are used. K=1 and K=KMAX=3 are the side planes 2D side plane boundary conditions are used (extrapolation type).

For L=1 and L=LMAX surfaces from J=2 to 19 and J=121 to 139 periodic, from J=20 to 120 surface type boundary conditions are applied. Fig. 4.8 summarizes the boundary conditions applied to the H-grid. Further explanations are available in Appendix A.

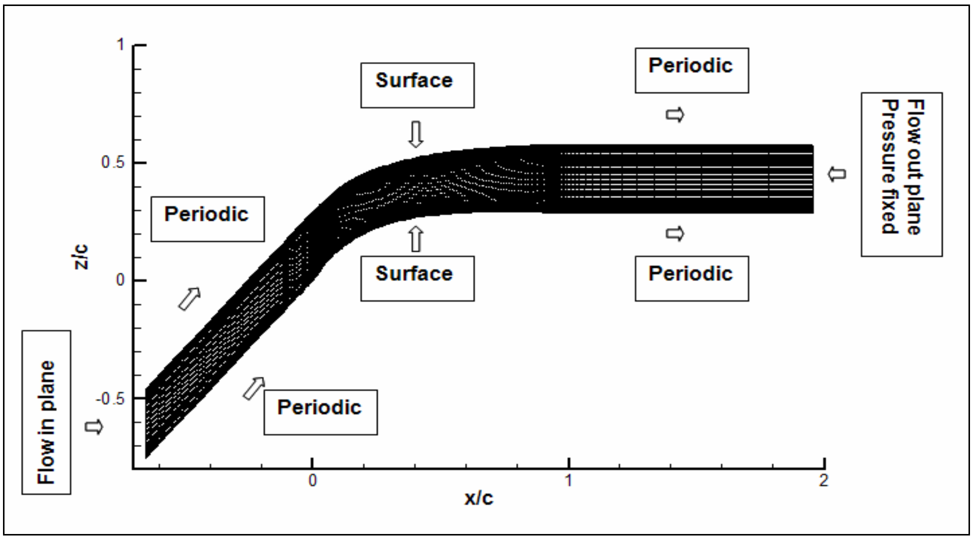

Fig. 4.8 Boundary Conditions applied to the H-grid

4.1.2.2. H-O-H Grid Boundary Conditions:

For the center O-Grid at L=LMAX top and Bottom surfaces are periodic. Matched Surface Boundary Conditions are applied at the common boundaries with the front and rear blocks. At L=1, the surface boundary conditions are applied. J=1 and J=JMAX boundaries coincides (the wake behind the T.E.) and the periodic boundary conditions are applied at those boundaries.

For the front grid at J=1 inflow (freestream) is specified. At J=JMAX Matched surface boundary conditions are applied with the central O-Block. L=1 (bottom surface) and L=LMAX (top surface) are periodic with each other.

For the rear grid at J=1 Matched surface boundary conditions are applied with the central O-Block. J=JMAX is the flow out plane pressure fixed extrapolation type boundary conditions are used. L=1 (bottom surface) and L=LMAX (top surface) are periodic with each other.

Fig. 4.9 summarizes the boundary conditions applied to the H-O-H grid. Further explanations are available in Appendix A.

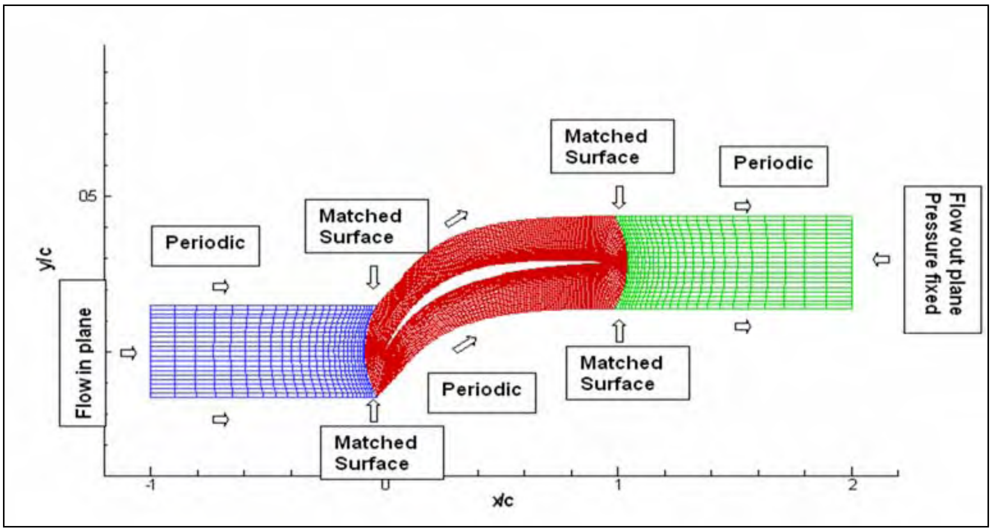

Fig. 4.9 Boundary Conditions applied to the H-O-H grid

4.1.2.3. Calculation of exit to inlet static pressure ratio:

In Fig. 4.10 the geometry of the flow domain is described.

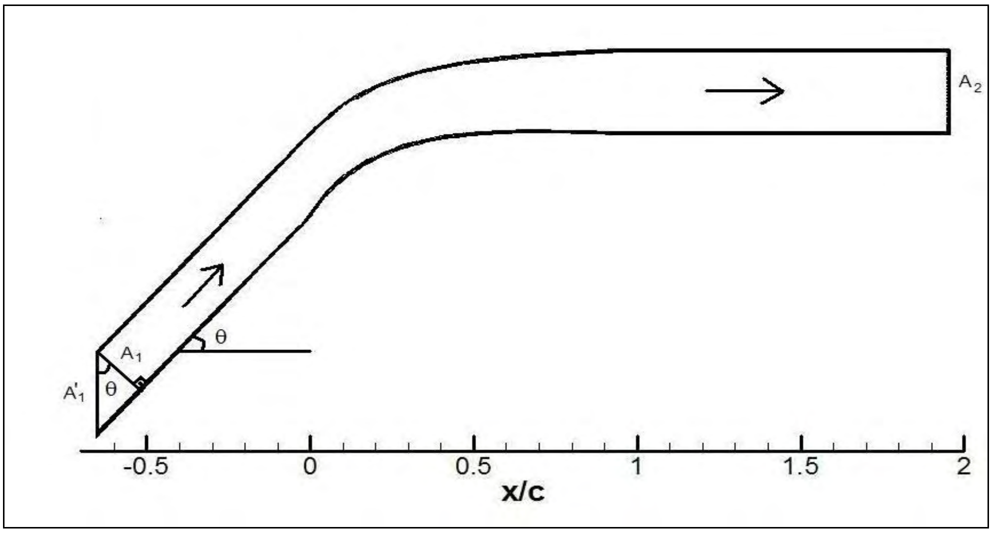

Fig. 4.10 Flow domain geometry

For the J=JMAX flow out plane pressure fixed extrapolation type boundary conditions, following procedure has been employed for calculation of exit to inlet static pressure ratio.

As shown in Fig. 4.10 A'_1 is the inlet plane and A_2 is the exit plane. At the bottom and top boundaries, the surface (no flow across) or periodic boundary conditions (flow coming in from bottom goes out from top) are specified. Therefore we may assume that mass flow coming in from section A'_1 is going out from section A_2.

According to the experimental data $\frac{P_{02}}{P_{01}} \cong 0.99$. 1.0 % loss is due to the boundary layer losses. Since we are performing an Euler solution $\frac{P_{02}}{P_{01}} \cong 1.0$ will be assumed. From the flow domain geometry described in the Fig. 4.10, the following measurements are made:

$$A_1^{'} = 0.2947 \tag{4.1.1}$$

$$A_2 = 0.2947 \tag{4.1.2}$$

In this section, pressure ratio of $M_1 = 0.7$ and $\beta = 49°$ case is calculated as an example. Therefore θ angle described in Fig. 4.10 is taken as:

$$\theta = \beta = 49° \tag{4.1.3}$$

Then, inlet area normal to the flow, A_1, is calculated as follows:

$$A_1 = A_1^{'} \cos\theta = 0.1933 \tag{4.1.4}$$

By using the isentropic tables for $M_1 = 0.7$:

$\frac{P_{01}}{P_1} = 1.387$, $\frac{A_1}{A_1^*} = 1.094$

Since $P_{01} = P_{02}$ then, $A_1^* = A_2^*$ (4.1.5)

$$\frac{A_2}{A_2^*} = \frac{A_2}{A_1}\frac{A_1}{A_1^*}\frac{A_1^*}{A_2^*} = \frac{0.2947}{0.1933} * 1.094 * 1.0 = 1.6679 \quad (4.1.6)$$

The area ratio found in Equation (4.1.6) is used to predict exit Mach number and presssure ratio from the isentropic tables and this leds to the inlet to exit pressure ratio as described in Equation (4.1.8);

$M_2 = 0.3777$, $\frac{P_{02}}{P_2} = 1.1037$ (4.1.7)

$$\frac{P_2}{P_1} = \frac{P_2}{P_{02}}\frac{P_{01}}{P_1} = \frac{1.387}{1.1037} = 1.257 \quad (4.)$$

As parameter β is varied, $\frac{A_1}{A_1^*}$ changes and both affect $\frac{P_2}{P_1}$. Calculated ratios for different β angles are presented in Table 4.1.

Table 4.1 Exit to inlet static pressure ratios for Euler solution

Mach number	β angle	$\frac{P_2}{P_1}$
0.7	49°	1.2570
0.7	51°	1.2690
0.7	53°	1.2807
0.7	55°	1.2890

4.1.3. Results:

In this section convergence of the L2 norm of the residuals of the H-grid and H-O-H grid, M=0.7 and β=49° are presented in Figs. 4.11 and 4.12 initially for comparison.

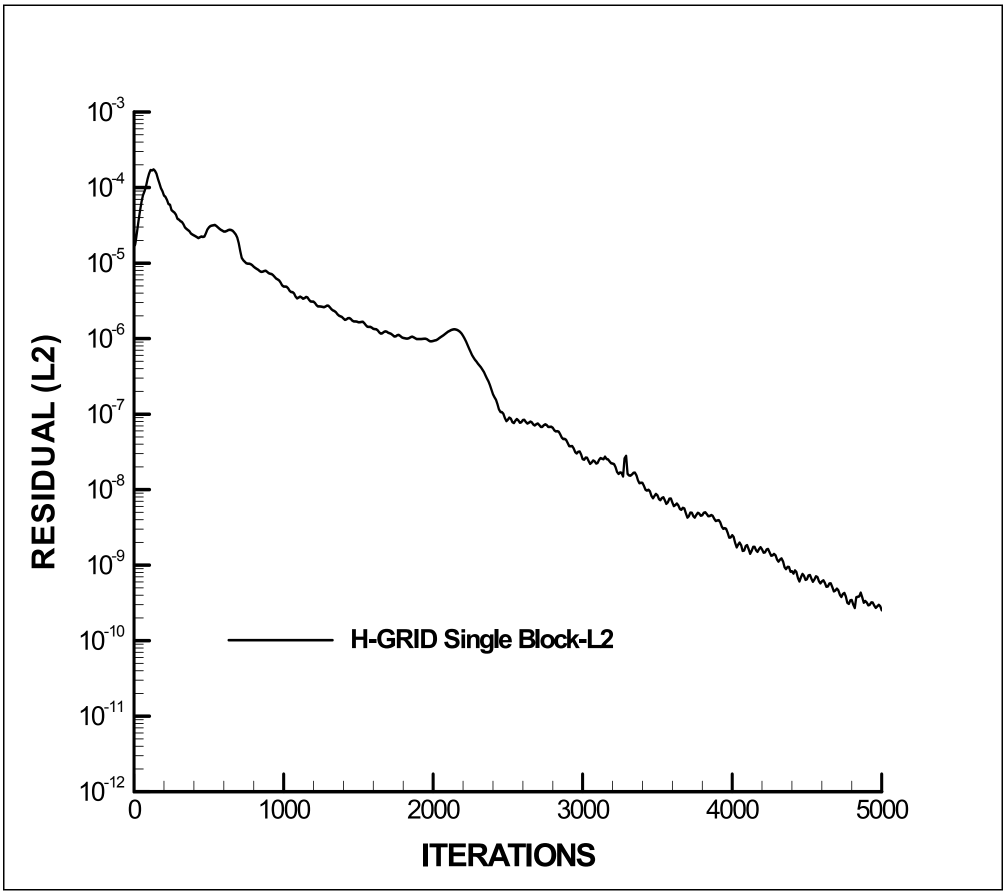

Fig. 4.11 H-Grid convergence history for M=0.7 and β =49°

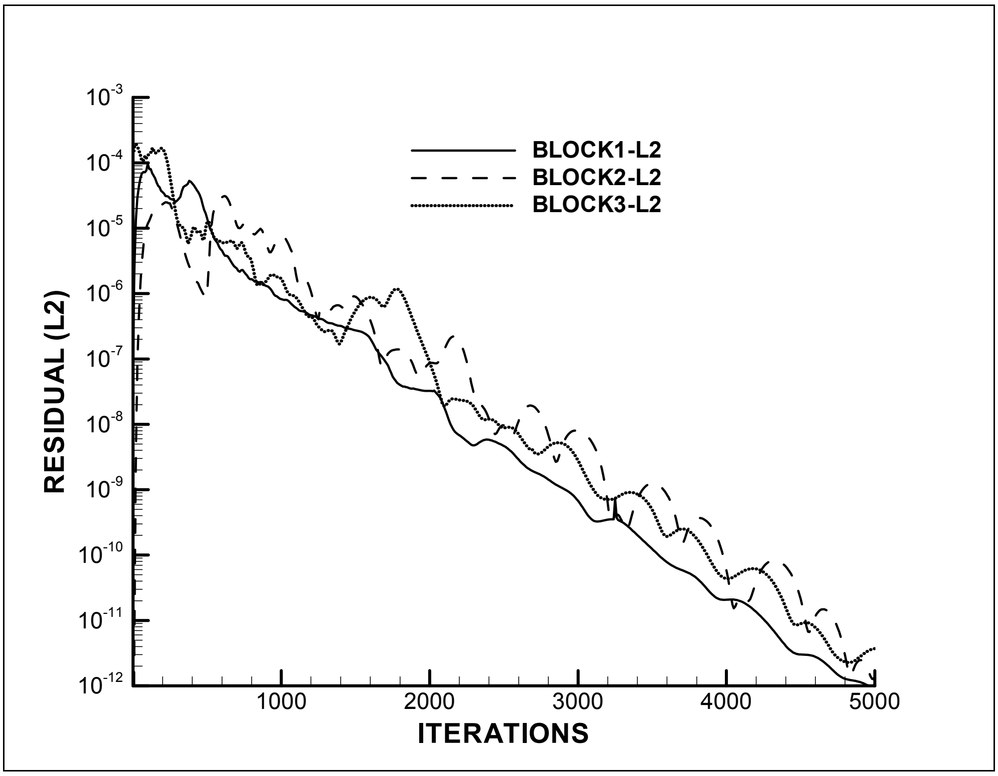

Fig. 4.12 H-O-H Grid convergence history for M=0.7 and β=49°

L2 norm converged about 5 orders in 5000 iterations for H-grid, M=0.7 and β=49° while Block-1 L2 norm converged about 8 orders in 5000 iterations of H-O-H grid, M=0.7 and β=49°. Another advantage of the H-O-H type grid is obviously better definitions of the leading and trailing edge regions. Therefore for the further test cases (M=0.7 and β=51°, 53°, 55°) H-O-H grid type is selected and computations have been done for that grid type only.

In the next figures (Figs. from 4.13 to 4.15) convergence of the L2 norms of the residuals of the H-O-H grid, test cases M=0.7 and β=51°, 53°, 55° are presented.

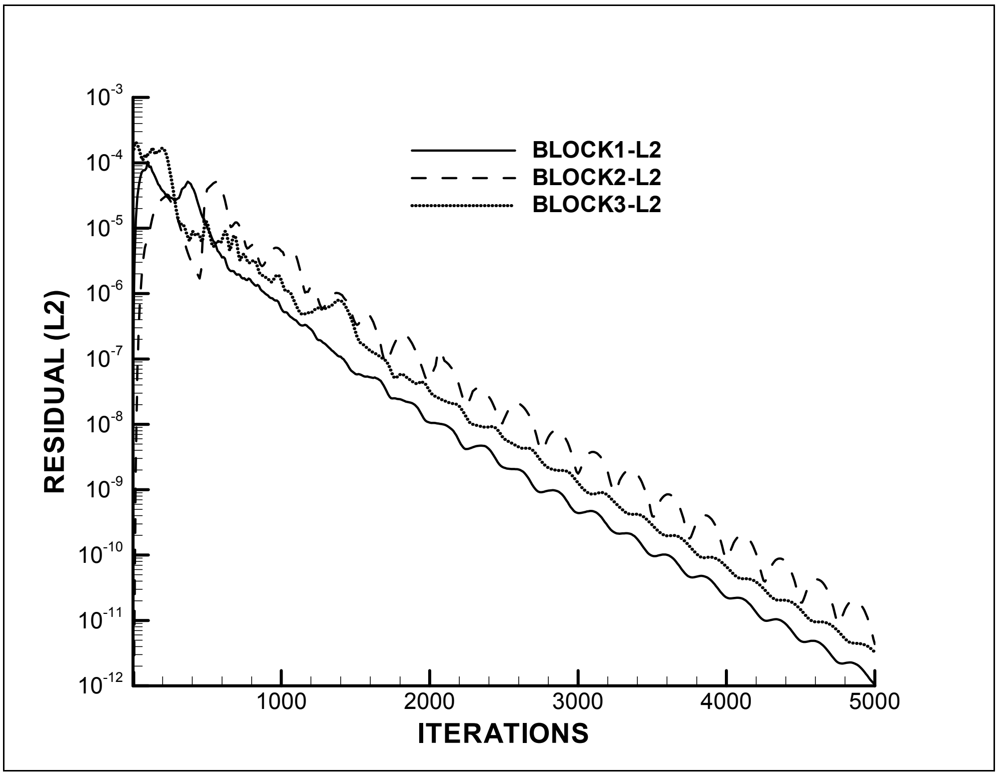

Fig. 4.13 H-O-H Grid convergence history for M=0.7 and β=51°

For Block-1 L2 norm converged about 8 orders in 5000 iterations for M=0.7 and β=51°.

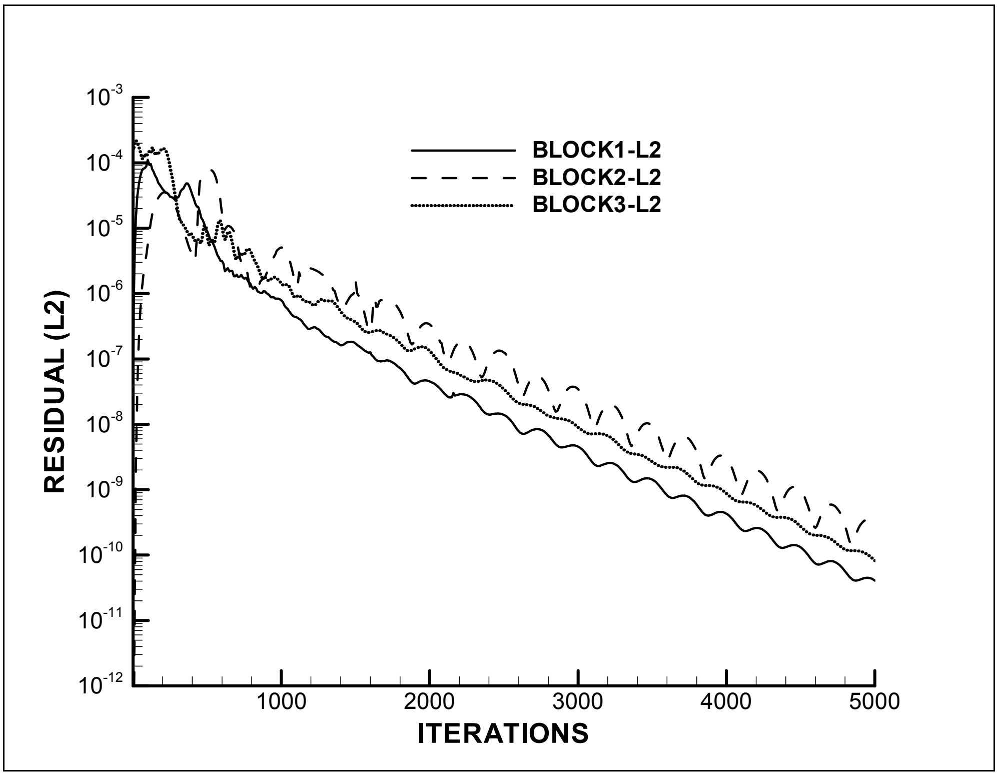

Fig. 4.14 H-O-H Grid convergence history for M=0.7 and β =53°

For Block-1 L2 norm converged more than 6 orders in 5000 iterations for M=0.7 and β =53°.

For Block-1 L2 norm does not converged for Euler solution for M=0.7 and β =55°.

In Ref. [13] the experimental surface pressure data is provided as the ratio of local static presure to inlet total pressure. In PML3D the pressures are nondimensionalized with $\rho_\infty a_\infty^2$. The nondimensional inlet total presssure is calculated as follows:

$$\frac{P_{i0}}{P_i} = \left(1 + \frac{\gamma - 1}{2} M_\infty^2\right)^{\frac{\gamma}{\gamma-1}} \tag{4.1.9}$$

$$\frac{P_{i0}}{\rho_\infty a_\infty^2} = \frac{P_i}{\rho_\infty a_\infty^2}\left(1 + \frac{\gamma - 1}{2} M_\infty^2\right)^{\frac{\gamma}{\gamma-1}} = \frac{1}{\gamma}\left(1 + \frac{\gamma - 1}{2} M_\infty^2\right)^{\frac{\gamma}{\gamma-1}} \tag{4.1.10}$$

Then local static pressure to inlet total pressure ratio $\frac{P}{P_{i0}}$ is obtained from the following equation

$$\frac{P}{P_{i0}} = \frac{\dfrac{P}{\rho_\infty a_\infty^2}}{\dfrac{P_{i0}}{\rho_\infty a_\infty^2}} \tag{4.1.11}$$

A post-processing program **postp2ds.for** reads the **BLOCK.001** and **qfile.001 files** and prepares a plot file **tec2ds.dat** by employing the above equations for plotting the selected variables along the selected two dimensional streamlines or surfaces. Following figures represents the results from the comparison of surface pressures with Euler solution with the experimental data.

In the experimantal data, there were no information on the suction side for M=0.7 and β=53° case. Again the results for M=0.7 and β=55° case does not agree with the available experimental results.

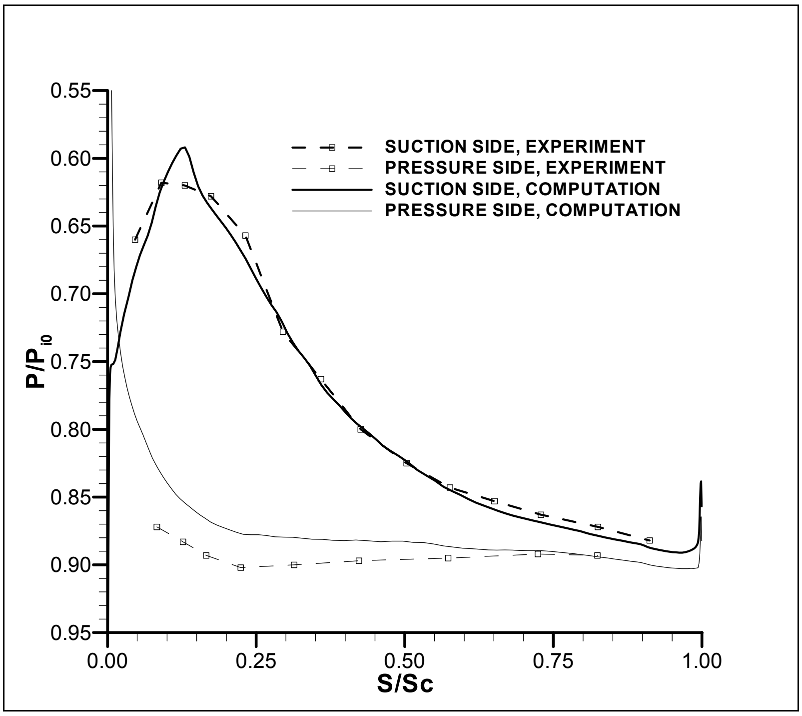

Fig. 4.15 H-O-H Grid comparison of surface pressures M=0.7 and β=49°

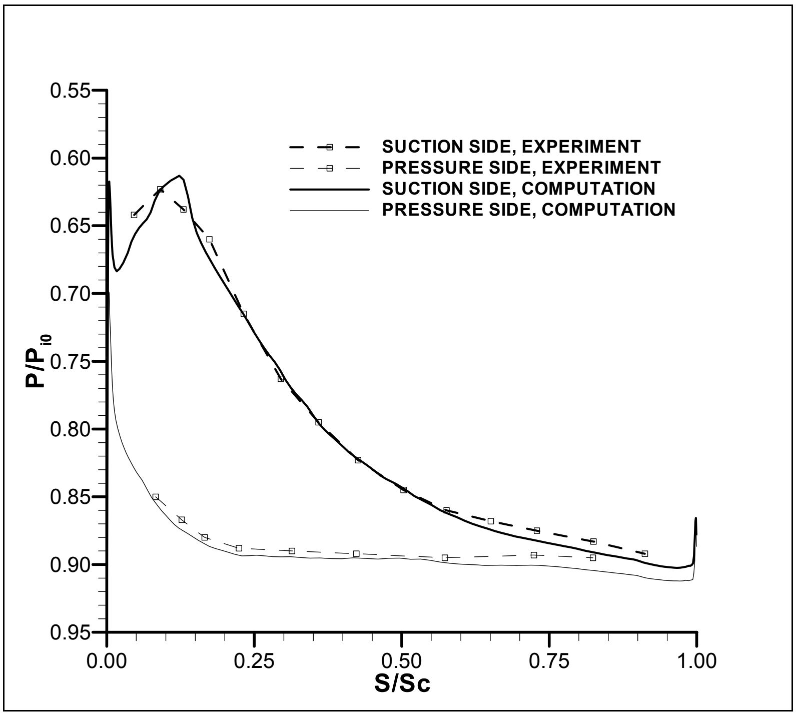

Fig. 4.16 Comparison of surface pressures M=0.7 and β=51°

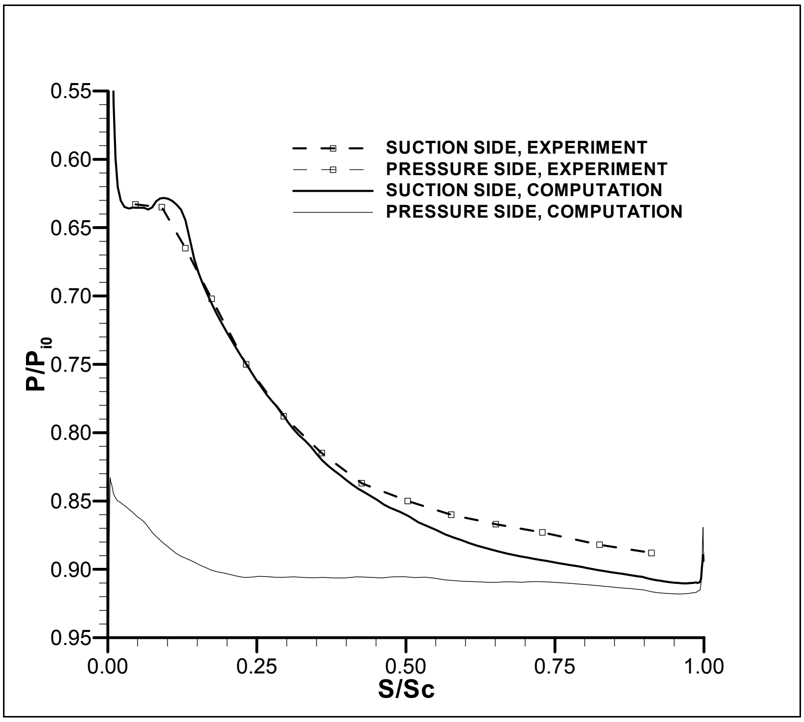

Fig. 4.17 Comparison of surface pressures M=0.7 and β =53°

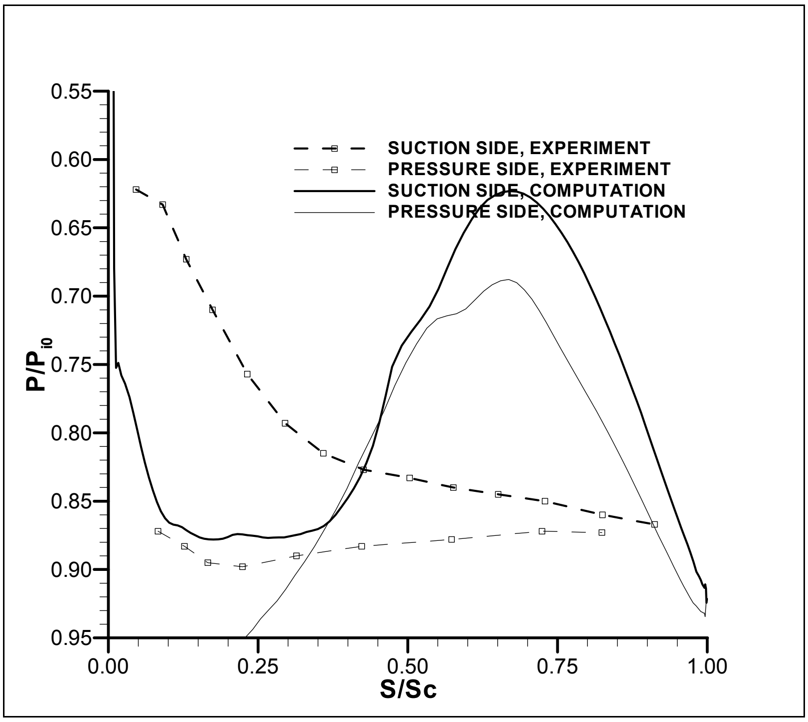

Fig. 4.18 Comparison of surface pressures M=0.7 and β =55°

Numerical results are compared with the experimental data in Figs. 4.15-4.18 and the agreement is found to be good excepting the results found for M=0.7 and β=55°. This is because the Euler solution does not converge for that large β angle. In the next sections Navier Stokes solution will be obtained for that β angle.

Results in the form of Mach number and Pressure Contours are also presented in the following figures (Figs. 4.19-4.24) for the converged Euler solutions. Note that M=0.7, β=55° test case pressure and Mach number contour results are not presented since there is no available converged Euler solution for that test case.

On the suction side of the cascade there are some bubbles with high velocity but the maximun velocity does not exceed speed of sound.

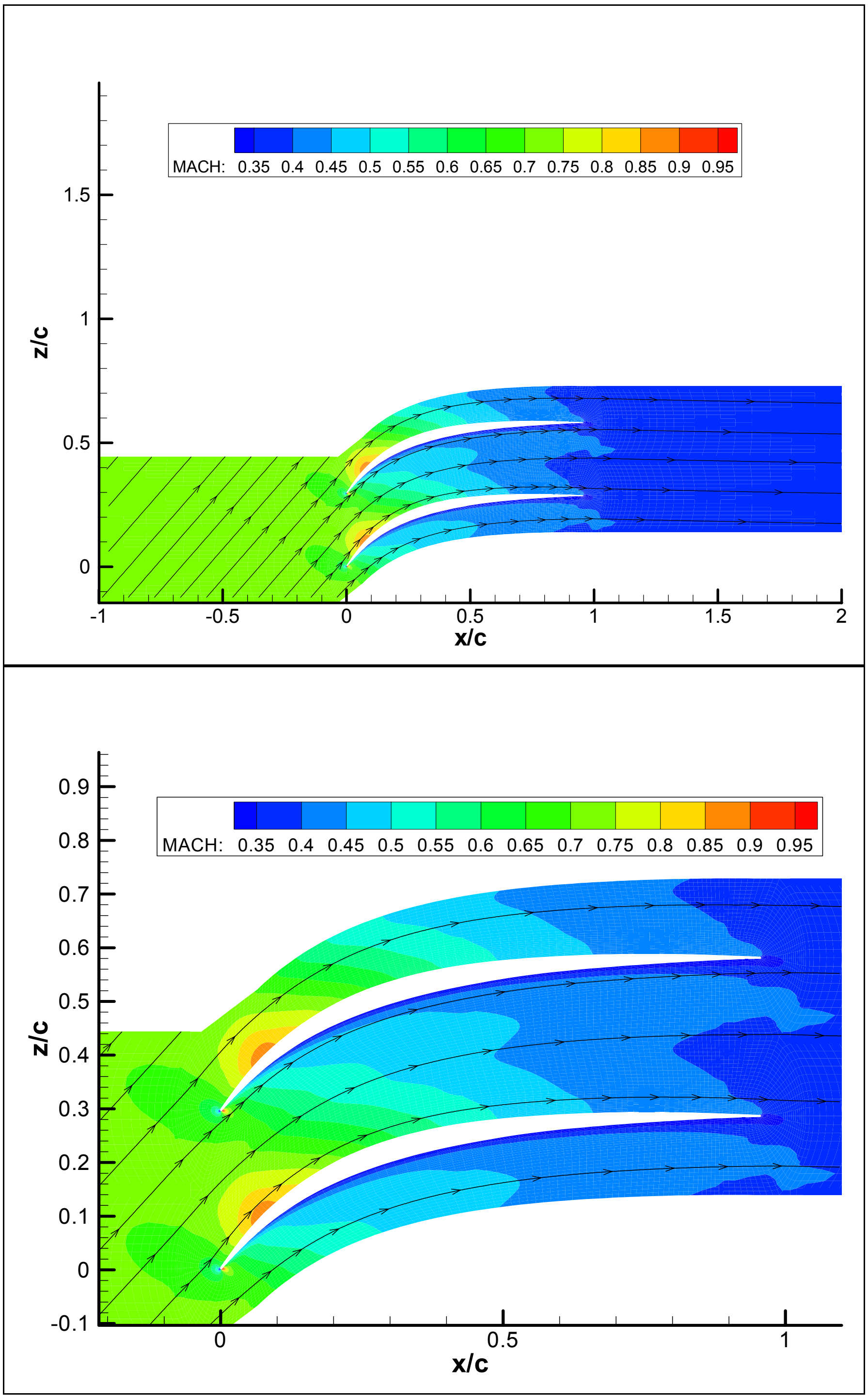

Fig. 4.19 Mach Contours obtained by using the H-O-H grid, M=0.7 and β=49°, Euler Solution. The lower figure is the enlarged view around the stator blades.

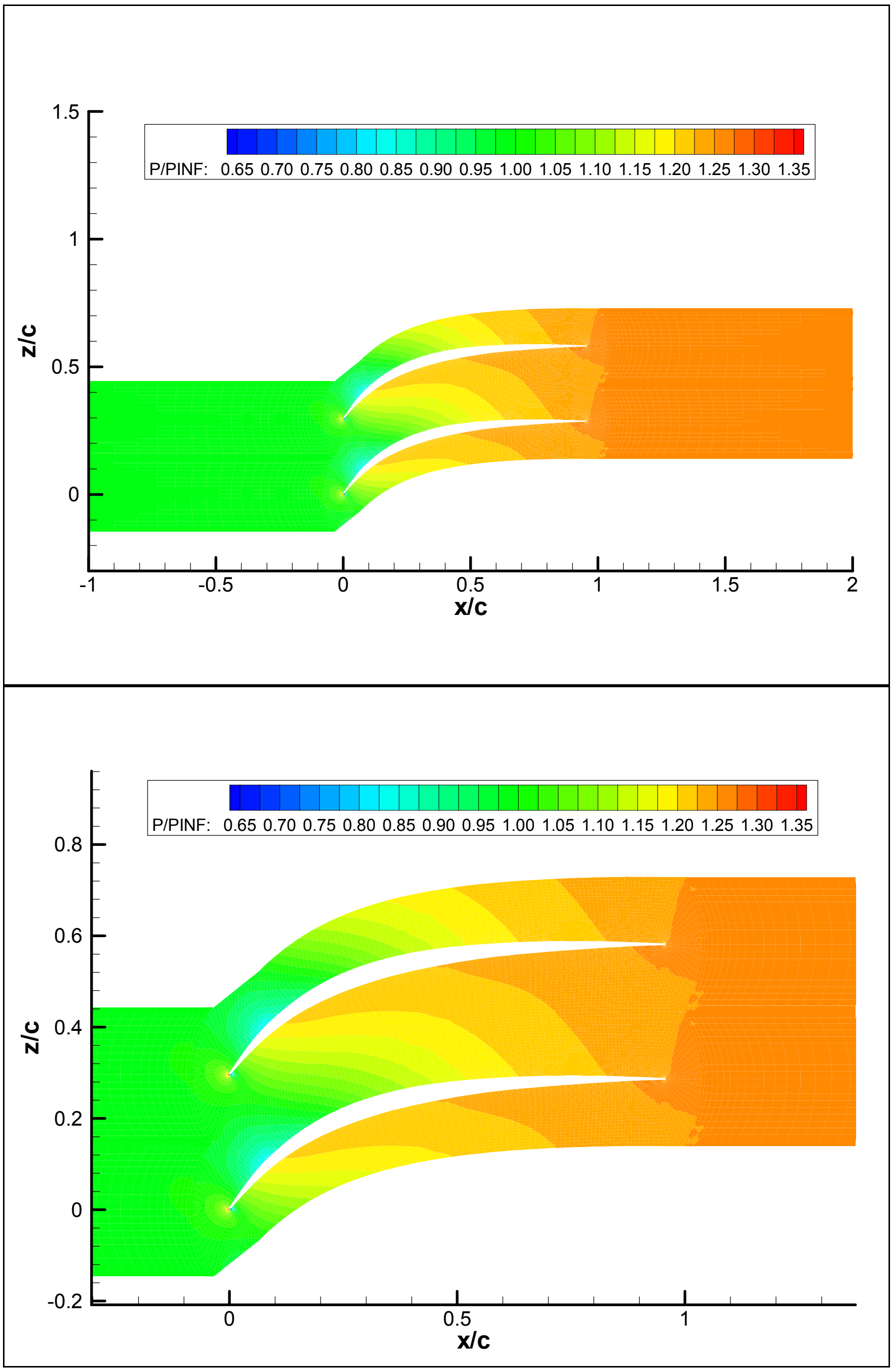

Fig. 4.20 Pressure Contours obtained by using the H-O-H grid, M=0.7 and β=49°, Euler Solution. The lower figure is the enlarged view around the stator blades.

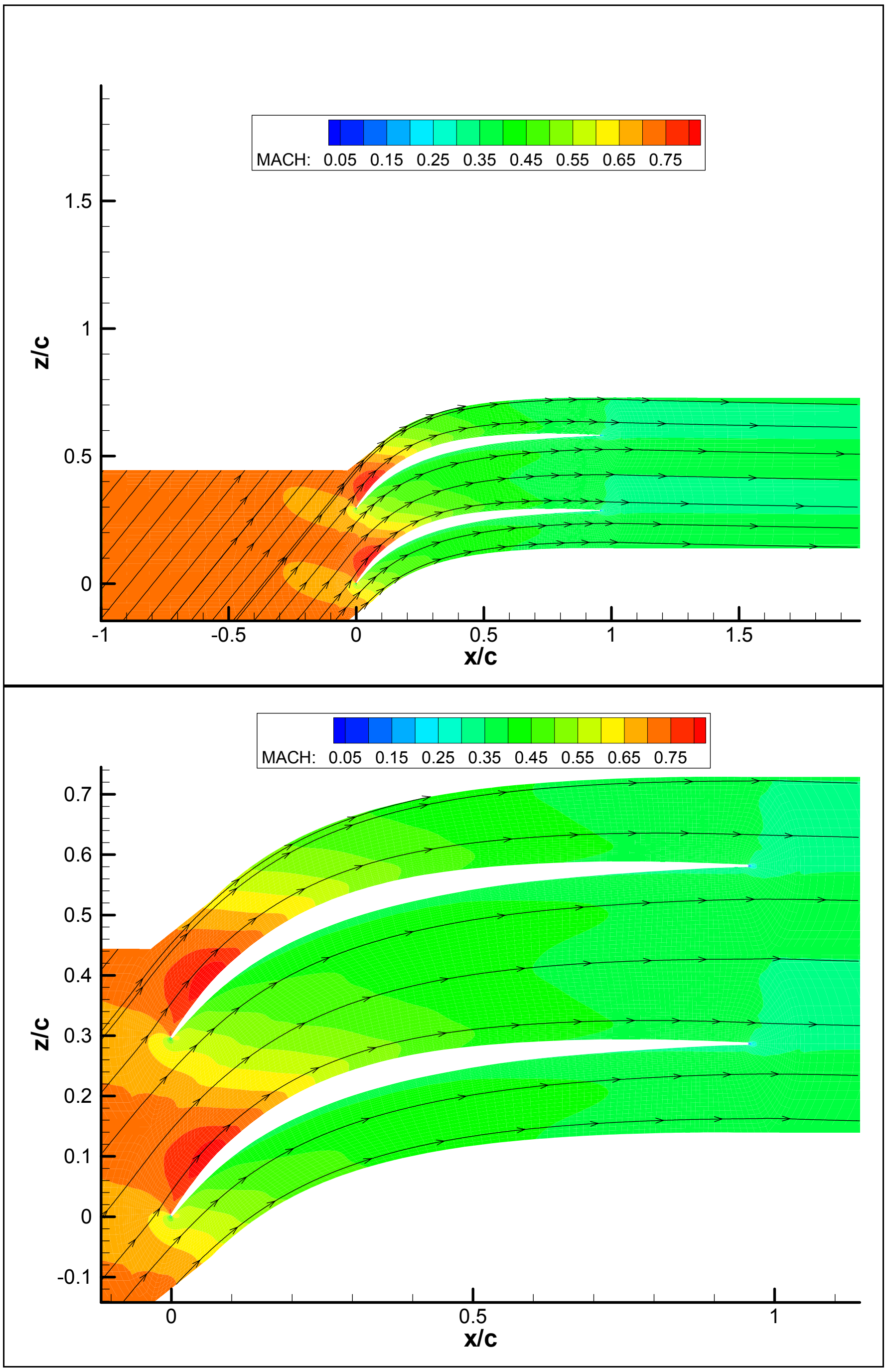

Fig. 4.21 Mach Contours obtained by using the H-O-H grid, M=0.7 and β=51°, Euler Solution. The lower figure is the enlarged view around the stator blades.

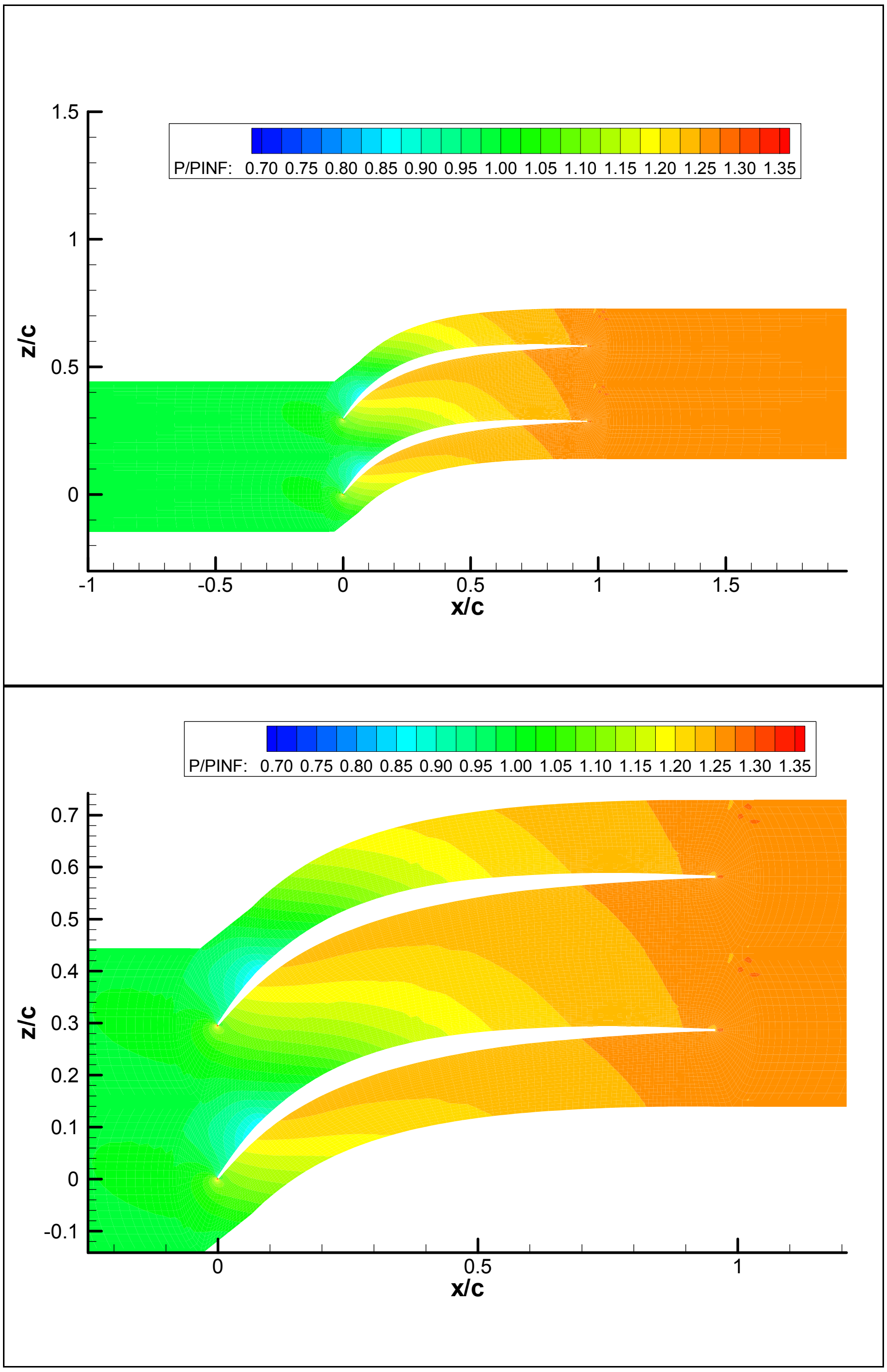

Fig. 4.22 Pressure Contours obtained by using the H-O-H grid, M=0.7 and β=51°, Euler Solution. The lower figure is the enlarged view around the stator blades.

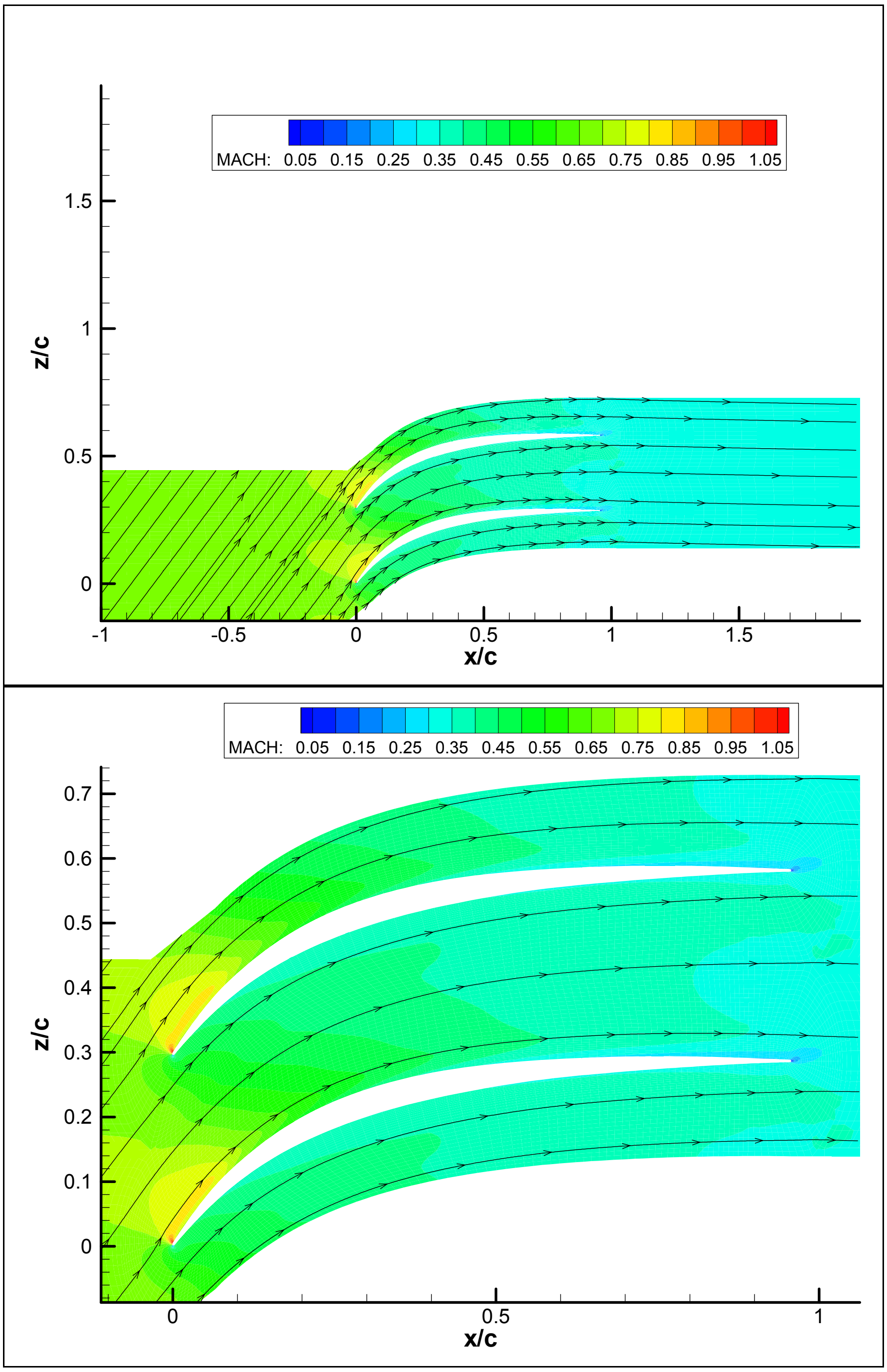

Fig. 4.23 Mach Contours obtained by using the H-O-H grid, M=0.7 and β=53°, Euler Solution. The lower figure is the enlarged view around the stator blades.

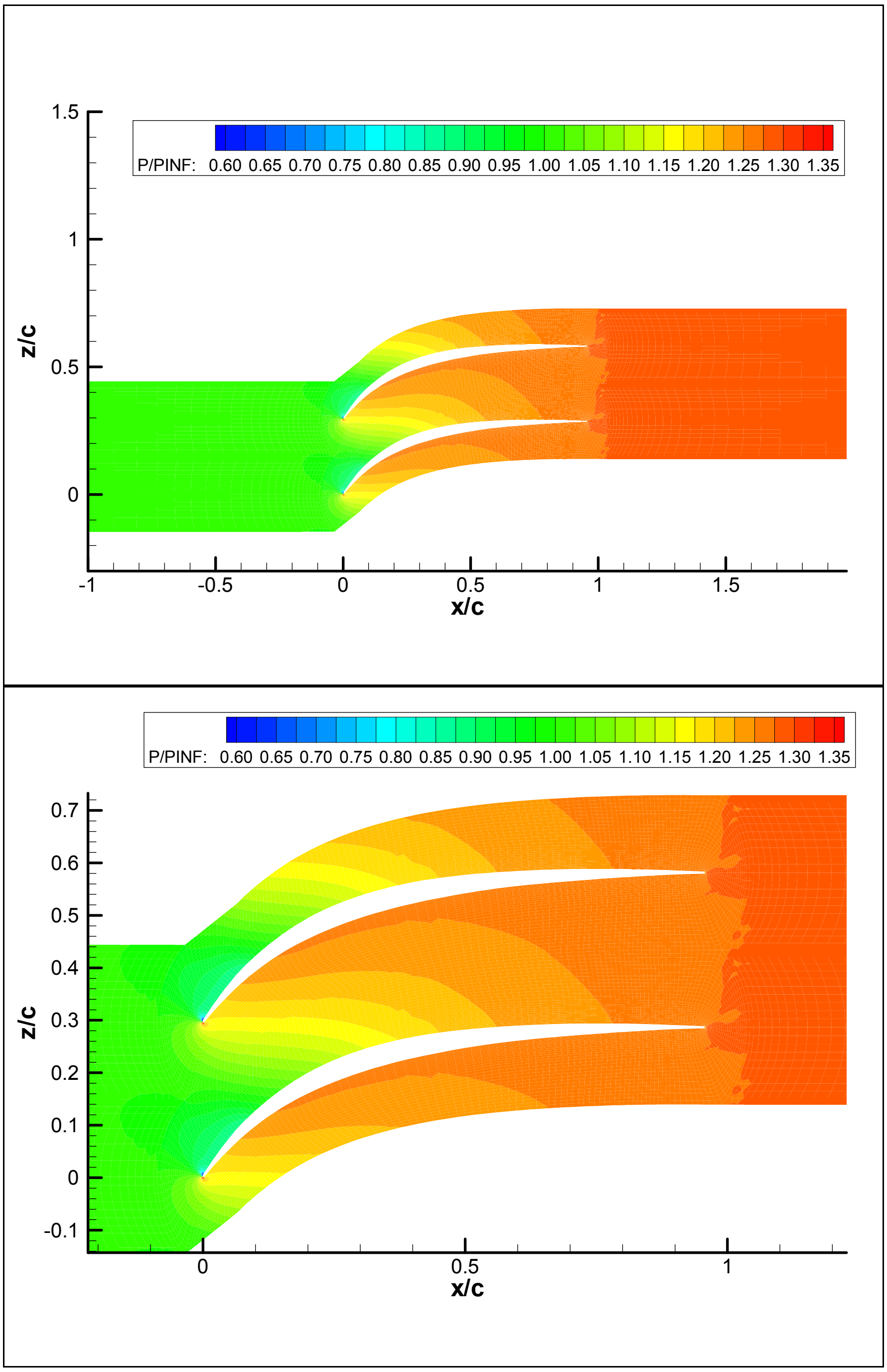

Fig. 4.24 Pressure Contours obtained by using the H-O-H grid, M=0.7 and β=53°, Euler Solution. The lower figure is the enlarged view around the stator blades.

4.2. Navier Stokes Solution with Uniform Inlet Velocity Profile:

4.2.1. Grid:

For the 2D Navier Stokes Solution of uniform inlet velocity profile H-O-H multi block type grid is modified. This grid is made of three blocks. The front block (Block 2), the center block (Block 1) and the rear block (Block 3). The center block is an O-type grid and its dimensions are 249*3*78 in ξ, η, and ζ directions (J,K,L). The normal distance between the surface and the first grid point above the surface is, $\Delta n / c = 0.00005$. L=1 corresponds to the airfoil surface. The front and rear block dimensions are 25*3*21 each in ξ, η, and ζ directions (J,K,L). The grid is shown in Figs. 4.25 and 4.26. The grid is nondimensionalized again with chord, *c*.

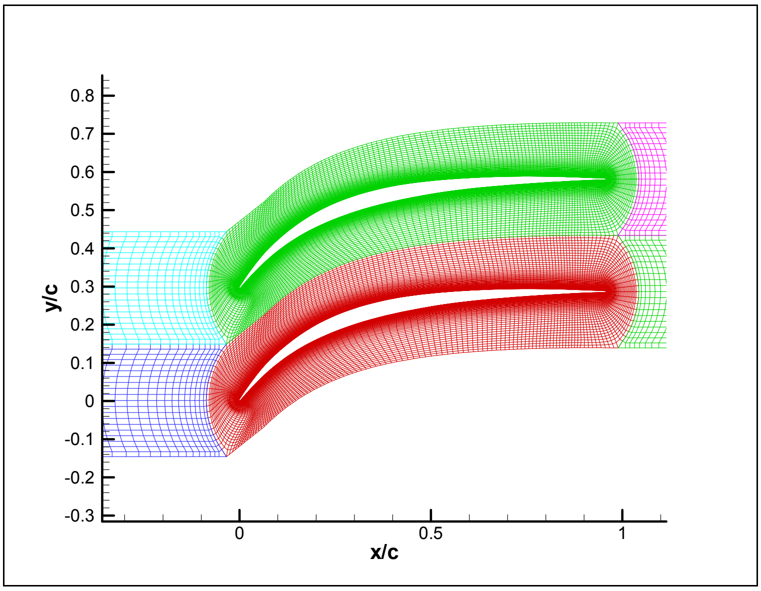

Fig. 4.25 H-O-H Grid, enlarged around the cascade

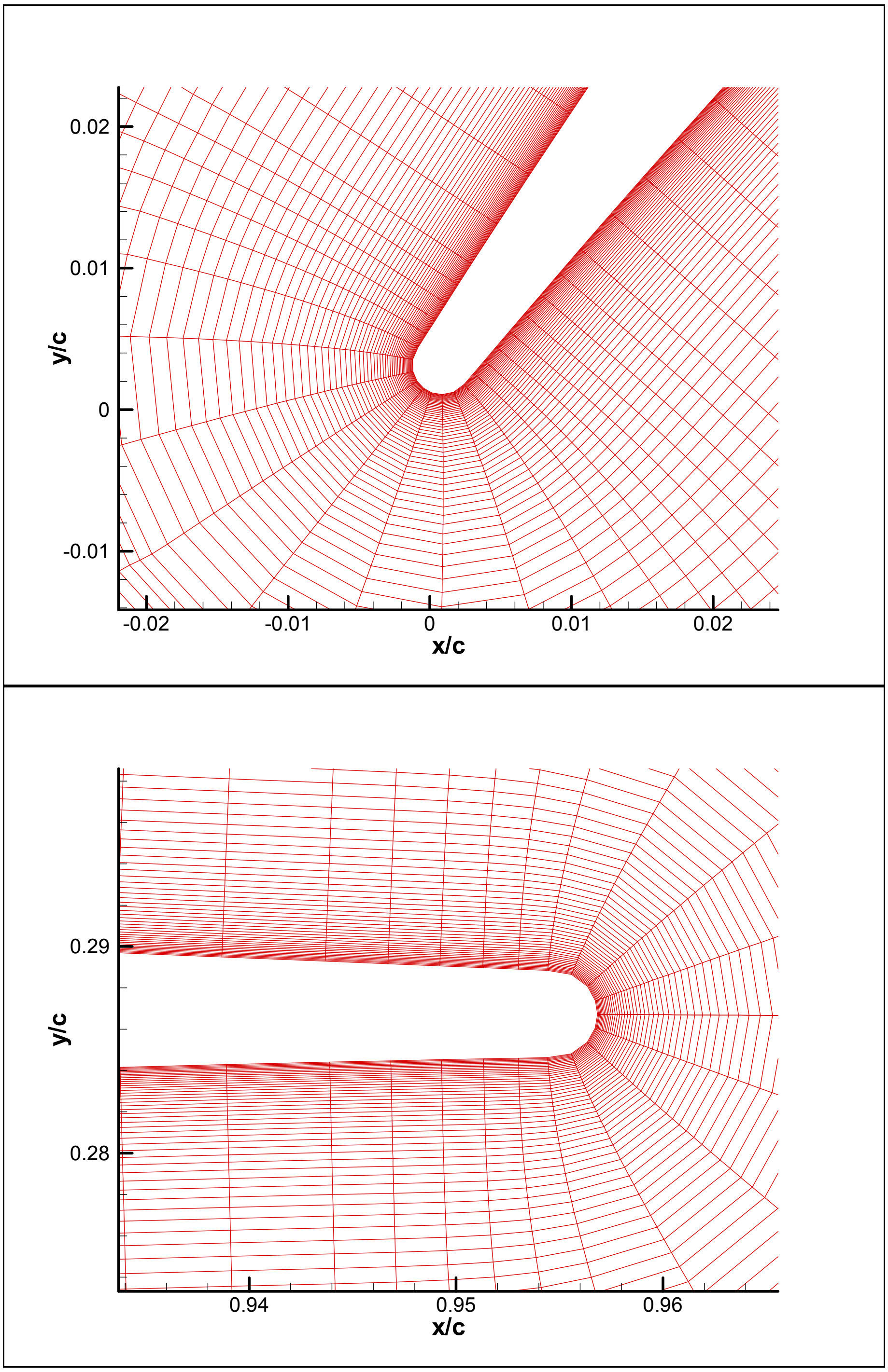

Fig. 4.26 Airfoil leading and trailing edge definition with the H-O-H grid

4.2.2. Boundary Conditions:

For the center O-Grid at L=LMAX top and Bottom surfaces are periodic. Matched Surface Boundary Conditions are applied at the common boundaries with the front and rear blocks. At L=1, the surface boundary conditions are applied. J=1 and J=JMAX boundaries coincides (the wake behind the T.E.) and the periodic boundary conditions are applied at those boundaries.

For the front grid at J=1 inflow (freestream) is specified. At J=JMAX Matched surface boundary conditions are applied with the central O-Block. L=1 (bottom surface) and L=LMAX (top surface) are periodic with each other.

For the rear grid at J=1 Matched surface boundary conditions are applied with the central O-Block. J=JMAX is the flow out plane pressure fixed extrapolation type boundary conditions are used. L=1 (bottom surface) and L=LMAX (top surface) are periodic with each other. Further explanations are available in Appendix A.

4.2.2.1. Calculation of exit to inlet static pressure ratio:

In Fig. 4.10 the geometry of the flow domain was described. For the J=JMAX flow out plane pressure fixed extrapolation type boundary condition, following procedure has been employed for calculation of exit to inlet static pressure ratio of the Navier Stokes solution.

1st Method:

This method is exactly the same as the method described in Section 4.1.3.3. For M=0.7 and β=49° $\frac{P_2}{P_1}$ has previously calculated as 1.257.

2nd Method:

Using **P2P1NS.for** program with the following inputs the program gives the proper outputs:

$$A_1^* = 0.2947 \qquad (4.2.1)$$

$$\theta = 49° \qquad (4.2.2)$$

$$M_1 = 0.7 \qquad (4.2.3)$$

$$\frac{P_{02}}{P_{01}} = 0.993 \qquad (4.2.4)$$

In this program following equations are used to evaluate the pressure ratio:

$$A_1 = A_1^{'} \cos\theta \qquad (4.2.5)$$

$$A_2 = A_1^{'} \qquad (4.2.6)$$

$$\frac{P_{01}}{P_1}=\left(1+\frac{\gamma-1}{2}M_1^{\ 2}\right)^{\frac{\gamma}{\gamma-1}} \tag{4.2.7}$$

$$\left(\frac{A_1}{A_1^{\ *}}\right)^2=\frac{1}{M_1^{\ 2}}\left[\frac{2}{\gamma+1}\left(1+\frac{\gamma-1}{2}M_1^{\ 2}\right)\right]^{\frac{\gamma+1}{\gamma-1}} \tag{4.2.8}$$

from Equaiton (4.2.8) $A_1^{\ *}$ is evaluated

$\frac{A_2^{\ *}}{A_1^{\ *}}=\frac{P_{01}}{P_{02}}$ then $A_2^{\ *}$ is obtained.

Since we know the LHS of the following equaion we can evaluate M_2

$$\left(\frac{A_2}{A_2^{\ *}}\right)^2=\frac{1}{M_2^{\ 2}}\left[\frac{2}{\gamma+1}\left(1+\frac{\gamma-1}{2}M_2^{\ 2}\right)\right]^{\frac{\gamma+1}{\gamma-1}} \tag{4.2.9}$$

and the ratio of P_{02}/P_2 is obtained:

$$\frac{P_{02}}{P_2}=\left(1+\frac{\gamma-1}{2}M_2^{\ 2}\right)^{\frac{\gamma}{\gamma-1}} \tag{4.2.10}$$

As a result pressure ratio is calculated:

$$\frac{P_2}{P_1}=\frac{P_2}{P_{02}}*\frac{P_{02}}{P_{01}}*\frac{P_{01}}{P_1} \tag{4.2.11}$$

and these steps in the program gives the following outputs:

$M_2 = 0.3803$,

$\frac{P_{02}}{P_2} = 1.1051$, $\frac{P_2}{P_1} = 1.246$

<u>3rd Method :</u>

The third method is the trial and error method. After a certain number of iterations P_2 / P_1 ratio is adjusted so that at the mid parts of Block 2 (front block) the P_2 / P_1 ratio is approximately equal to 1. The final P_2 / P_1 ratios for different β angles are presented in Table 4.2.

More detailed information about the CPU time and P_2 / P_1 values employed in the analysis can be found in Appendix C.

Table 4.2 Exit to inlet static pressure ratios for Navier Stokes solution

Mach number	β angle	$\frac{P_2}{P_1}$
0.7	49°	1.255
0.7	51°	1.260
0.7	53°	1.260
0.7	55°	1.251

4.2.3. Results:

In this section convergence of the L2 norm of the residuals of the H-O-H grid, M=0.7 and β=49°, 51°, 53°, 55° are presented in Figs. 4.27 and 4.30 initially for comparison.

For Navier Stokes solution Block-1 L2 norm converged about 7 orders in 100000 iterations of H-O-H grid, M=0.7 and β=49°.

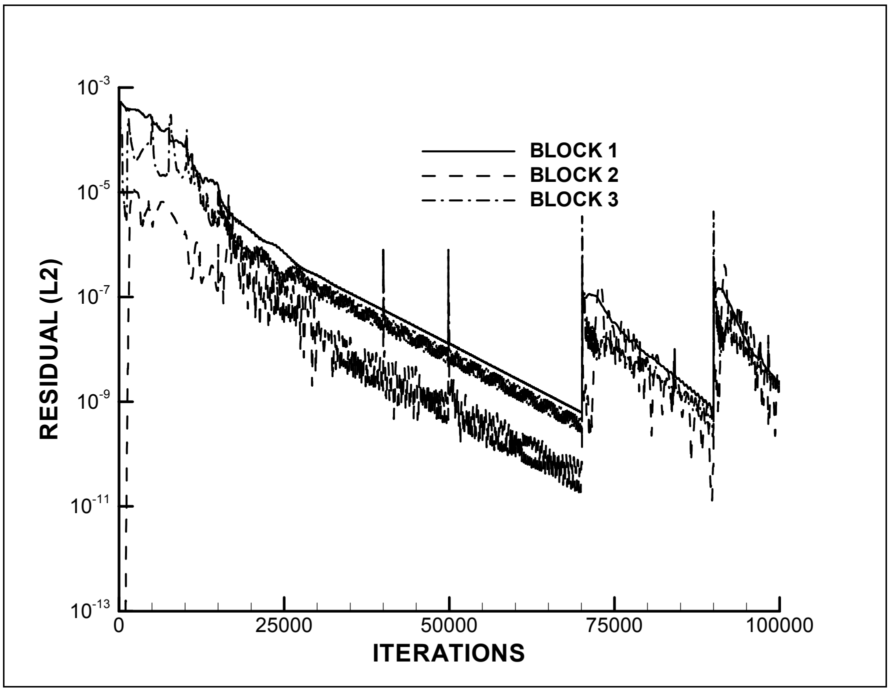

Fig. 4.27 N-S Solution convergence history for M=0.7 and β=49°

From Fig. 4.27 it can be seen that after iterations 70000 and 90000 there are jumps on the residuals. This is because after 70000 and 90000 iterations P_2/P_1 ratio is changed to a larger value in order to get P/P_1 value close to the 1.0 at the inlet region (mid parts of front block).

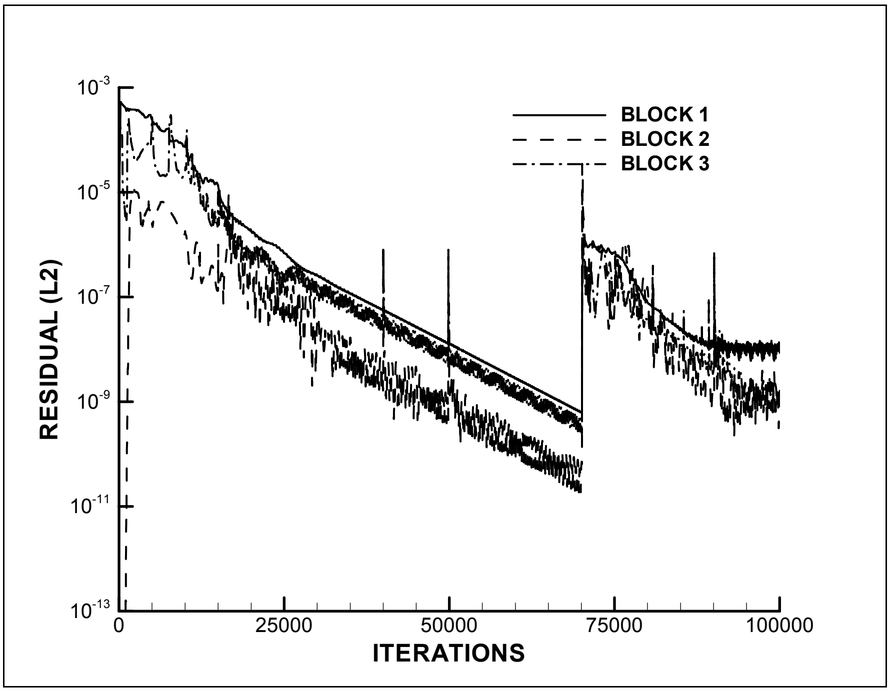

Fig. 4.28 N-S Solution convergence history for M=0.7 and β=51°

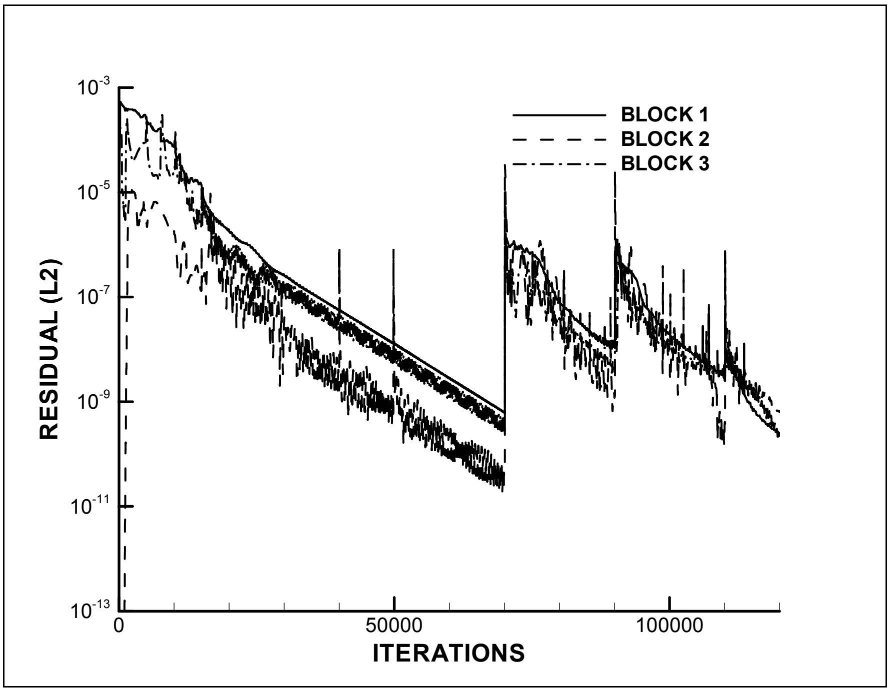

Fig. 4.29 N-S Solution convergence history for M=0.7 and β=53°

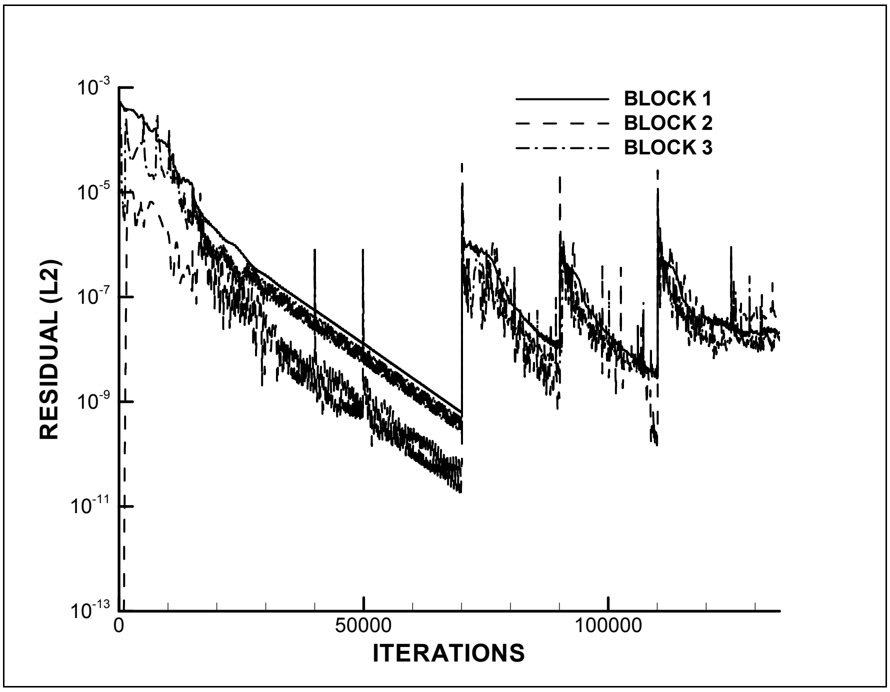

Fig. 4.30 N-S Solution convergence history for M=0.7 and β=55°

Convergence of the L2 norm of the residuals are given in Fig. 4.28 for β=51° for blocks 1 (central), 2 (front) and 3 (rear). For Block-1 L2 norm has converged about 6 orders in 100000 iterations. Except for the results of M=0.7 and β=49°, all runs initiated with the previous runs such as in M=0.7 and β=51° solution first 70000 iterations taken from M=0.7 and β=49° solution. Similarly for the M=0.7 and β=53° solution, first 90000 iterations comes from the solution for M=0.7 and β=51°. This is the other reason for the jumps in the convergence histories. Some small jumps also occur in the figures due to the CNBR changes which are also presented in Appendix C.

Again in Fig. 4.29 convergence history of M=0.7 and β=53° test case is presented. For Block-1 L2 norm has converged about 7 orders in 120000 iterations at the end.

Convergence of the L2 norm of the residuals are given in Fig. 4.30 for M=0.7 and β=53° for blocks 1 (central), 2 (front) and 3 (rear). For Block-1 L2 norm converged about 6 orders in 135000 iterations.

The same post-processing program **postp2ds.for** employed to prepare the plot file **tec2ds.dat** for plotting the selected variables along the selected two dimensional streamlines or surfaces.

Following figures represents the results from the comparison of surface pressures with Euler and Navier Stokes solution with the experimental data.

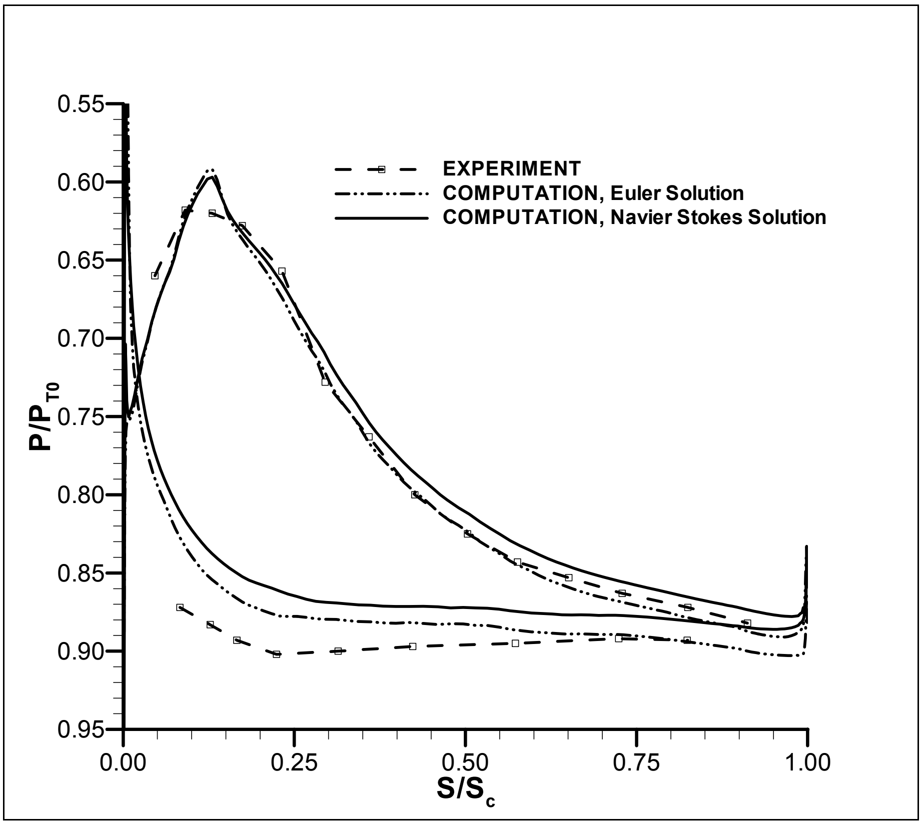

Fig. 4.31 N-S and Euler Solution comparison of surface pressures for M=0.7 and β=49°

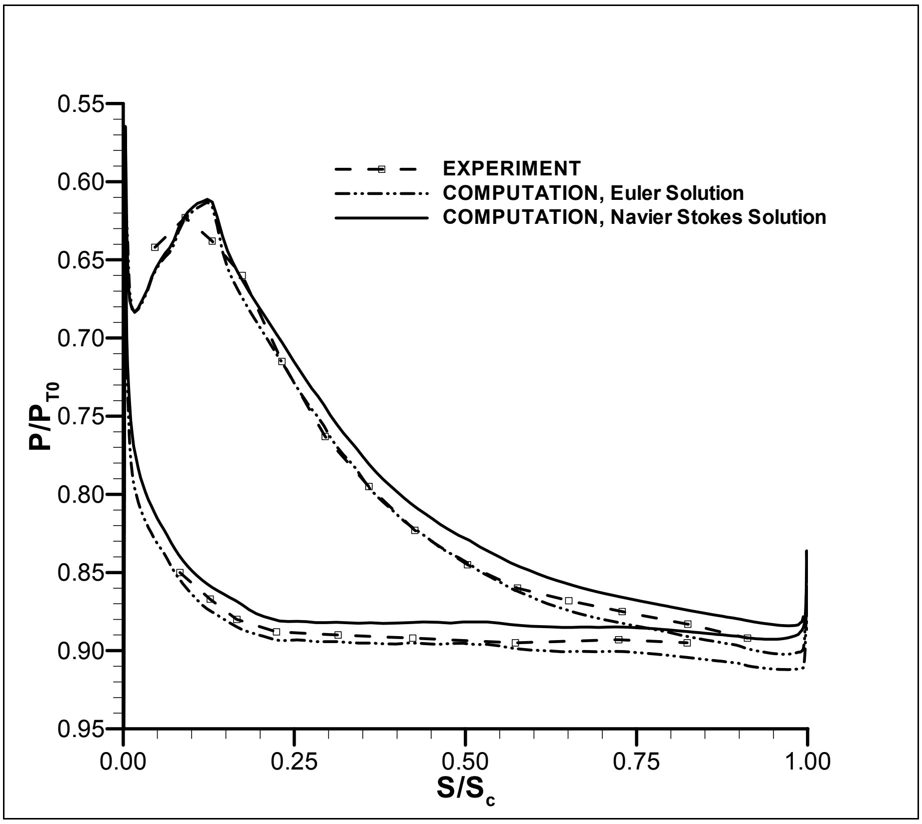

Fig. 4.32 N-S and Euler Solution comparison of surface pressures for M=0.7 and β=51°

Figs. 4.31 and 4.32 show that Euler and Navier Stokes solutions have good agreement with the experimental data. The reader should remember that there can be also a 0.3% change in the experimental data as mentioned in Chapter 3.

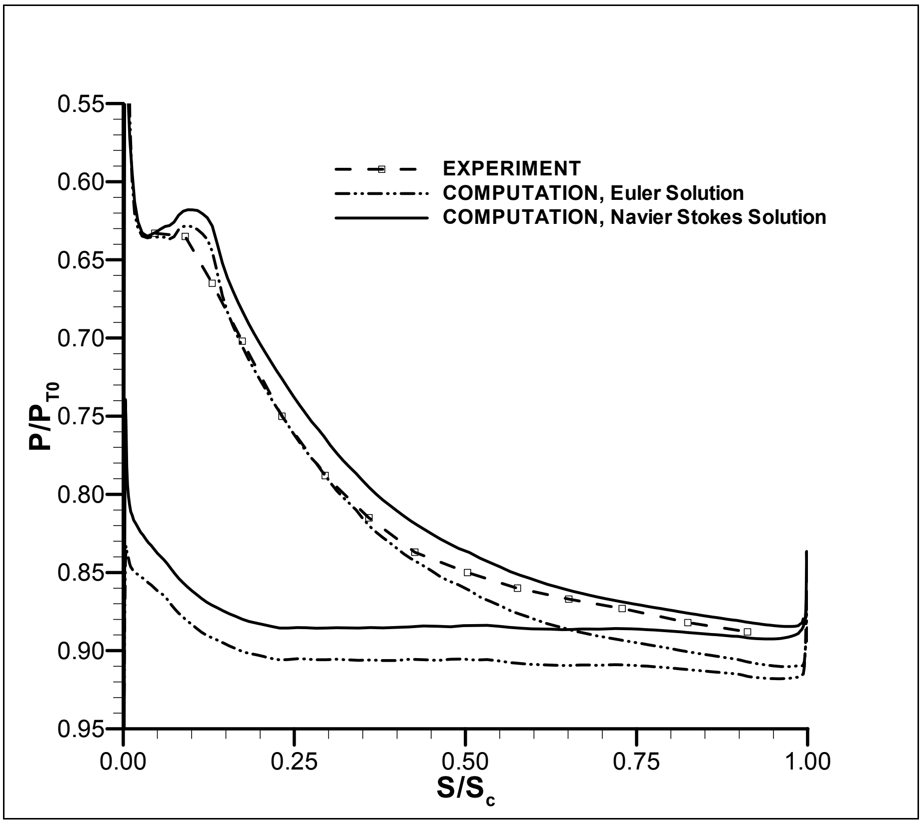

Fig. 4.33 N-S and Euler Solution comparison of surface pressures for M=0.7 and β=53°

In Fig. 4.34 the reader should notice that there is no available experimental data on the pressure side for M=0.7 and β=53°.

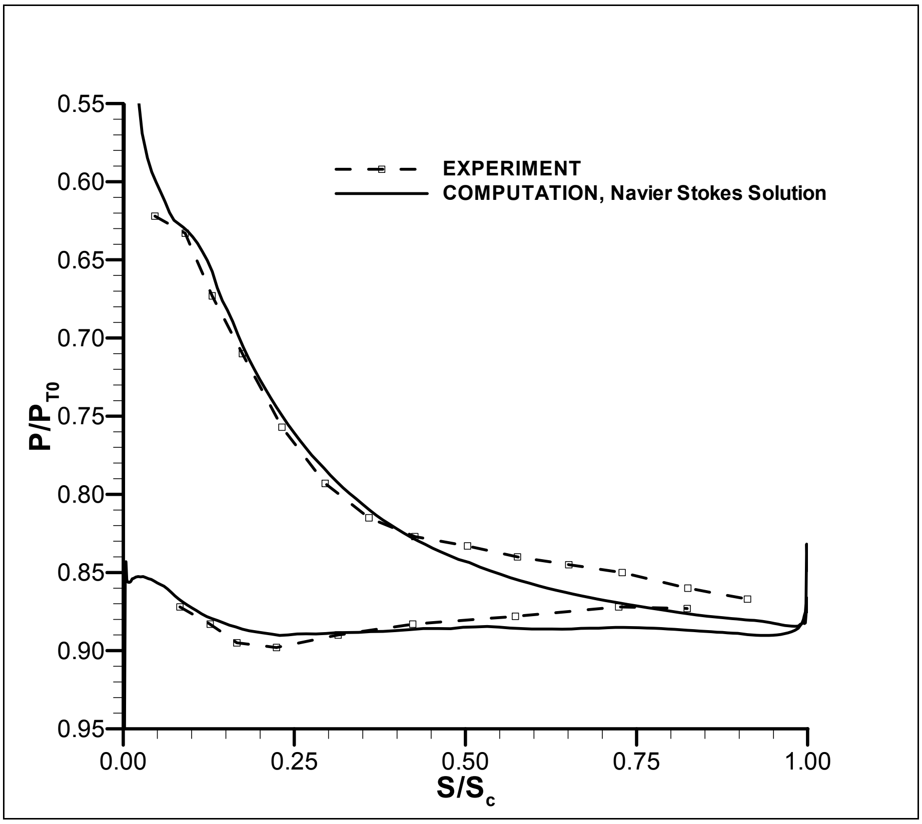

Fig. 4.34 N-S comparison of surface pressures for M=0.7 and β =55°

Figs. 4.33 and 4.34 show that Navier Stokes solutions have better agreement with the experimental data. It is obvious that Euler solution fails for β=55° angle. Navier Stokes gives better results for higher angles.

Results in the form of Mach number and Pressure Contours are presented in the following figures (Figs. 4.35-4.42) for the converged Navier Stokes solutions.

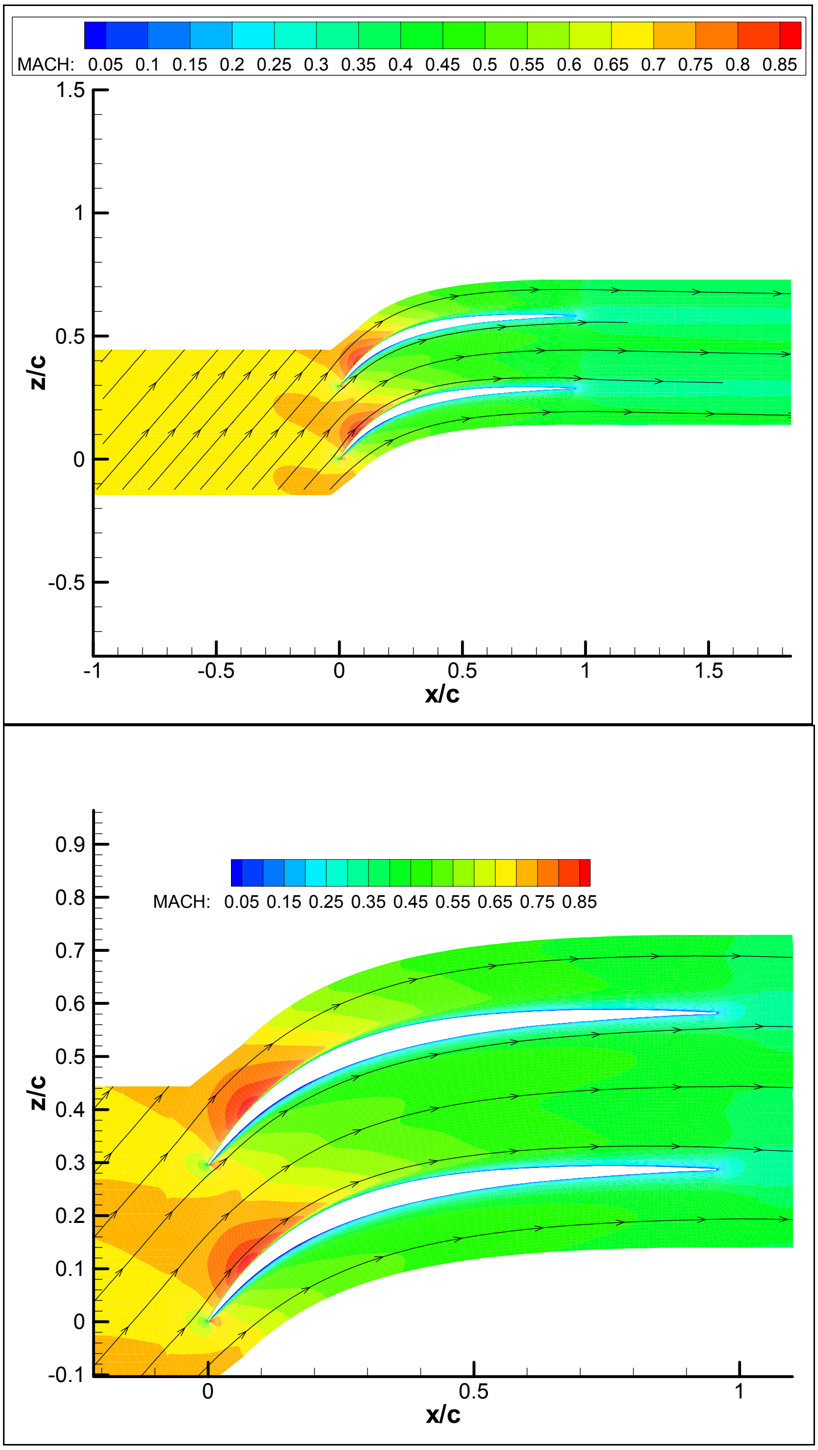

Fig. 4.35 Mach Contours obtained by using the H-O-H grid, M=0.7 and β=49°, N-S Solution. The lower figure is the enlarged view around the stator blades.

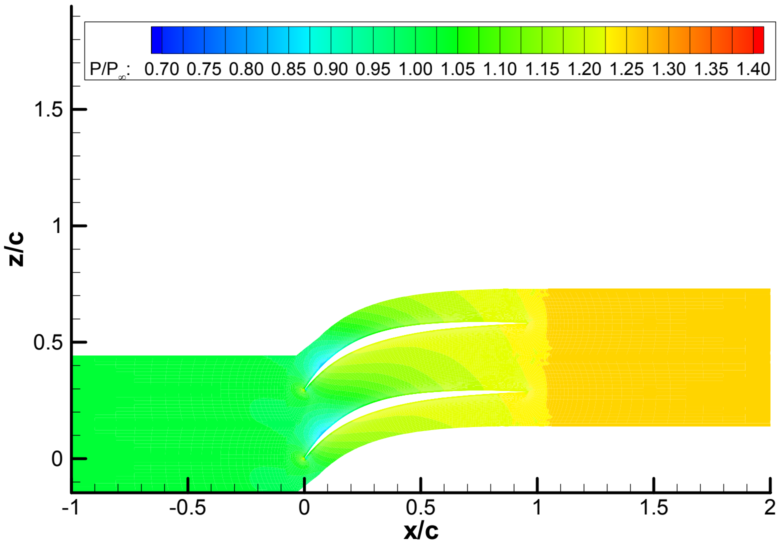

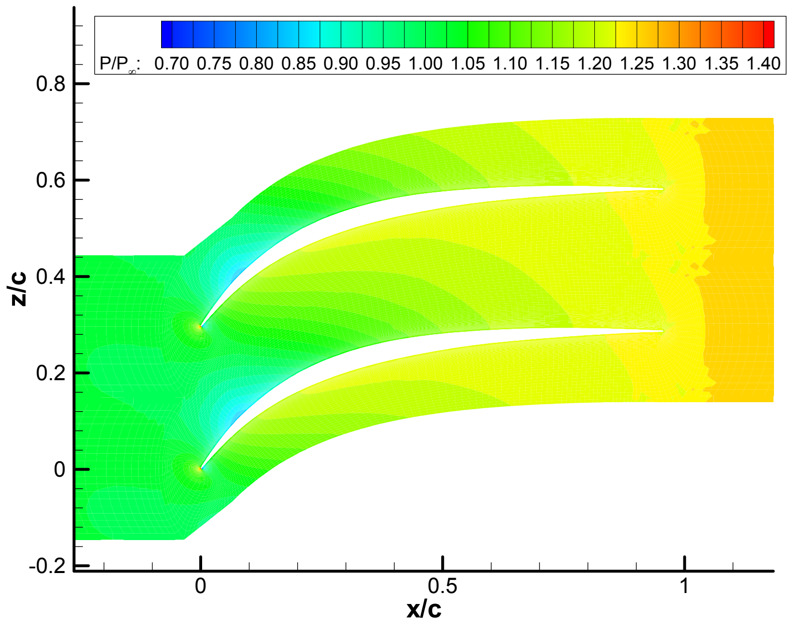

Fig. 4.36 Pressure Contours obtained by using the H-O-H grid, M=0.7 and β=49°, N-S Solution. The lower figure is the enlarged view around the stator blades.

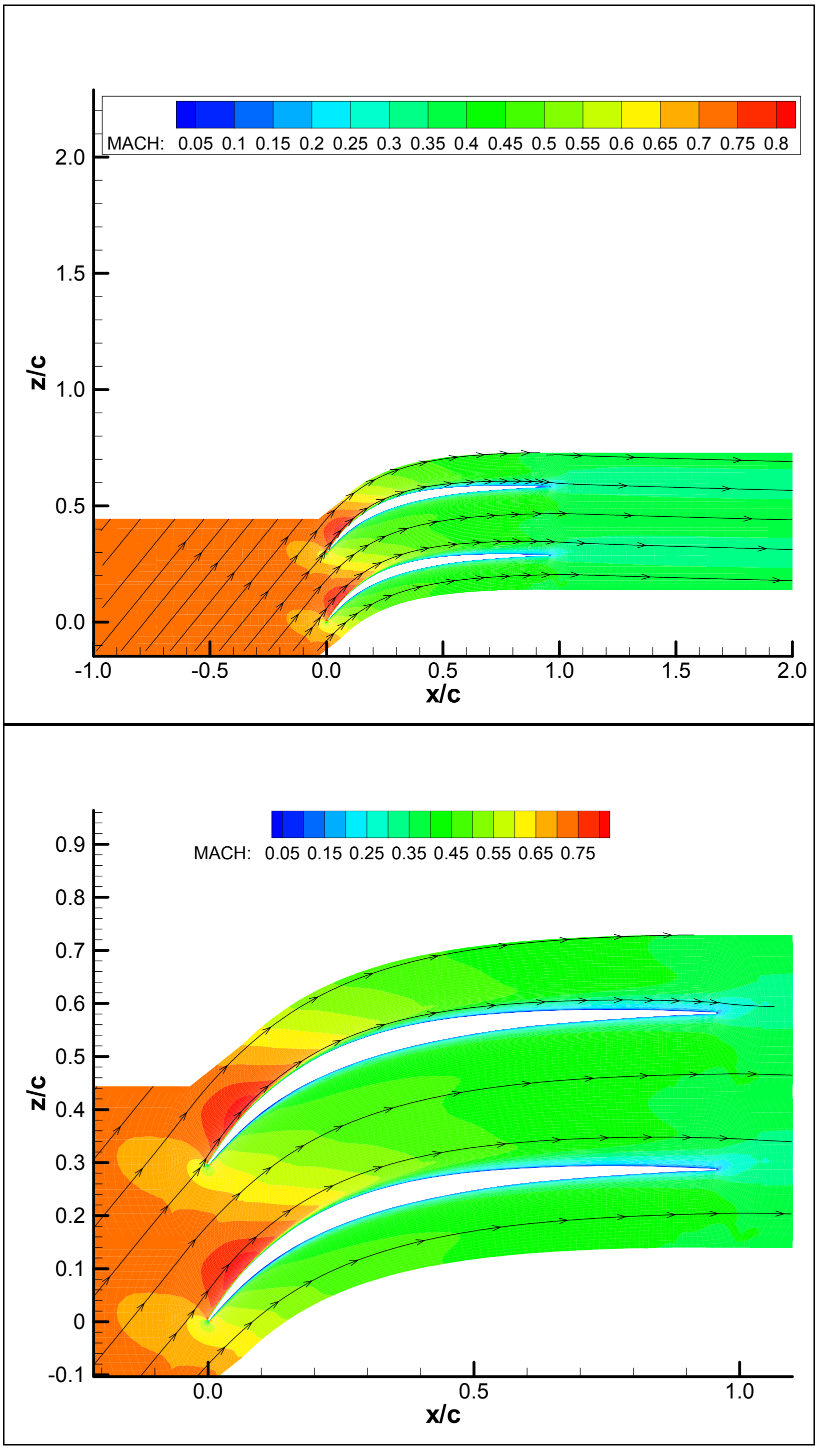

Fig. 4.37 Mach Contours obtained by using the H-O-H grid, M=0.7 and β=51°, N-S Solution. The lower figure is the enlarged view around the stator blades.

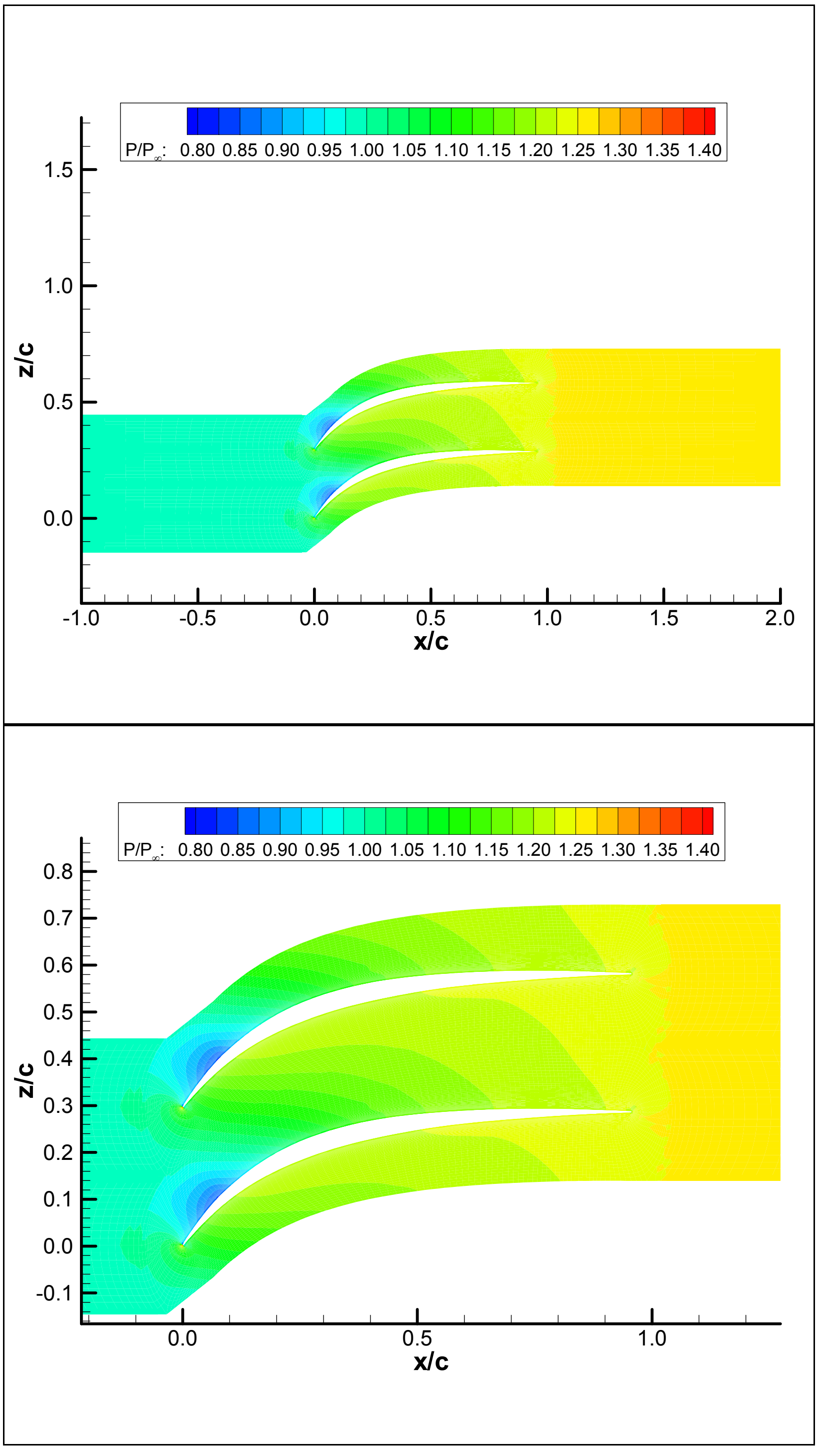

Fig. 4.38 Pressure Contours obtained by using the H-O-H grid, M=0.7 and β=51°, N-S Solution. The lower figure is the enlarged view around the stator blades.

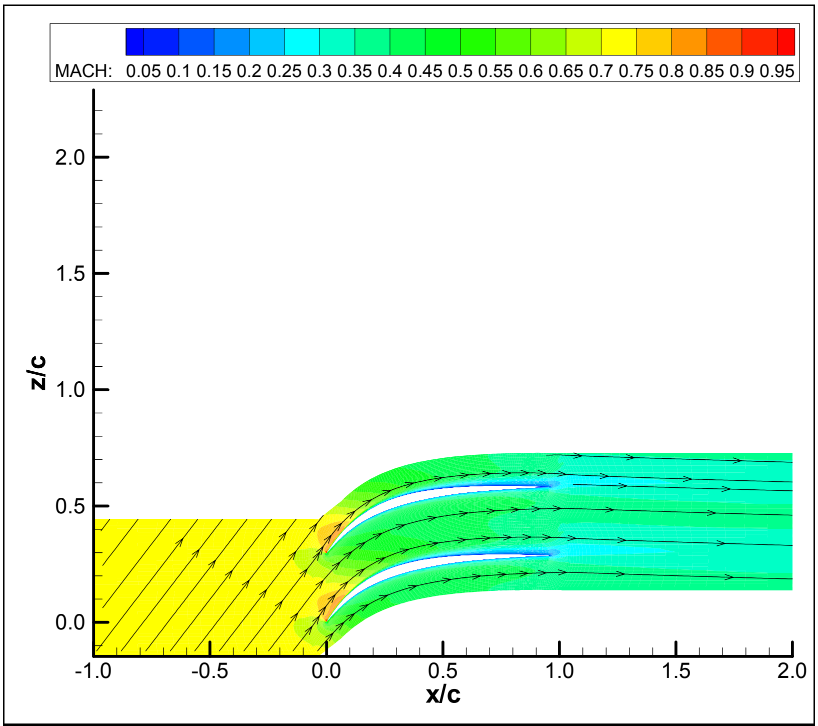

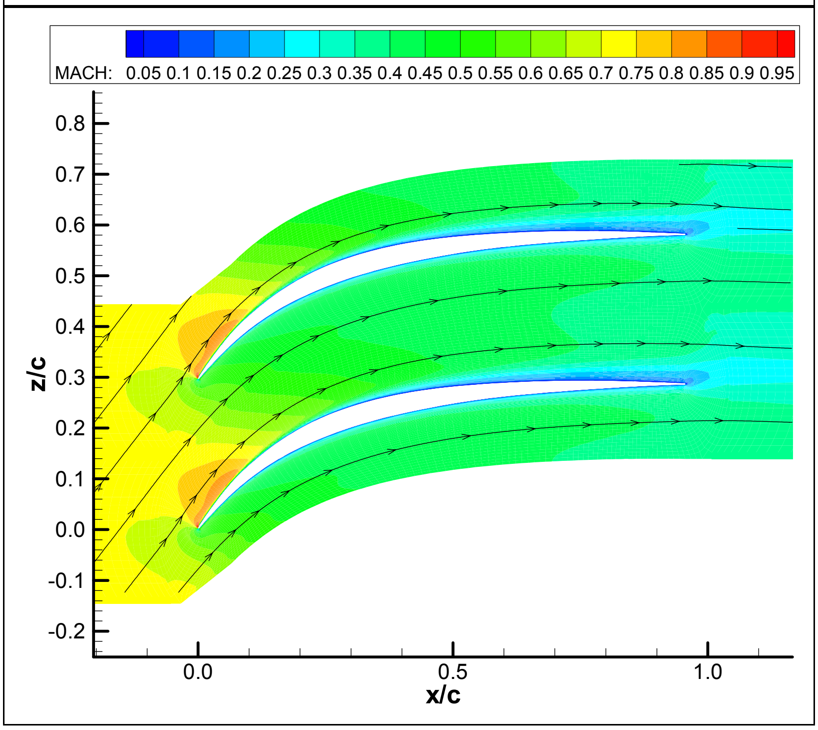

Fig. 4.39 Mach Contours obtained by using the H-O-H grid, M=0.7 and β=53°, N-S Solution. The lower figure is the enlarged view around the stator blades.

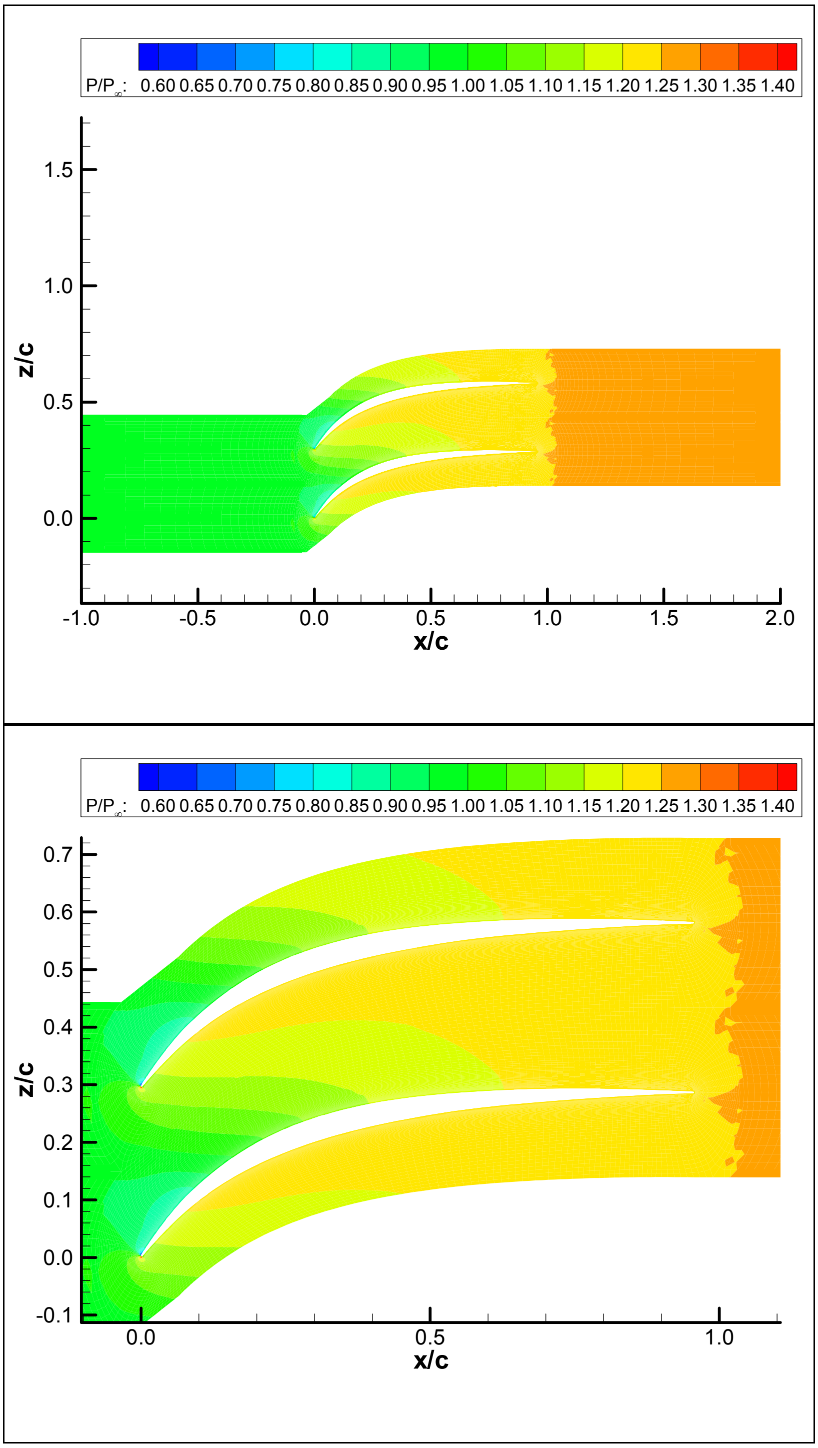

Fig. 4.40 Pressure Contours obtained by using the H-O-H grid, M=0.7 and β=53°, N-S Solution. The lower figure is the enlarged view around the stator blades.

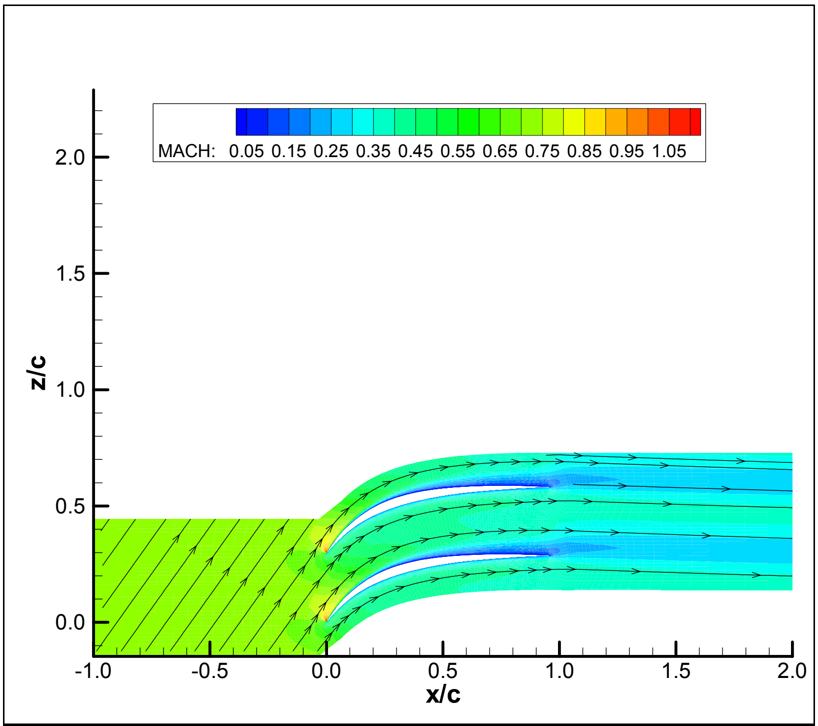

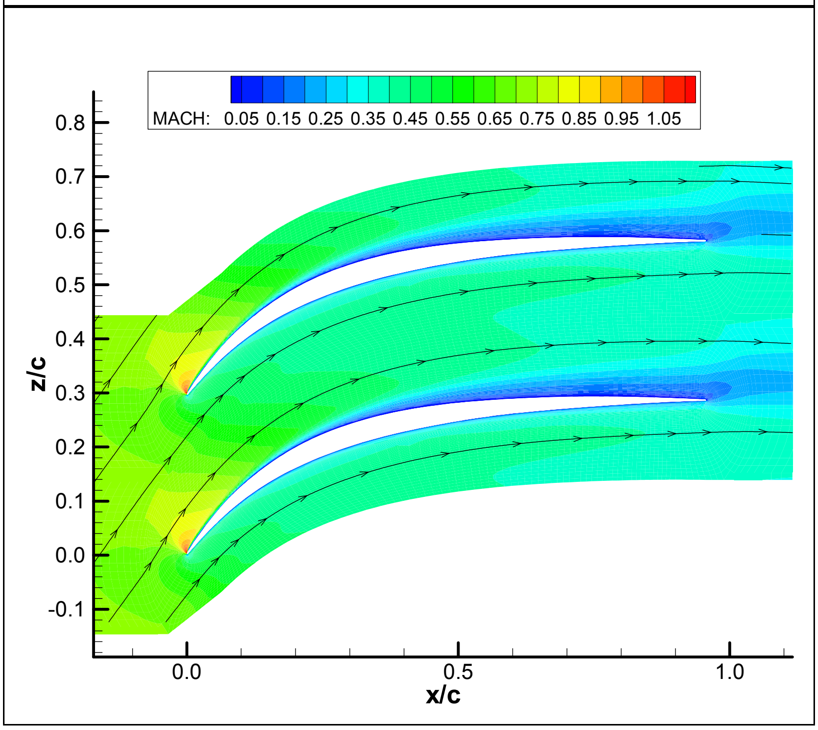

Fig. 4.41 Mach Contours obtained by using the H-O-H grid, M=0.7 and β=55°, N-S Solution. The lower figure is the enlarged view around the stator blades.

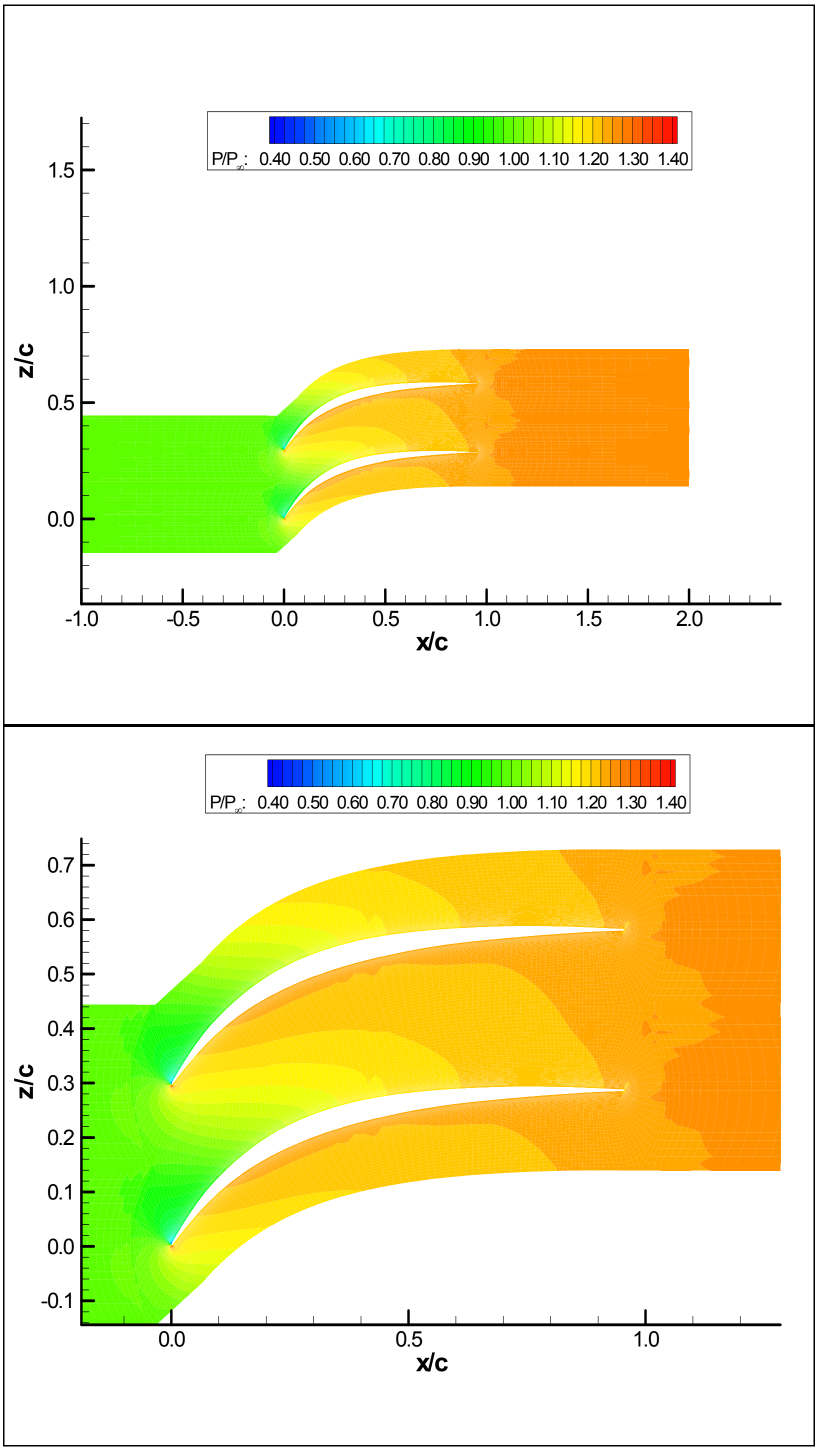

Fig. 4.42 Pressure Contours obtained by using the H-O-H grid, M=0.7 and β=55°, N-S Solution. The lower figure is the enlarged view around the stator blades.

In the following figures boundary layer comparisons of Navier Stokes solutions with the experimental data are presented. In order to obtain the boundary layer parameters **postbl2.for** post processing program is employed.

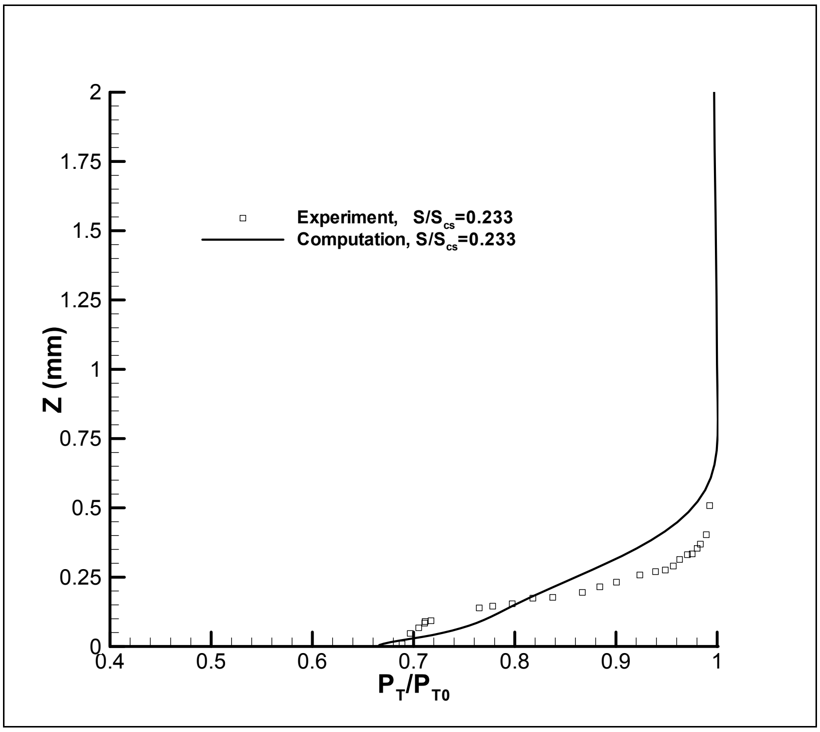

Fig. 4.43 Boundary Layer total pressure profile comparison for M=0.7 and β=49° (Station 1)

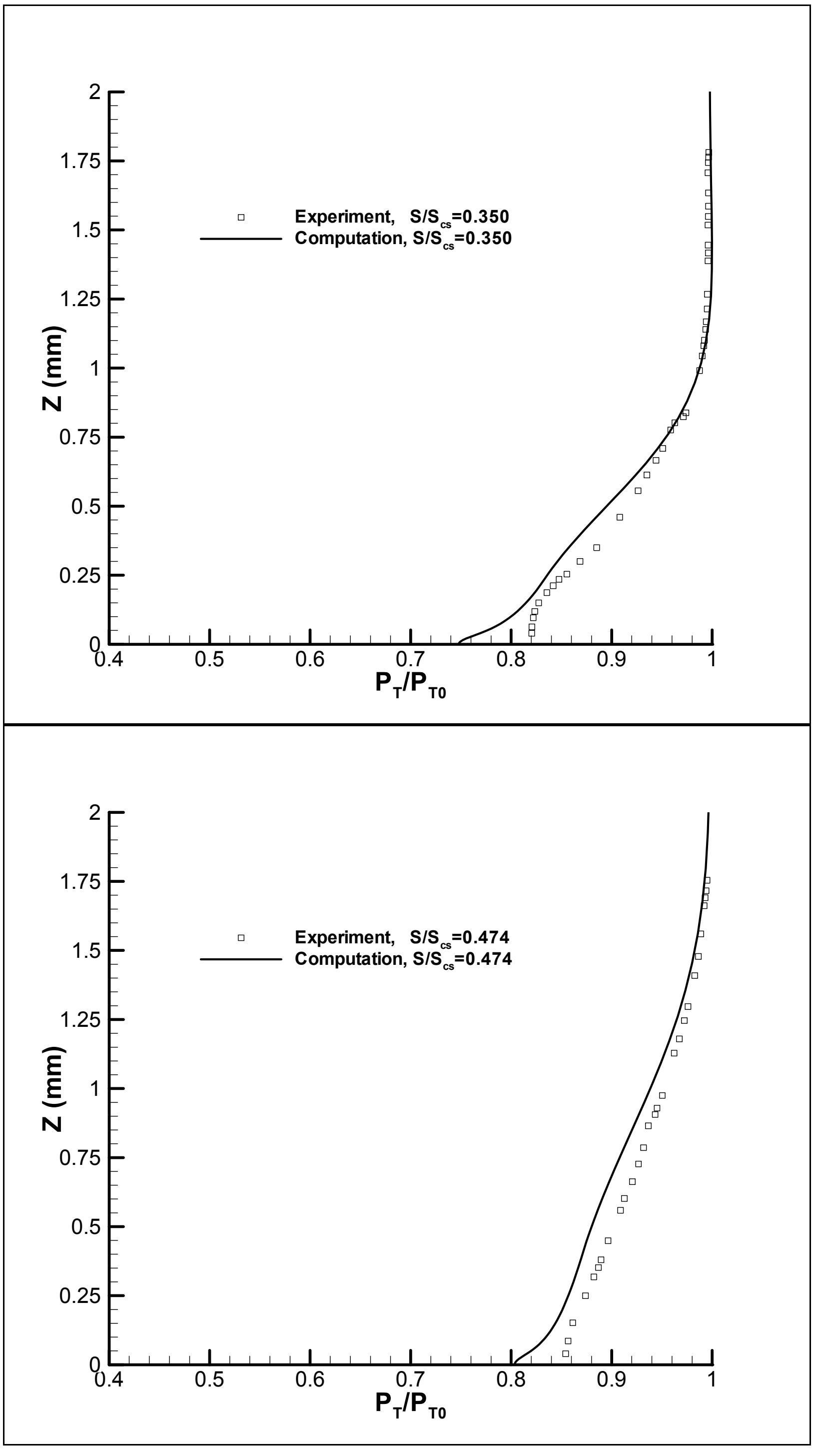

Fig. 4.44 Boundary Layer total pressure profile comparison for M=0.7 and β=49° (Upper Figure:Station 2, Lower Figure: Station 3)

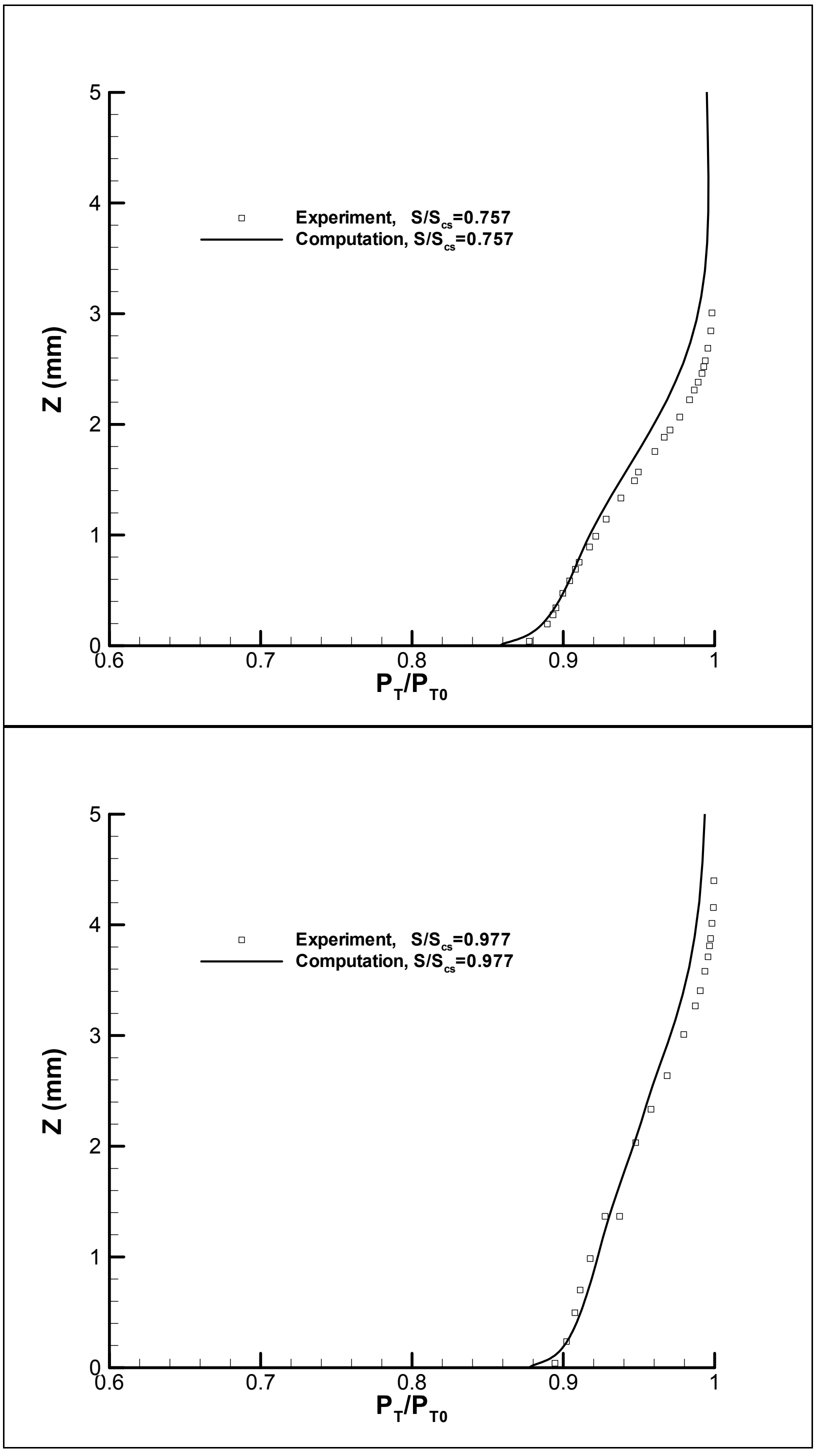

Fig. 4.45 Boundary Layer total pressure profile comparison for M=0.7 and β=49° (Upper Figure: Station 4, Lower Figure: Station 5)

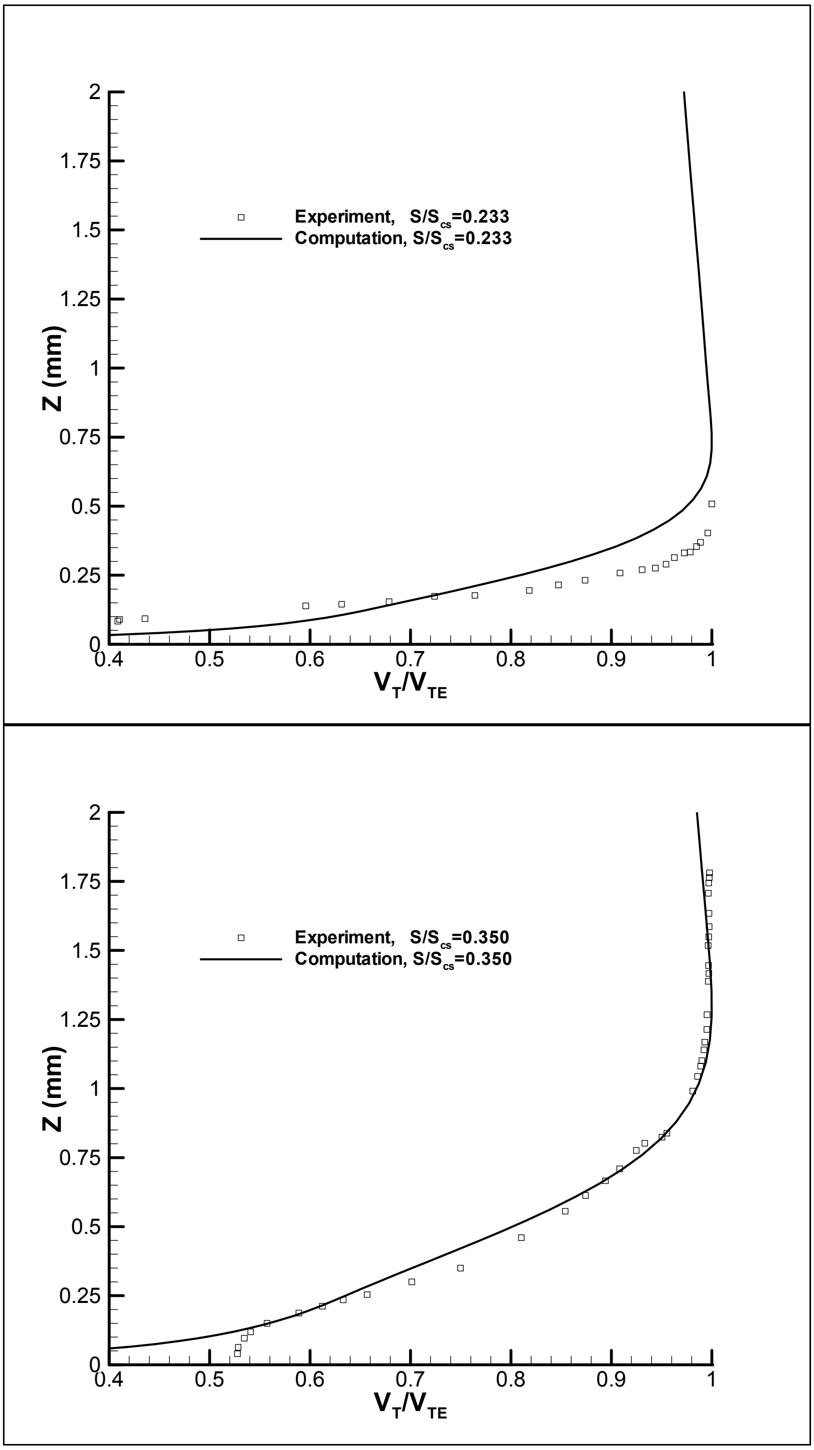

Fig. 4.46 Boundary Layer velocity profile comparison for M=0.7 and β =49° (Upper Figure: Station 1, Lower Figure: Station 2)

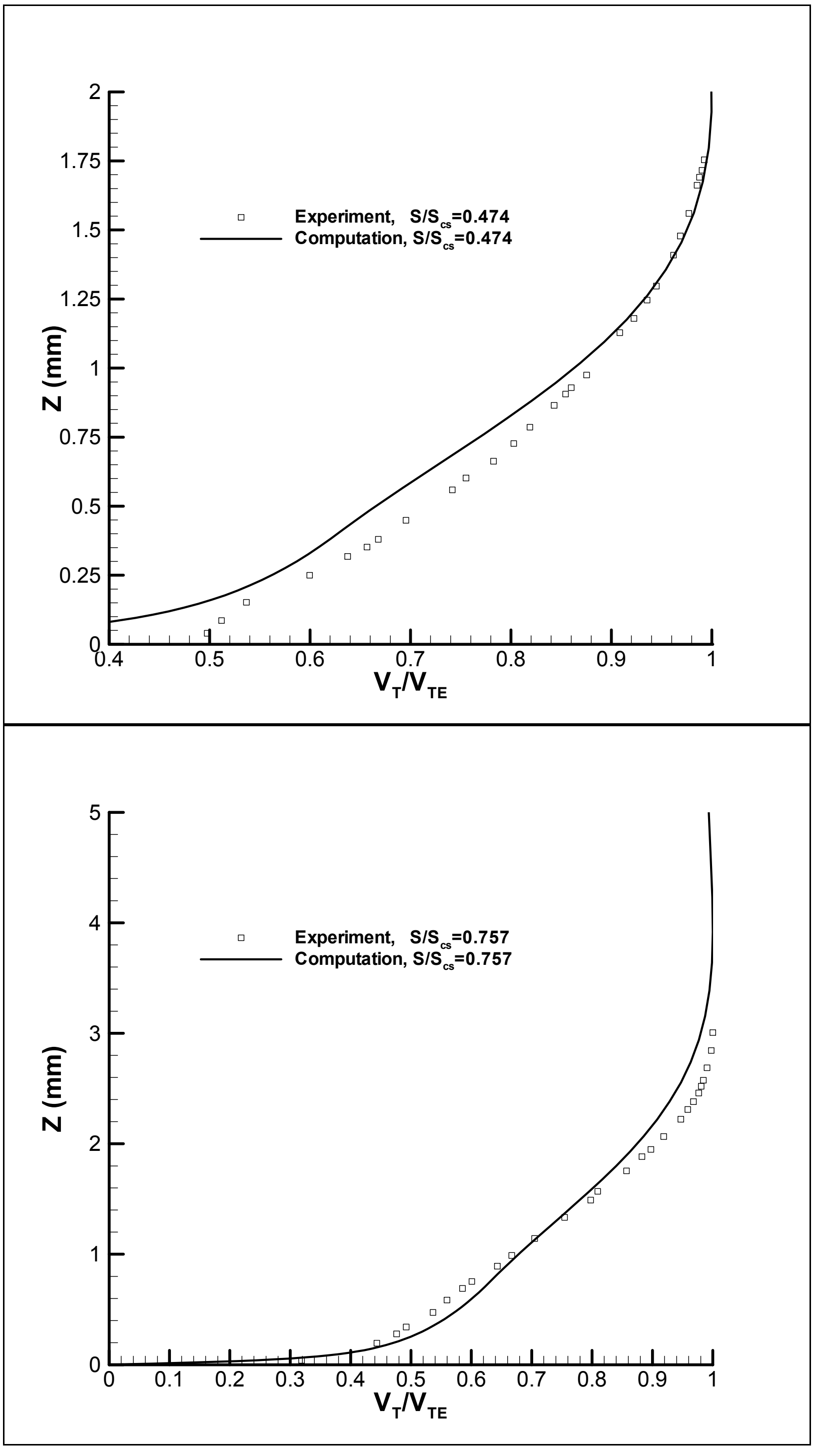

Fig. 4.47 Boundary Layer velocity profile comparison for M=0.7 and β=49° (Upper Figure: Station 3, Lower Figure: Station 4)

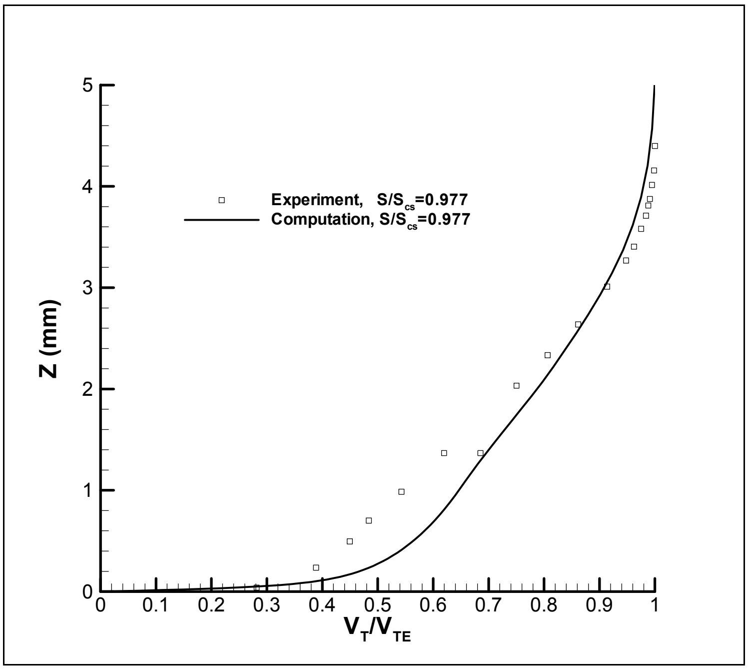

Fig. 4.48 Boundary Layer velocity profile comparison for M=0.7 and β=49° (Station 5)

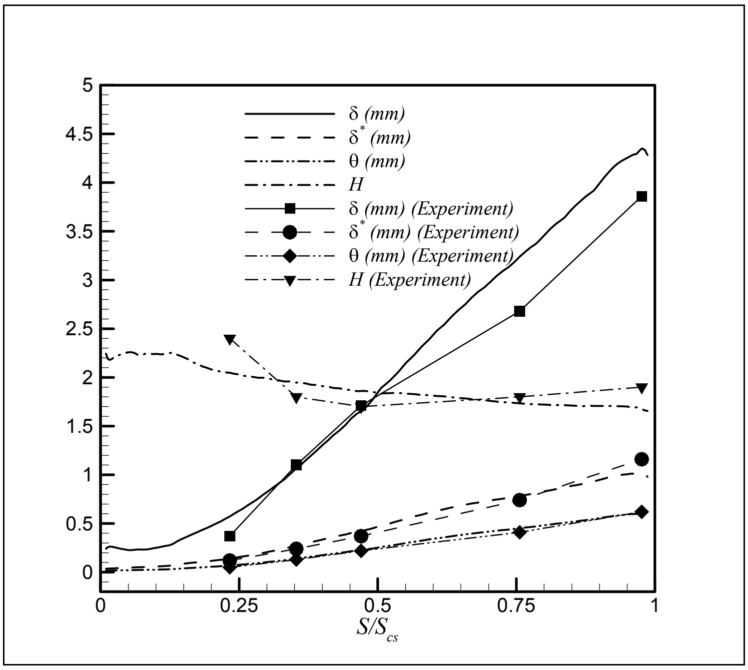

Fig. 4.49 Boundary Layer integral parameters comparison for M=0.7 and β=49°

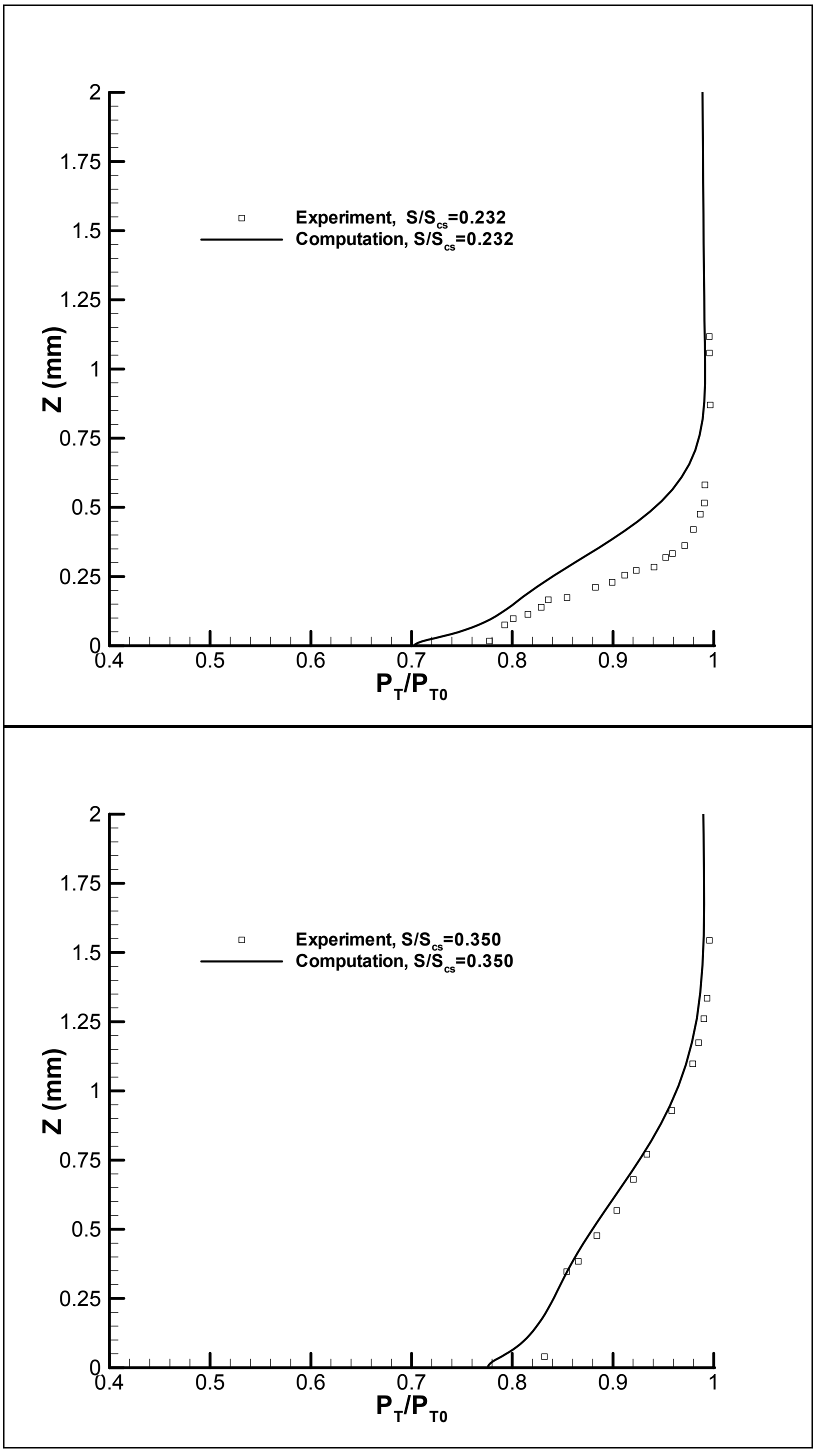

Fig. 4.50 Boundary Layer total pressure profile comparison for M=0.7 and β =51° (Upper Figure: Station 1, Lower Figure: Station 2)

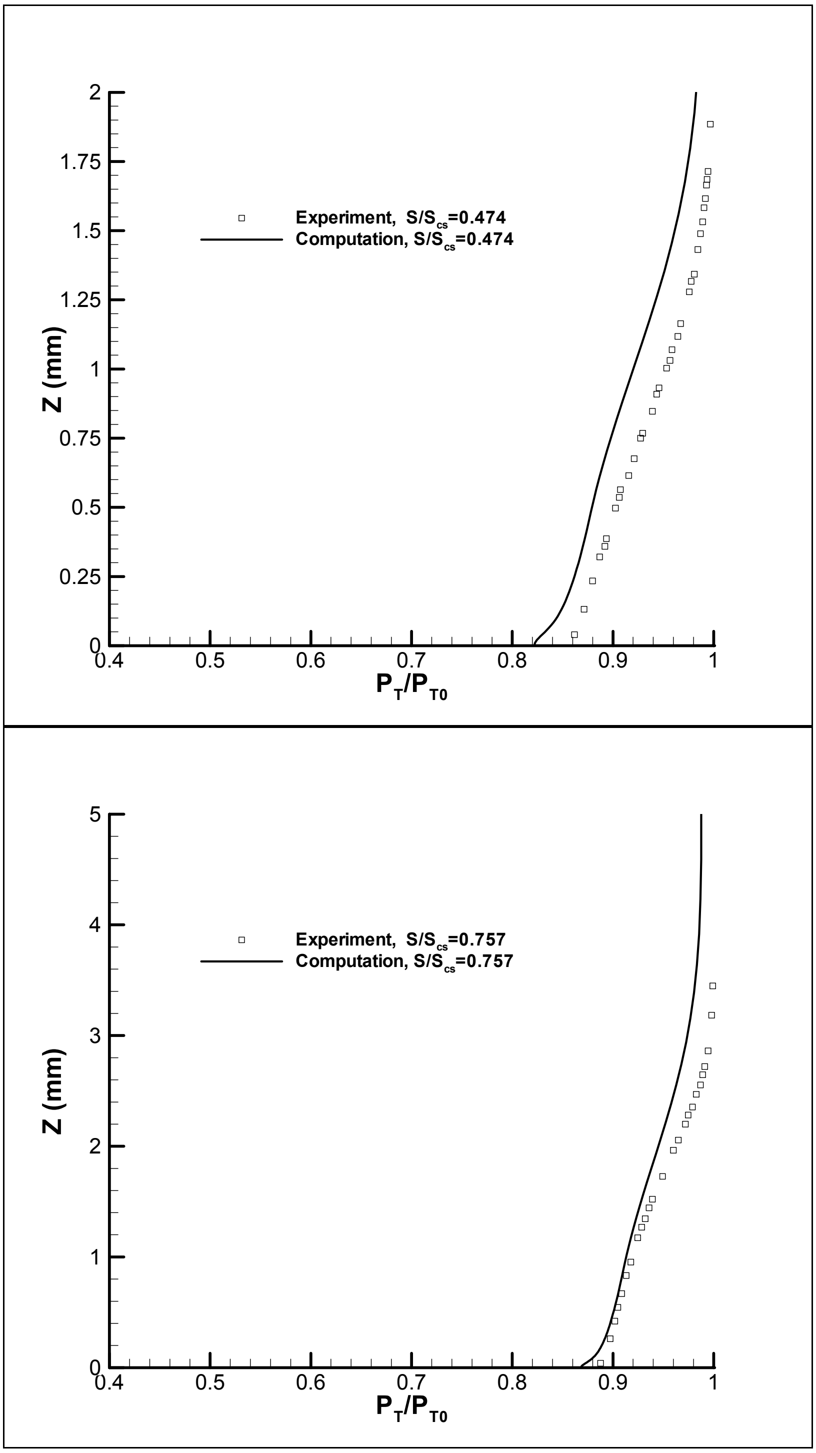

Fig. 4.51 Boundary Layer total pressure profile comparison for M=0.7 and β=51° (Upper Figure: Station 3, Lower Figure: Station 4)

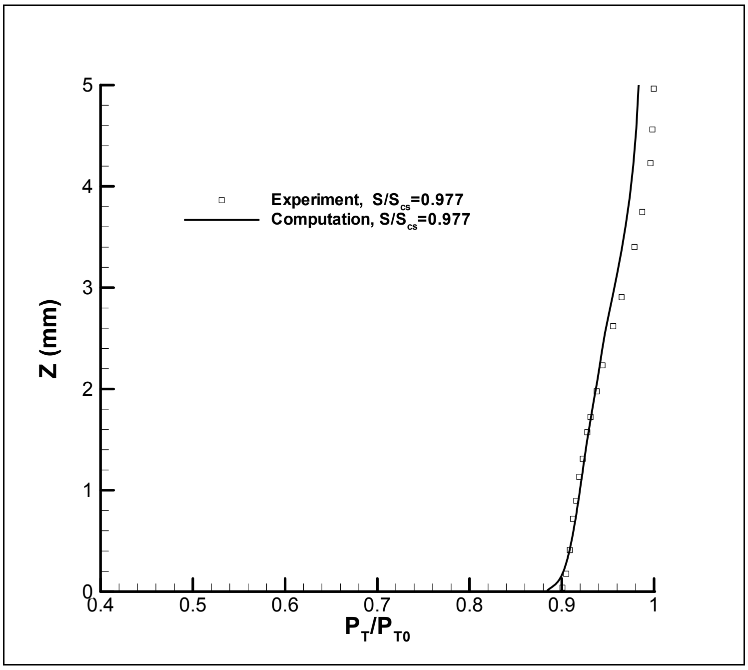

Fig. 4.52 Boundary Layer total pressure profile comparison for M=0.7 and β=51° (Station 5)

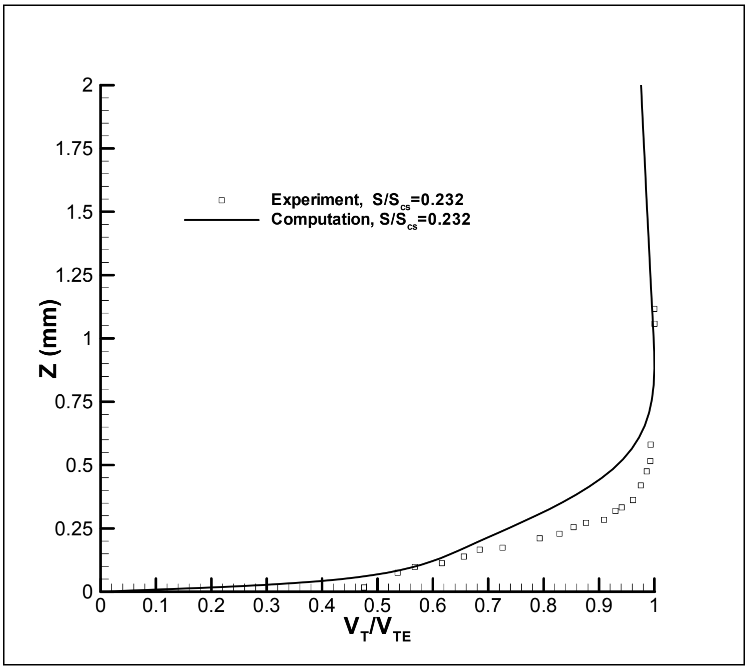

Fig. 4.53 Boundary Layer velocity profile comparison for M=0.7 and β=51° (Station 1)

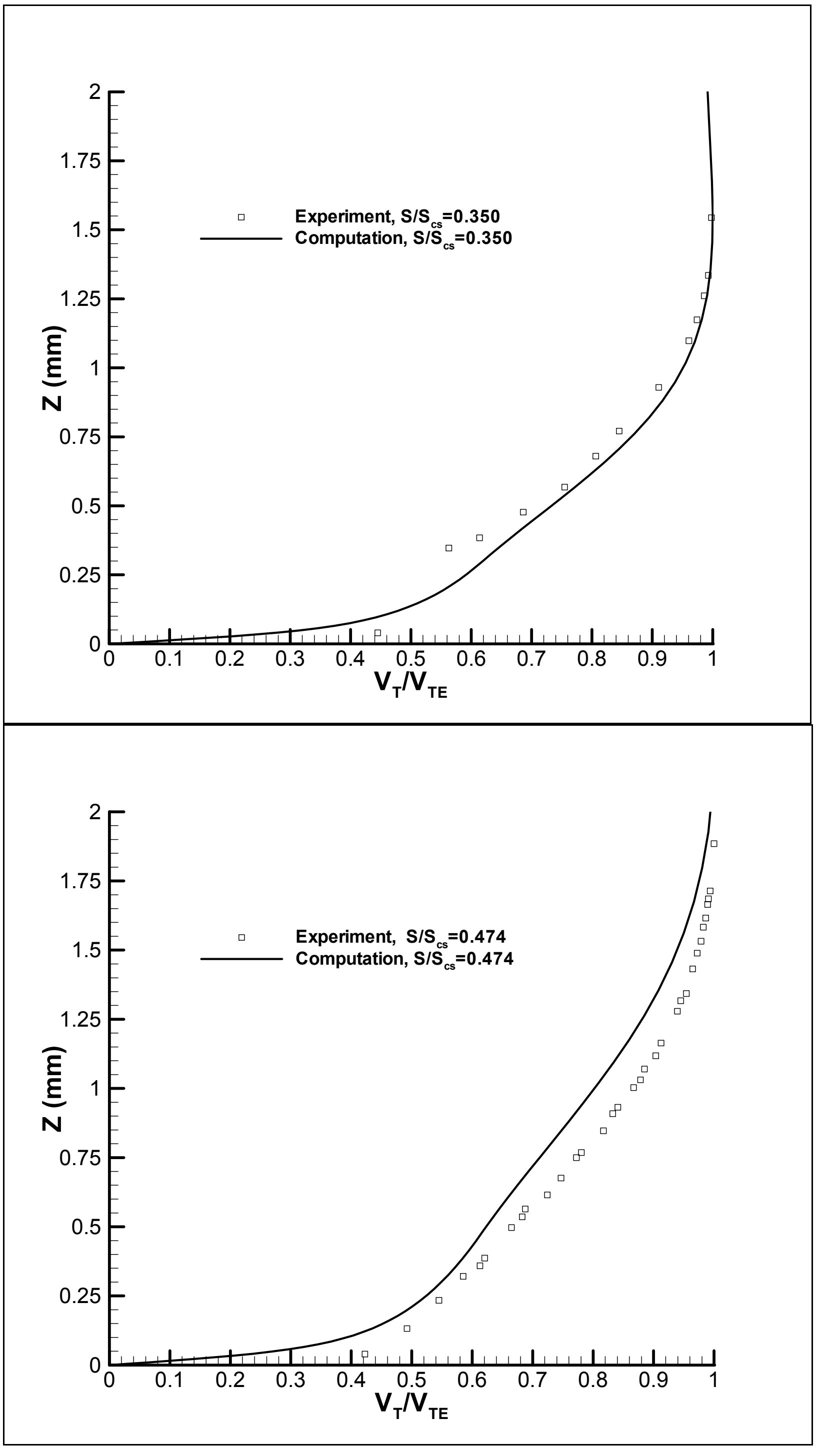

Fig. 4.54 Boundary Layer velocity profile comparison for M=0.7 and β =51° (Upper Figure: Station 2, Lower Figure: Station 3)

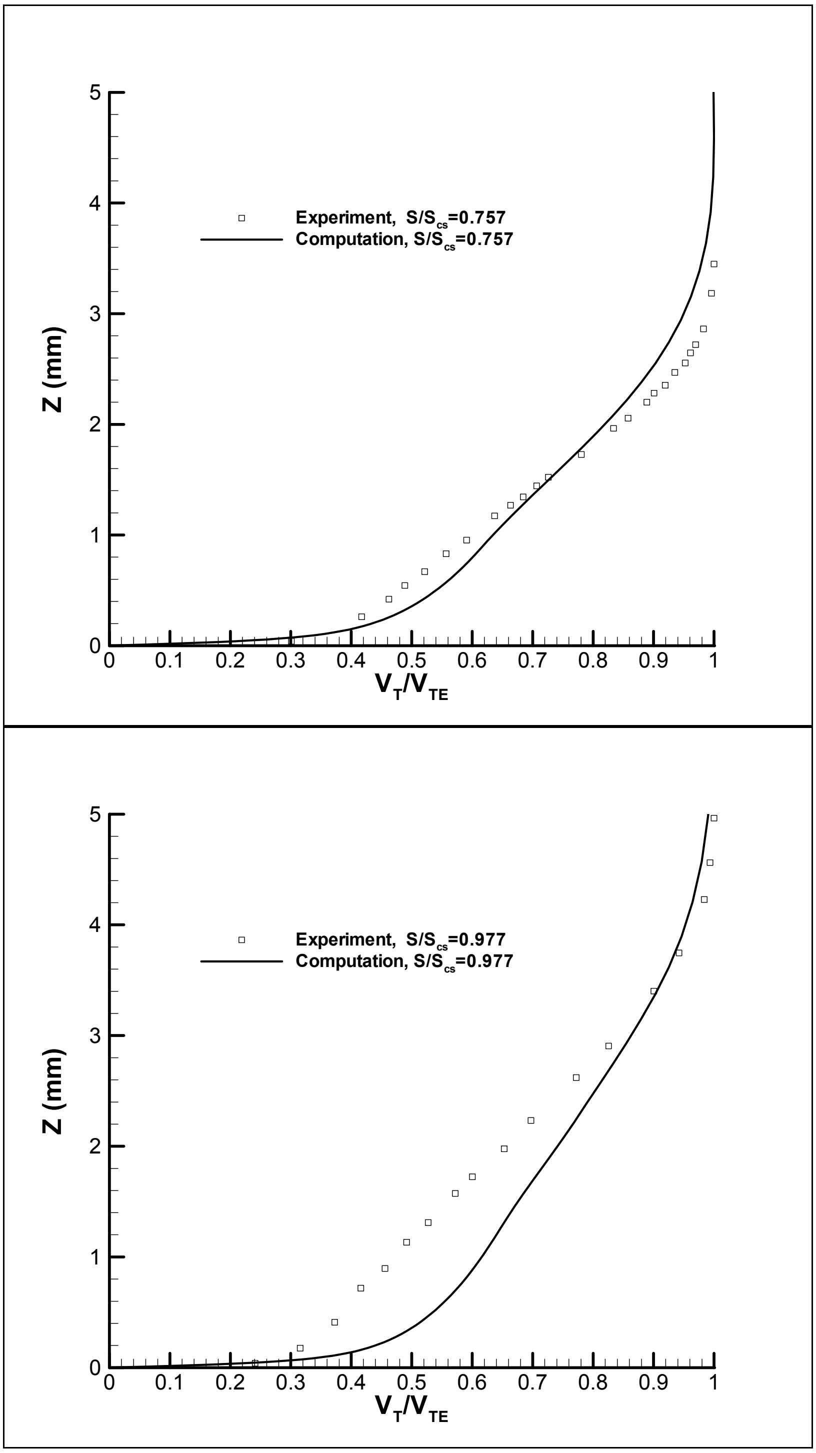

Fig. 4.55 Boundary Layer velocity profile comparison for M=0.7 and β =51° (Upper Figure: Station 4, Lower Figure: Station 5)

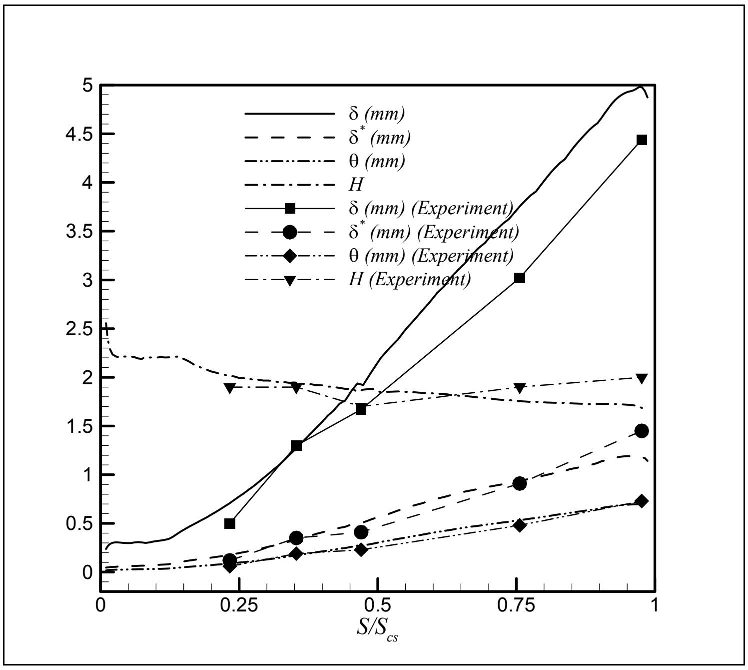

Fig. 4.56 Boundary Layer integral parameters comparison for M=0.7 and β=51°

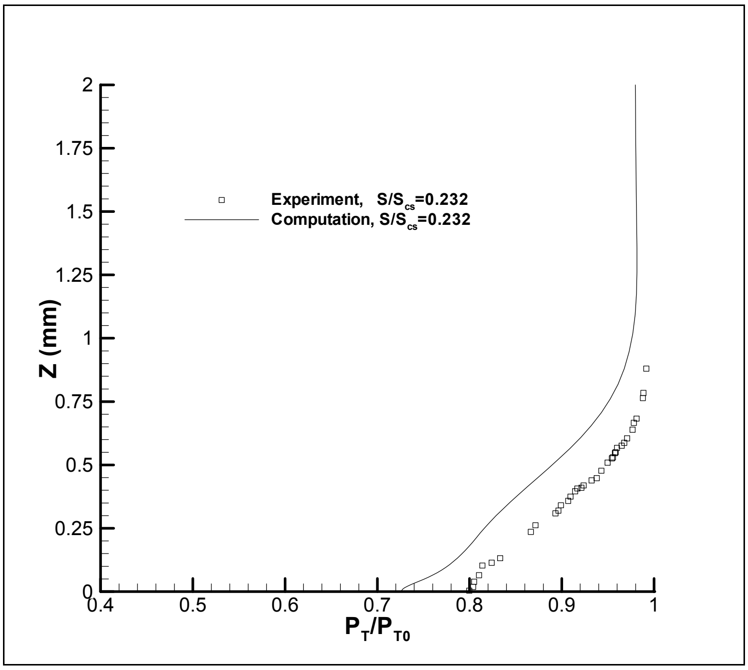

Fig. 4.57 Boundary Layer total pressure profile comparison for M=0.7 and β=53° (Station 1)

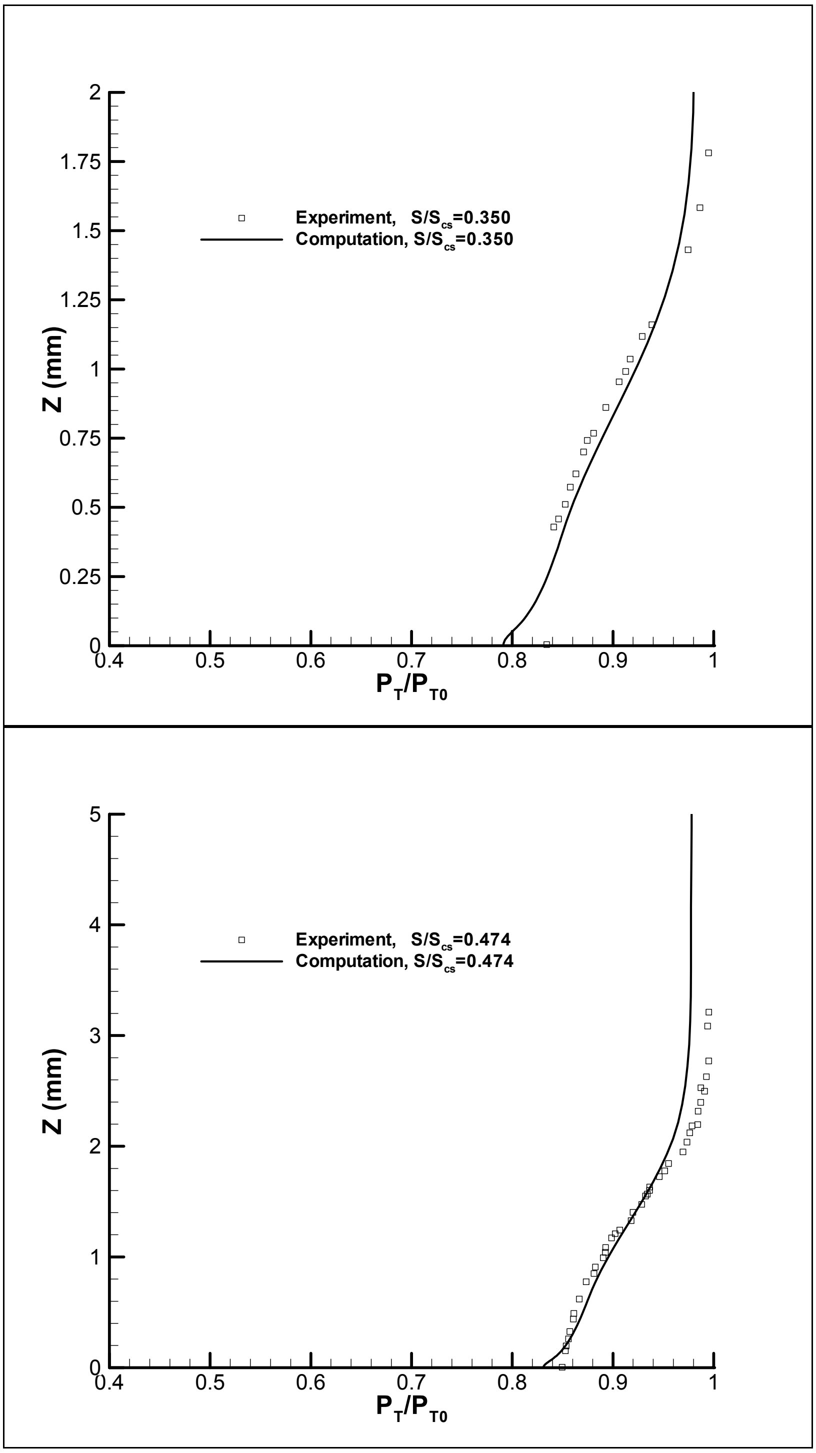

Fig. 4.58 Boundary Layer total pressure profile comparison for M=0.7 and β=53° (Upper Figure: Station 2, Lower Figure: Station 3)

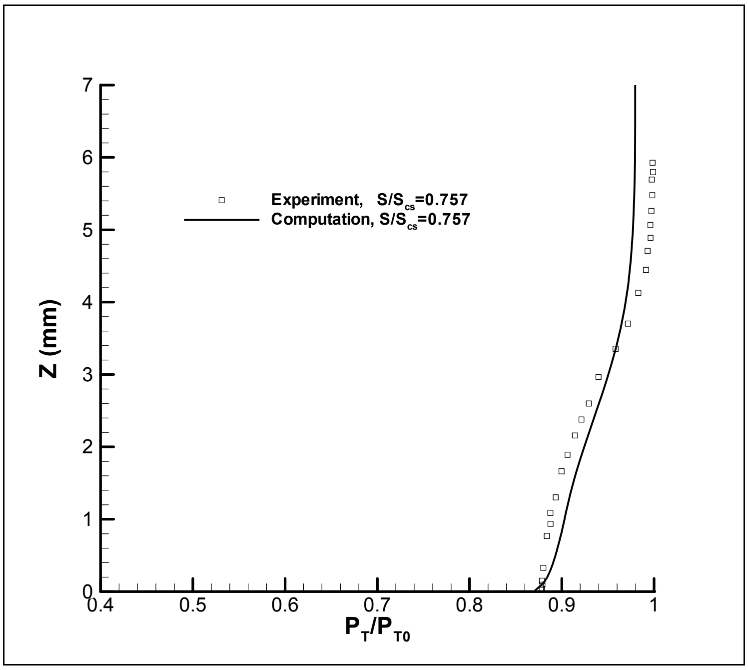

Fig. 4.59 Boundary Layer total pressure profile comparison for M=0.7 and β =53° (Station 4)

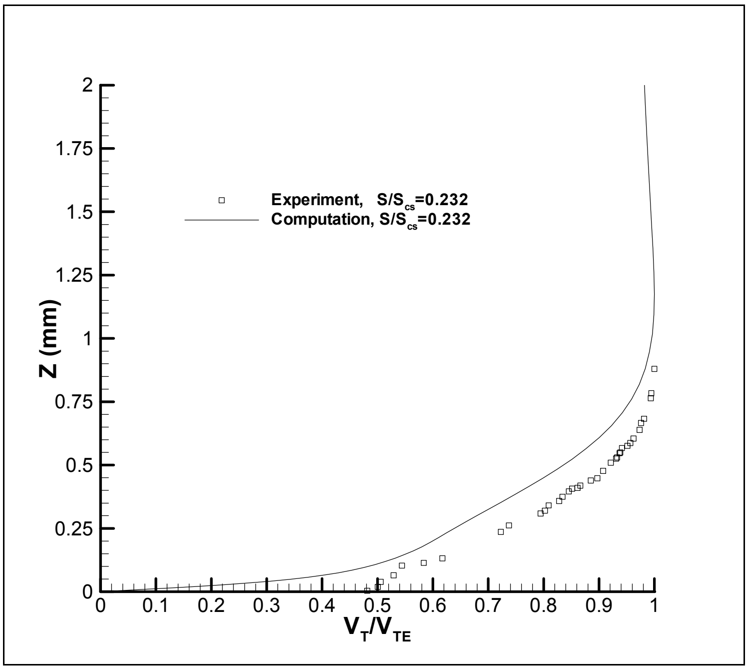

Fig. 4.60 Boundary Layer velocity profile comparison for M=0.7 and β =53° (Station 1)

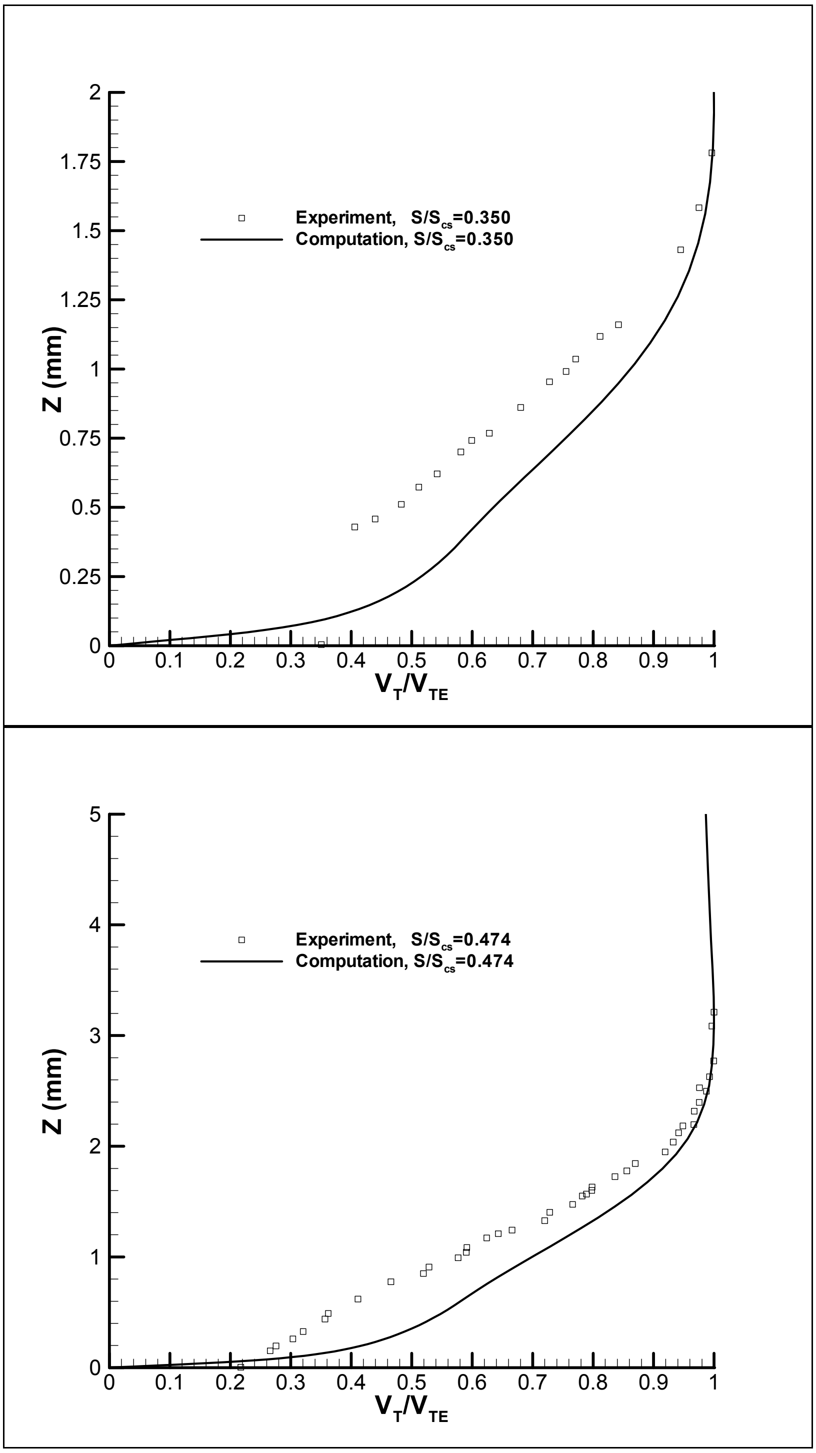

Fig. 4.61 Boundary Layer velocity profile comparison for M=0.7 and β =53° (Upper Figure: Station 2, Lower Figure: Station 3)

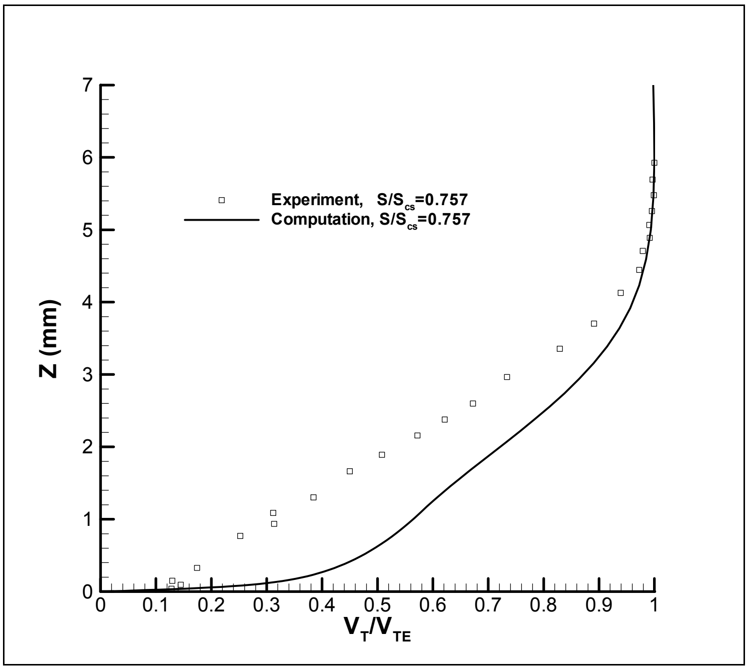

Fig. 4.62 Boundary Layer velocity profile comparison for M=0.7 and β=53° (Station 4)

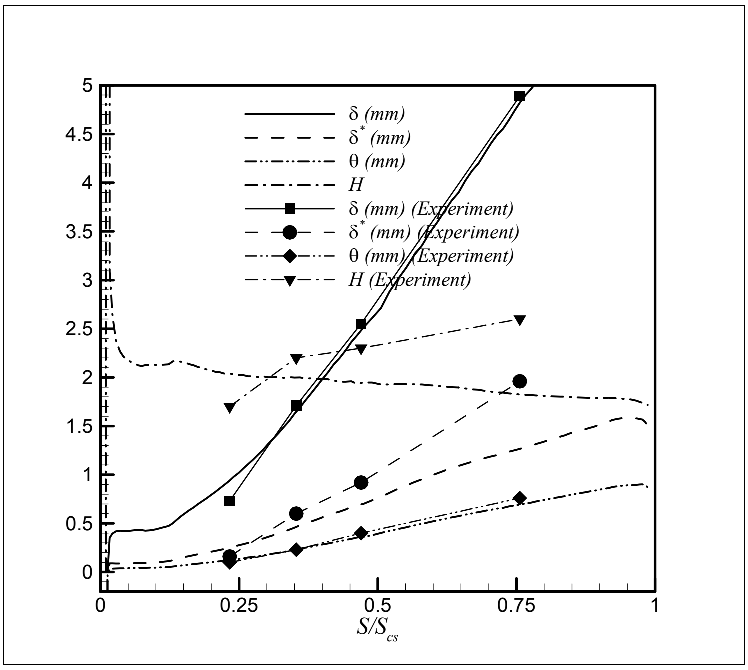

Fig. 4.63 Boundary Layer integral parameters comparison for M=0.7 and β=53°

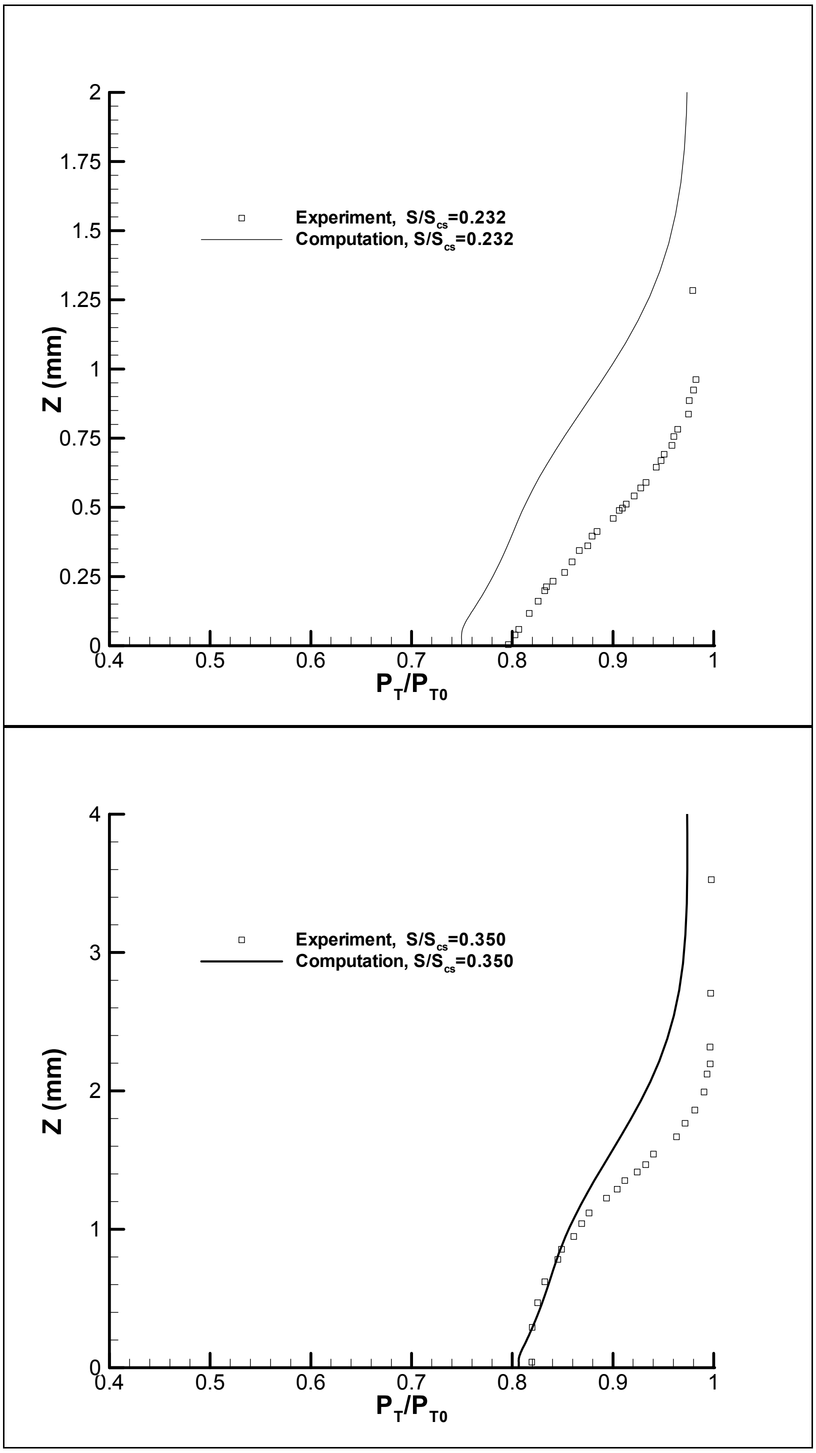

Fig. 4.64 Boundary Layer total pressure profile comparison for M=0.7 and β=55° (Upper Figure: Station 1, Lower Figure: Station 2)

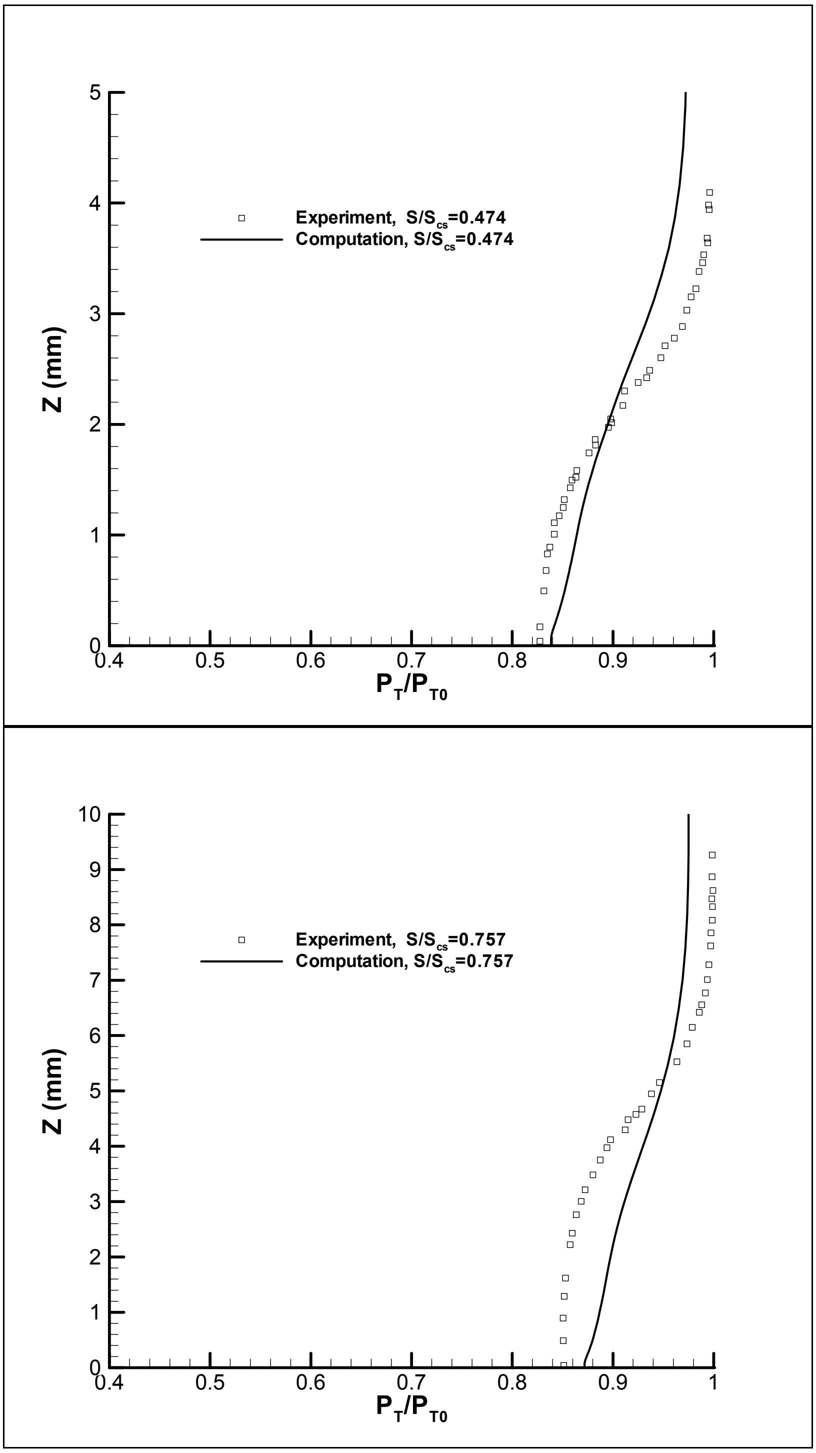

Fig. 4.65 Boundary Layer total pressure profile comparison for M=0.7 and β =55° (Upper Figure: Station 3, Lower Figure: Station 4)

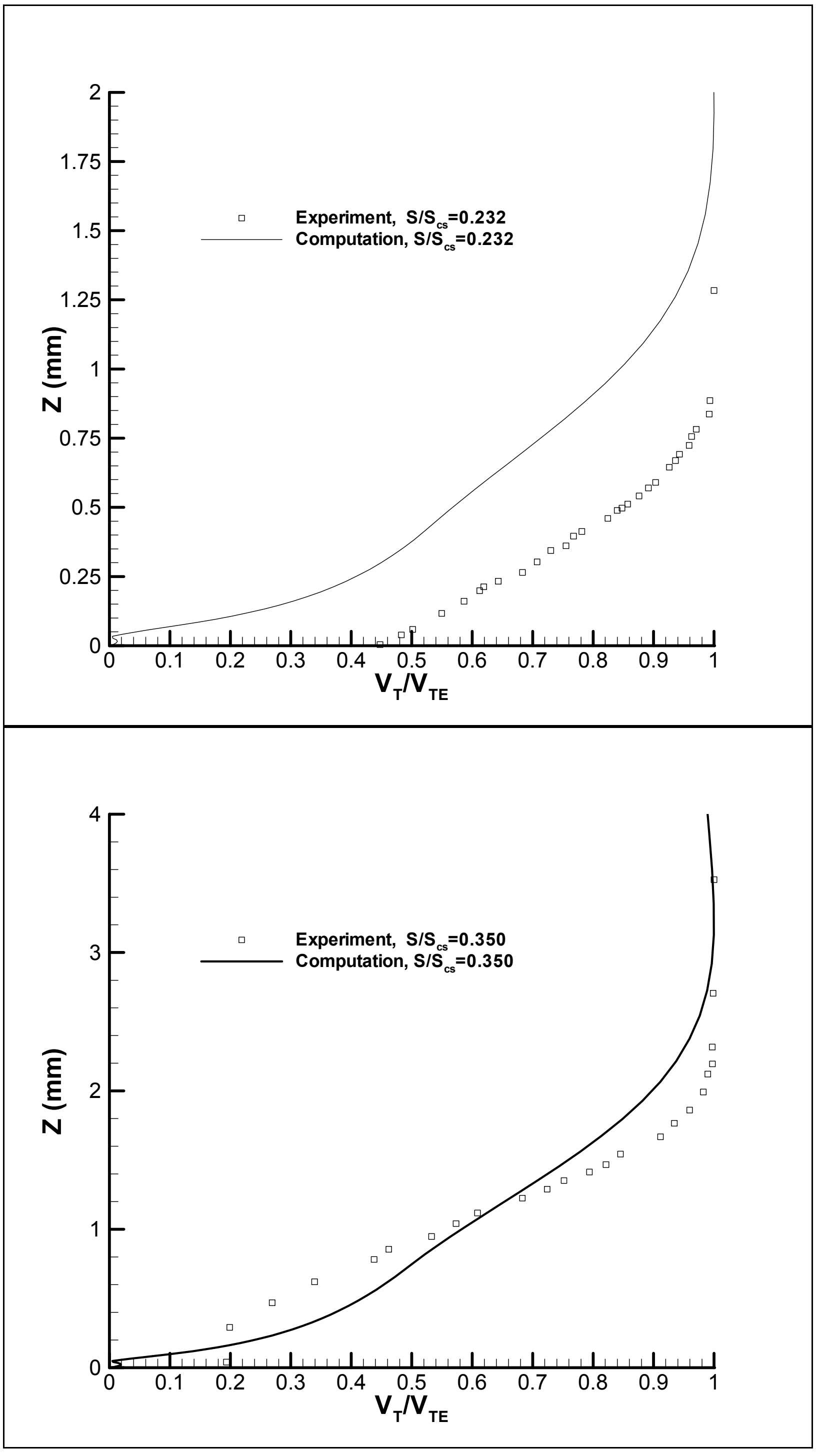

Fig. 4.66 Boundary Layer velocity profile comparison for M=0.7 and β =55° (Upper Figure: Station 1, Lower Figure: Station 2)

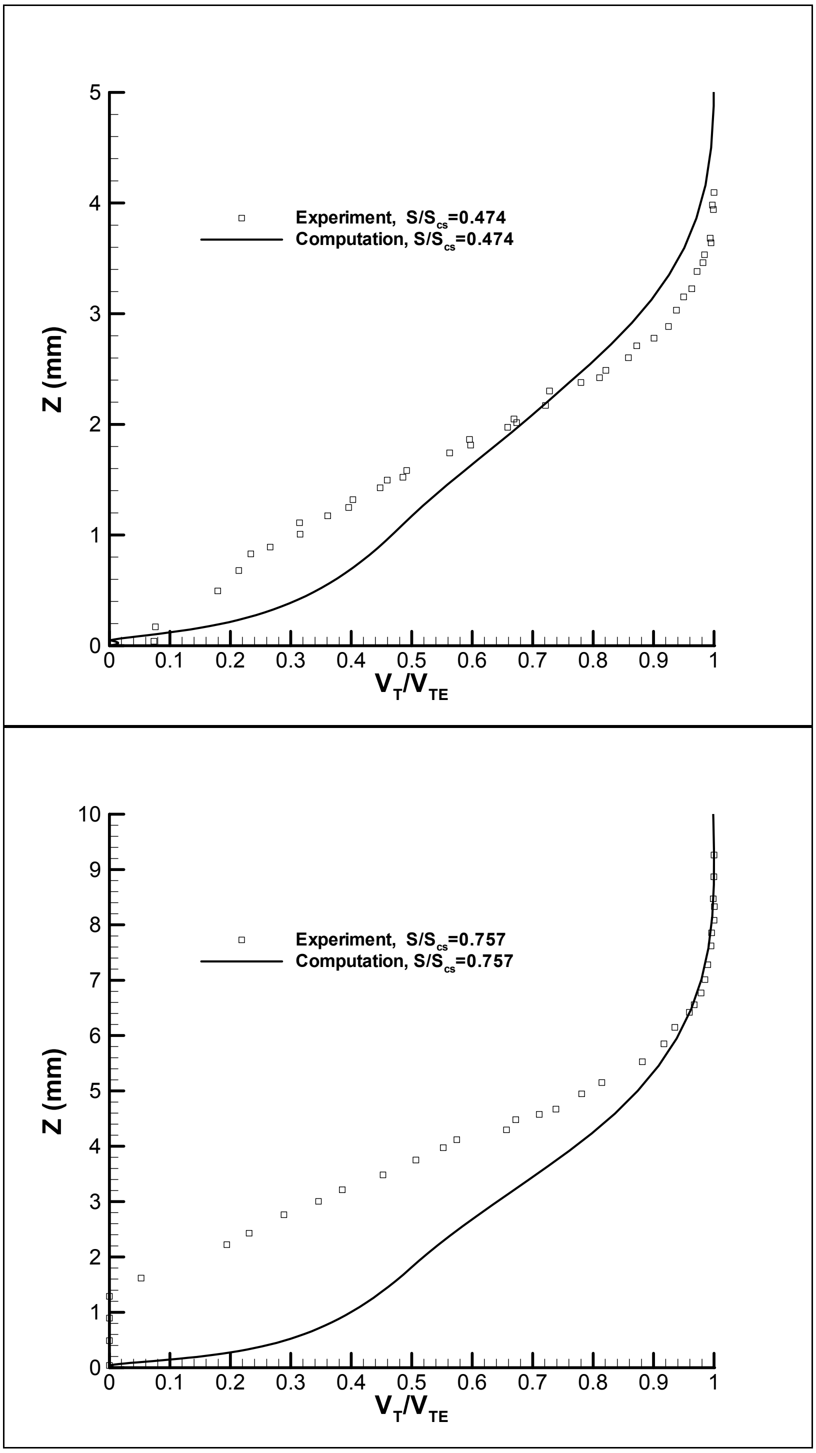

Fig. 4.67 Boundary Layer velocity profile comparison for M=0.7 and β =55° (Upper Figure: Station 3, Lower Figure: Station 4)

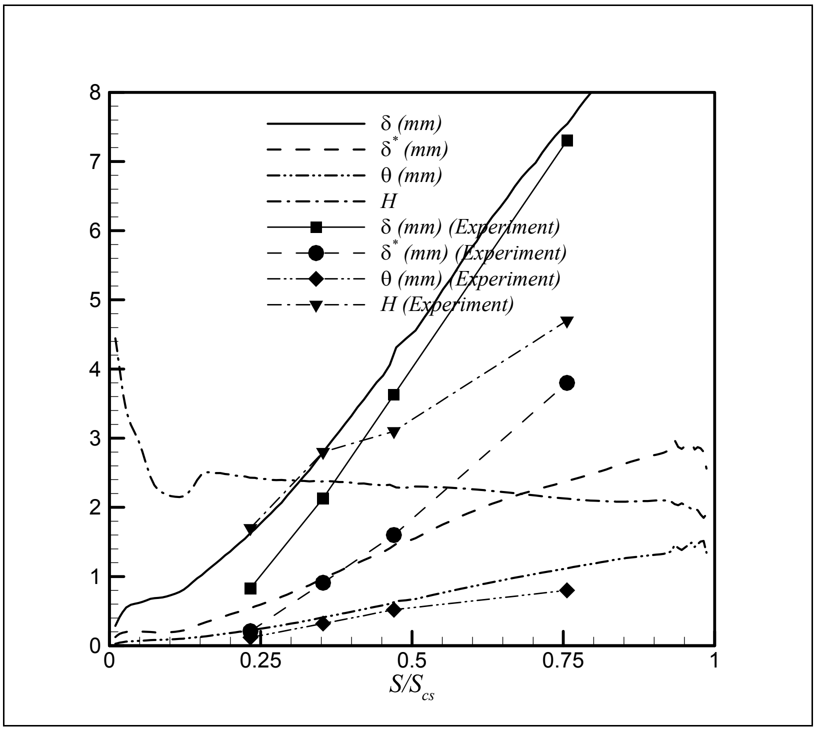

Fig. 4.68 Boundary Layer integral parameters comparison for M=0.7 and β=55°

In the above figures the results of the comparison of boundary layer parameters with the experimental data [13] has been presented and it is obvious that results of Navier Stokes solution show relatively good agreement with the experimental data.

As a result, the numerical solution of the test problem presented in Chapter 3 and Ref. [13] reasonably agrees to the experimental results, and the validation work shows that the modified PML3D code is a powerful tool to calculate the test case E/CA-3 high subsonic compressor cascade 115.

In the following section non-uniform inlet velocity profile Navier Stokes solution is presented.

4.3. Navier Stokes Solution with Nonuniform Inlet Velocity Profile:

In this section an inlet wake in the velocity profile is introduced and this velocity wake has moved in the vertical direction for four different shift values in order to simulate one cycle of the wake movement.

NASA Rotor 37 wake (Ref. [14]) has been used for the definition of the wake presented in Fig. 4.70 for M=0.7 and β=49°. The rest of the test cases (M=0.7; β=51°, 53°, 55°) has the same wake positions and similar configuration.

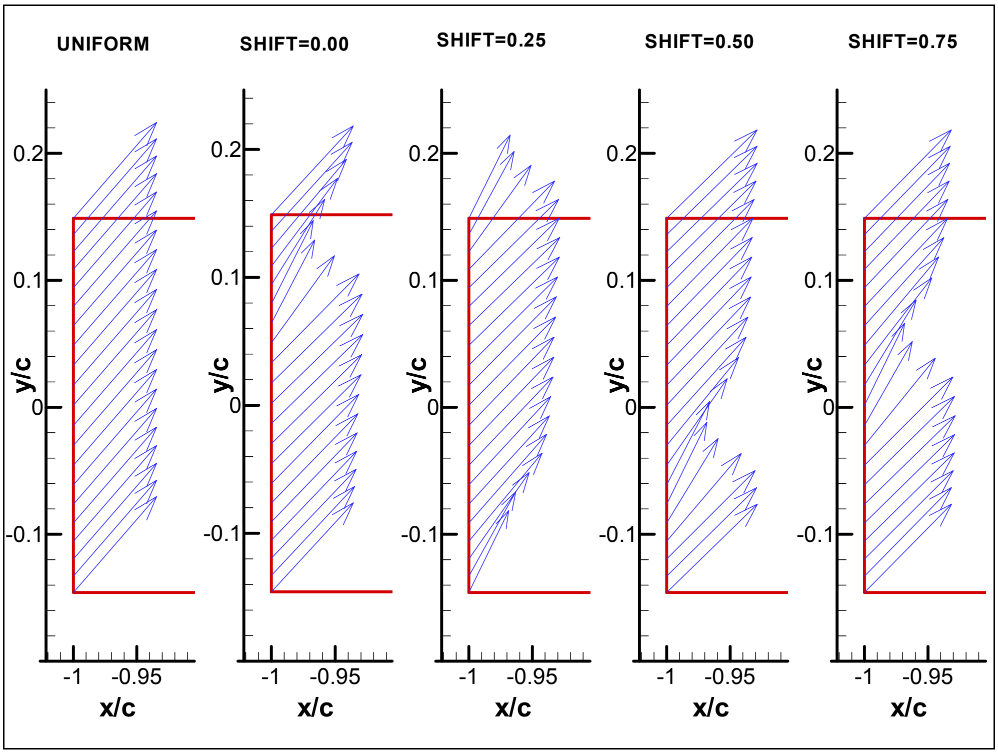

Fig. 4.69 Typical wake positions for different shift values (example is for M=0.7 and β=49°) .

4.3.1. Grid:

For the 2D Navier Stokes Solution of nonuniform inlet velocity profile again H-O-H multi block type grid is modified. This grid is made of three blocks. The front block, the center block and the rear block. The center block is an O-type grid and its dimensions are 249*3*78 in ξ, η, and ζ directions (J,K,L). The normal distance between the surface and the first grid point above the surface is, $\Delta n / c = 0.2947$ (0.00005). L=1 corresponds to the airfoil surface. The front block dimensions are 100*3*21 and rear block dimensions are 25*3*21 each in ξ, η, and ζ directions (J,K,L).

The front block is modified due to the introduction of the nonuniform inlet velocity profile that is described in Fig. 4.69. The grid is shown in Fig. 4.70 and Fig. 4.71.

The grid is nondimensionalized again with chord, *c*.

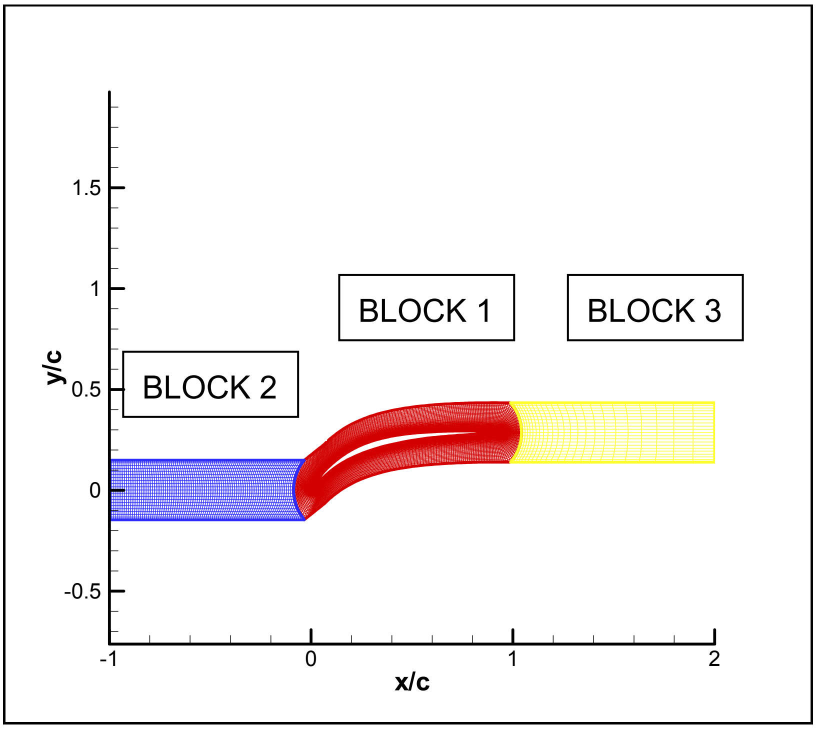

Fig. 4.70 H-O-H Grid

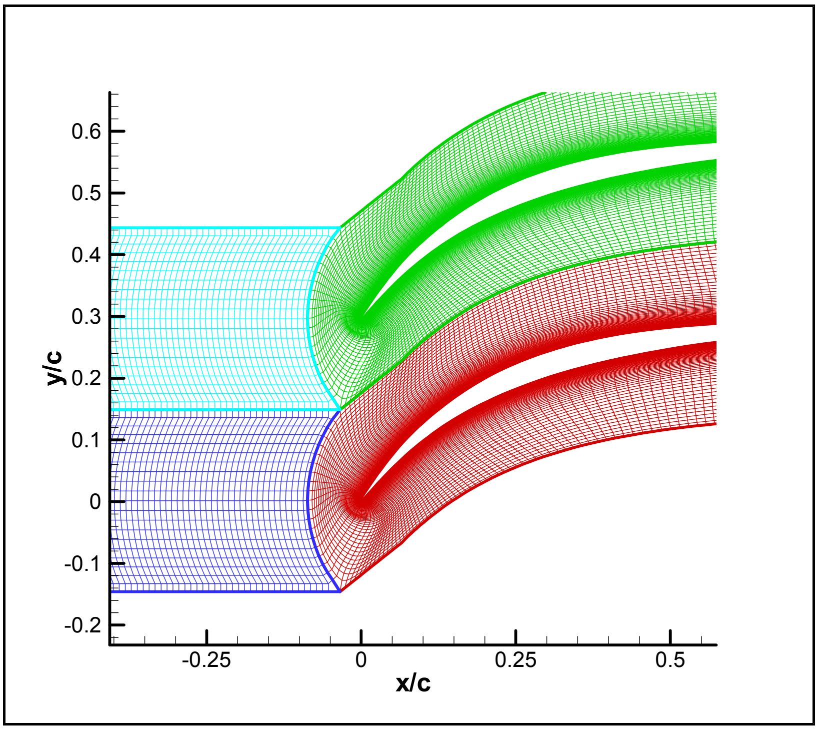

Fig. 4.71 H-O-H Grid, enlarged around leading edge

4.3.2. Boundary Conditions:

For the center O-Grid at L=LMAX top and Bottom surfaces are periodic. Matched Surface Boundary Conditions are applied at the common boundaries with the front and rear blocks. At L=1, the surface boundary conditions are applied. J=1 and J=JMAX boundaries coincides (the wake behind the T.E.) and the periodic boundary conditions are applied at those boundaries.

For the front grid at J=1 a special boundary condition for CA115 stator cascade in rotor wake problem nonuniform inlet velocity profile is specified. At J=JMAX Matched surface boundary conditions are applied with the central O-Block. L=1 (bottom surface) and L=LMAX (top surface) are periodic with each other.

For the rear grid at J=1 Matched surface boundary conditions are applied with the central O-Block. J=JMAX is the flow out plane pressure fixed extrapolation type boundary conditions are used. L=1 (bottom surface) and L=LMAX (top surface) are periodic with each other.

4.3.2.1. Calculation of exit to inlet static pressure ratio:

For the J=JMAX, flow out plane, pressure fixed extrapolation type boundary condition is applied. A computer program named as **P2P1NSP.f90** is used to estimate initial value of the P_2 / P_1 ratio. This program is similar to the **P2P1NS.f90** program which is mentioned at the uniform inlet velocity profile Navier Stokes solutions section. The main difference is that P2P1NSP.f90 also takes into account the momentum loss due to rotor wake (non-uniform inlet velocity profile).

The final value of the P_2/P_1 ratio is again obtained by using the trial and error method mentioned before. After a certain number of iterations P_2/P_1 ratio is adjusted so that at the mid parts of block 2 (the front block) the P/P_1 ratio is approximately equal to 1.0. The final P_2/P_1 ratios for different β angles are presented in Table 4.3.

More detailed information about the CPU time and P_2/P_1 values employed in the analysis can be found in Appendix C.

Table 4.3 Exit to inlet static pressure ratios for Navier Stokes nonuniform inlet profile solution

Mach number	β angle	Shift	$\frac{P_2}{P_1}$
0.7	49°	0.00	1.187
		0.25	1.192
		0.50	1.186
		0.75	1.187
0.7	51°	0.00	1.196
		0.25	1.202
		0.50	1.195
		0.75	1.195
0.7	53°	0.00	1.205
		0.25	1.201
		0.50	1.203
		0.75	1.205
0.7	55°	0.00	1.213
		0.25	1.219
		0.50	1.212
		0.75	1.212

4.3.3. Results:

In this section convergence in form of force and moment coefficients C_z and C_m vs iteration plots of the H-O-H grid, M=0.7, β=49°, 51°, 53°, 55° and for each β 4 different shifts are presented in Figs. 4.30 and 4.33 initially.

Shifts indicate the location of the wake in the inlet profile. Such that shift=0.0 means wake is in the most down position in the inlet. For the other shift values (shift=0.25, 0.50, 0.75) wake moves upward position.

The most important result from that section is to show the different surface pressure values that have been obtained with different wake locations. These results are also presented in Figs. 4.80 through 4.84. Also all the force values obtained with the wake profile are less than that for the uniform profile Navier Stokes solution.

One topic that should be mentioned here is the convergence of the runs. As seen from the below figures, no problem has been encountered for all runs in that section.

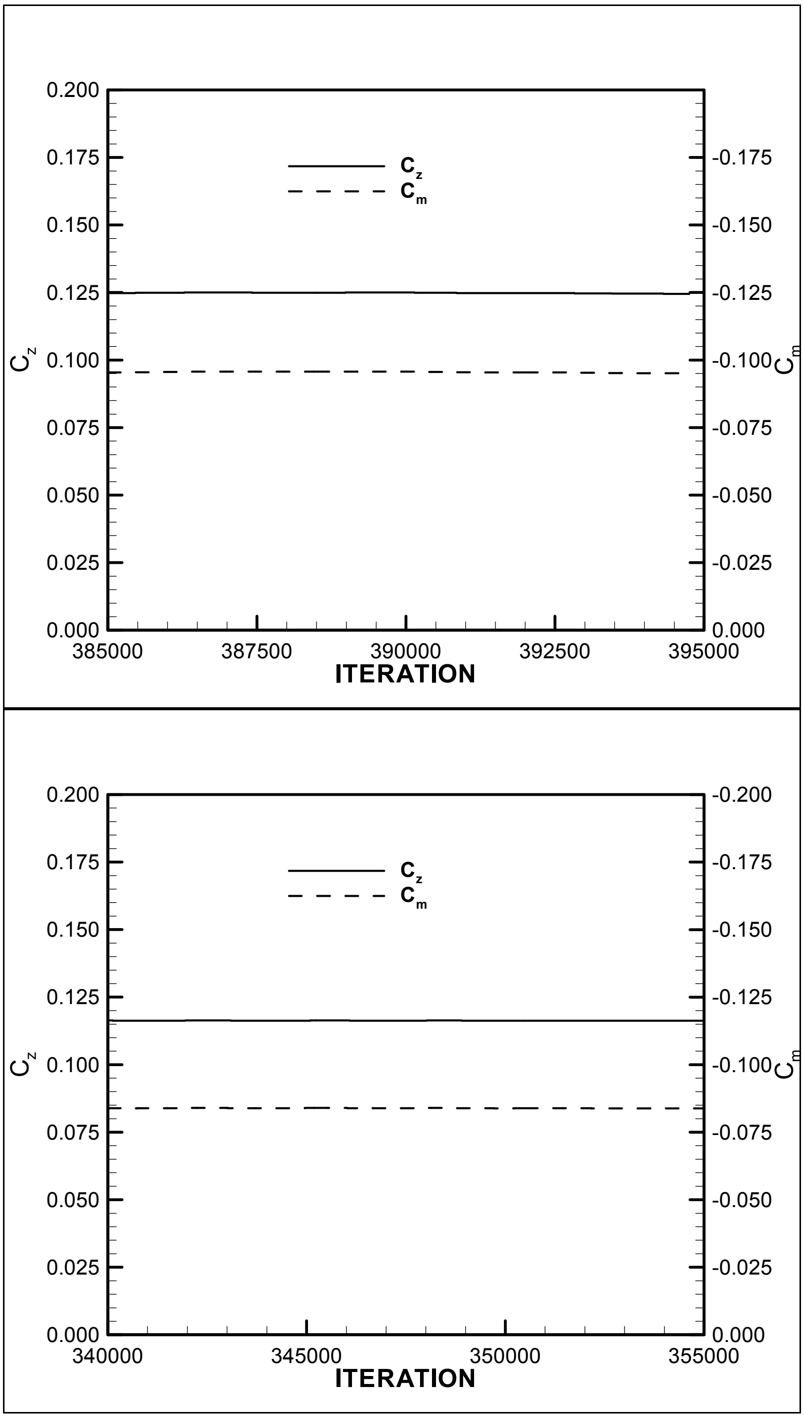

Fig. 4.72 N-S Nonuniform Inlet Velocity Profile Solution for M=0.7, β=49° and shift=0.0 and shift=0.25

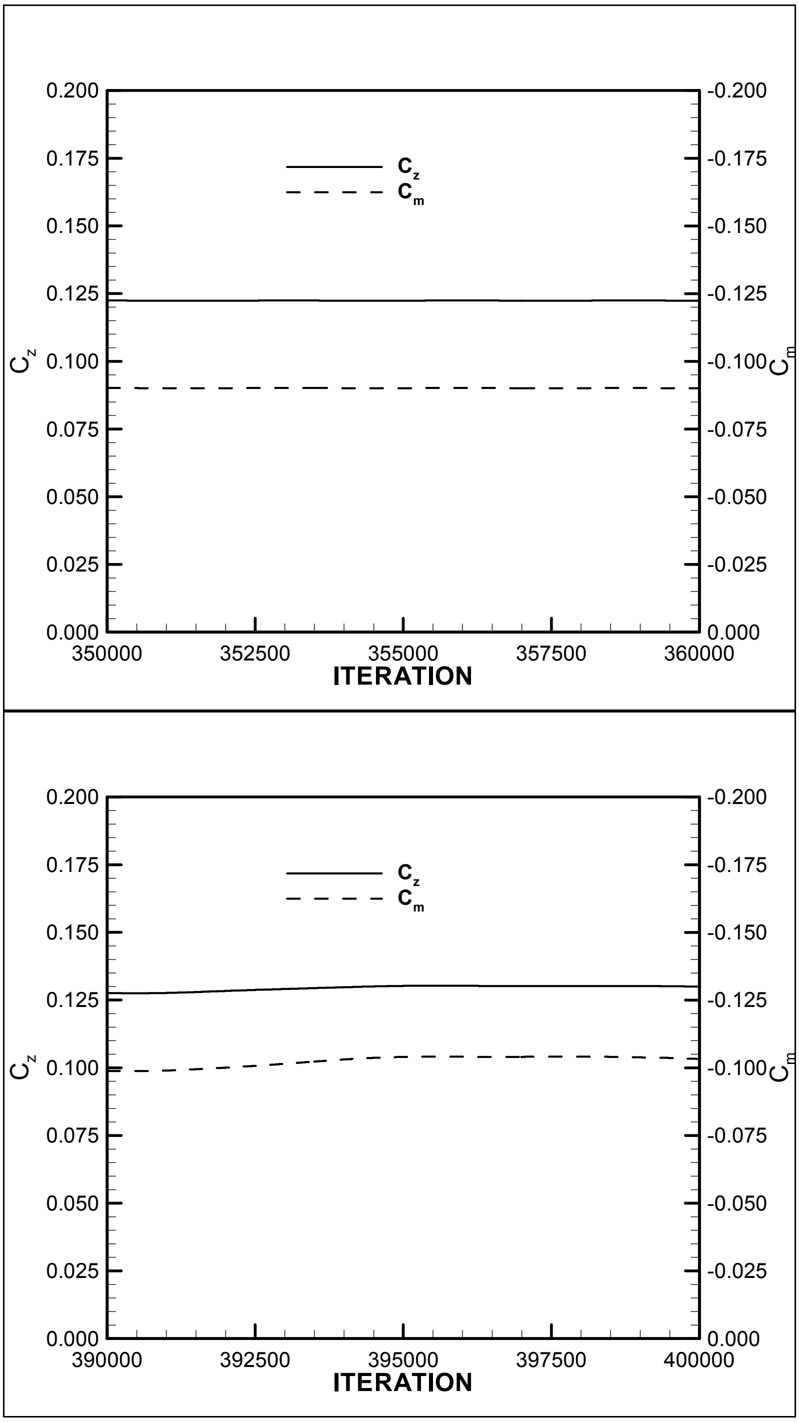

Fig. 4.73 N-S Nonuniform Inlet Velocity Profile Solution for M=0.7, β =49° and shift=0.50 and shift=0.75

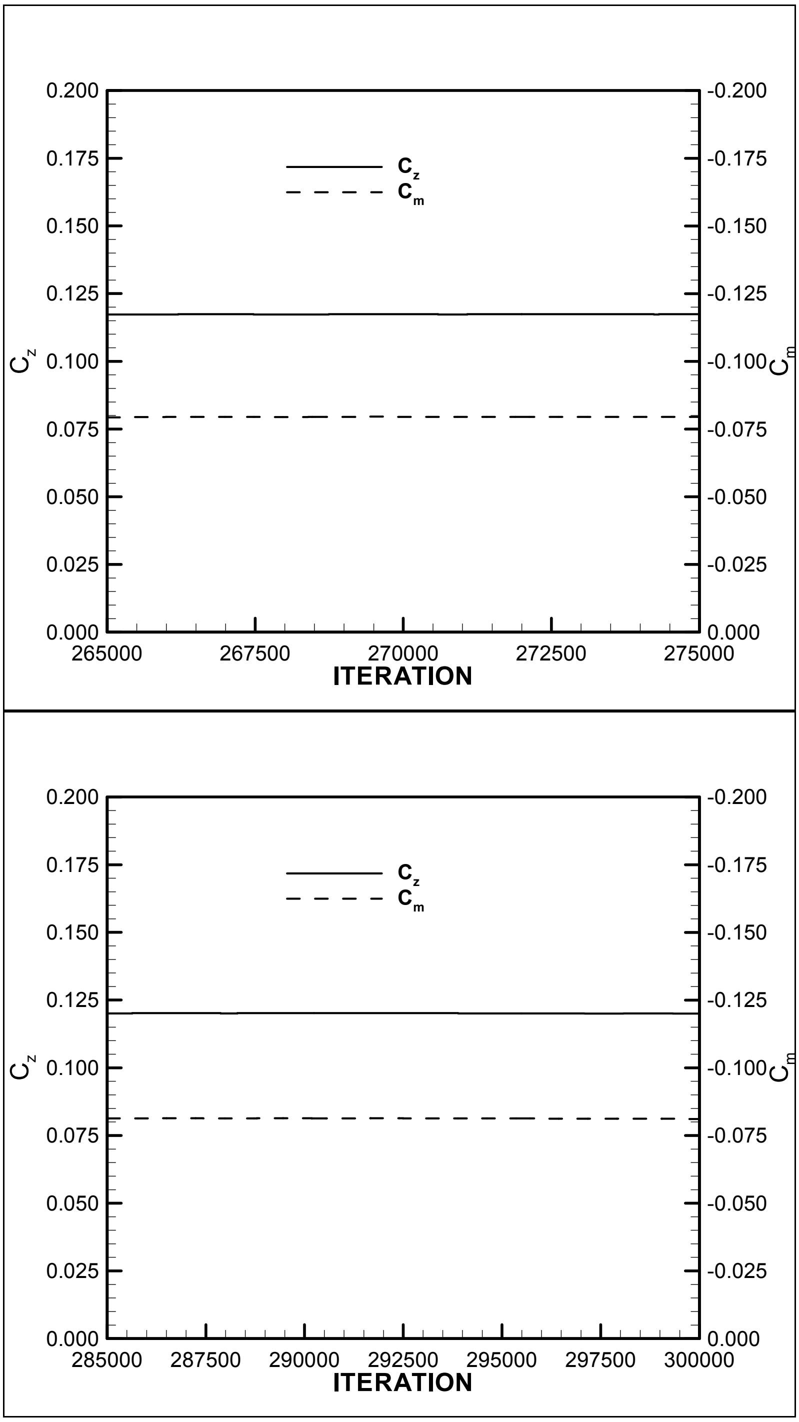

Fig. 4.74 N-S Nonuniform Inlet Velocity Profile Solution for M=0.7, β =51° and shift=0.0 and shift=0.25

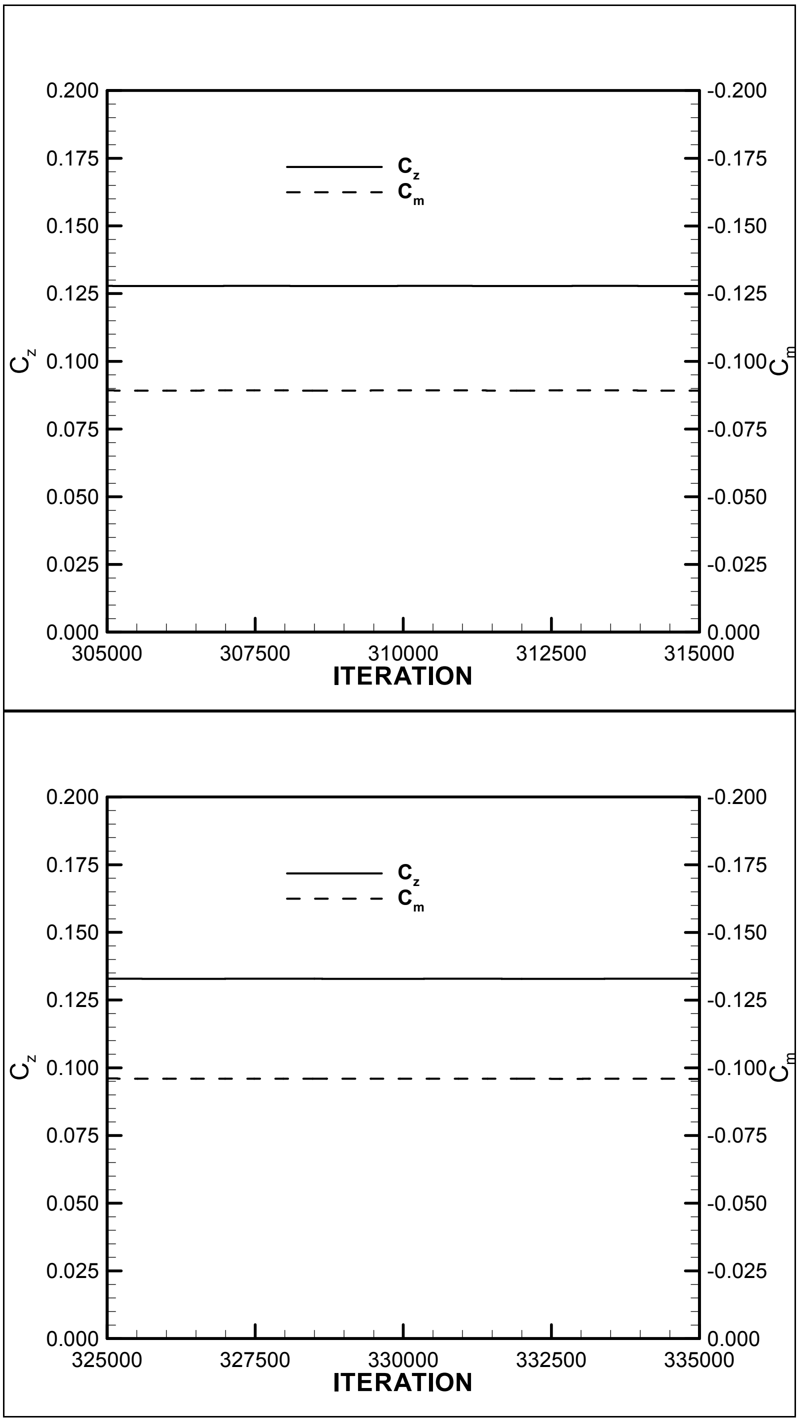

Fig. 4.75 N-S Nonuniform Inlet Velocity Profile Solution for M=0.7, β =51° and shift=0.50 and shift=0.75

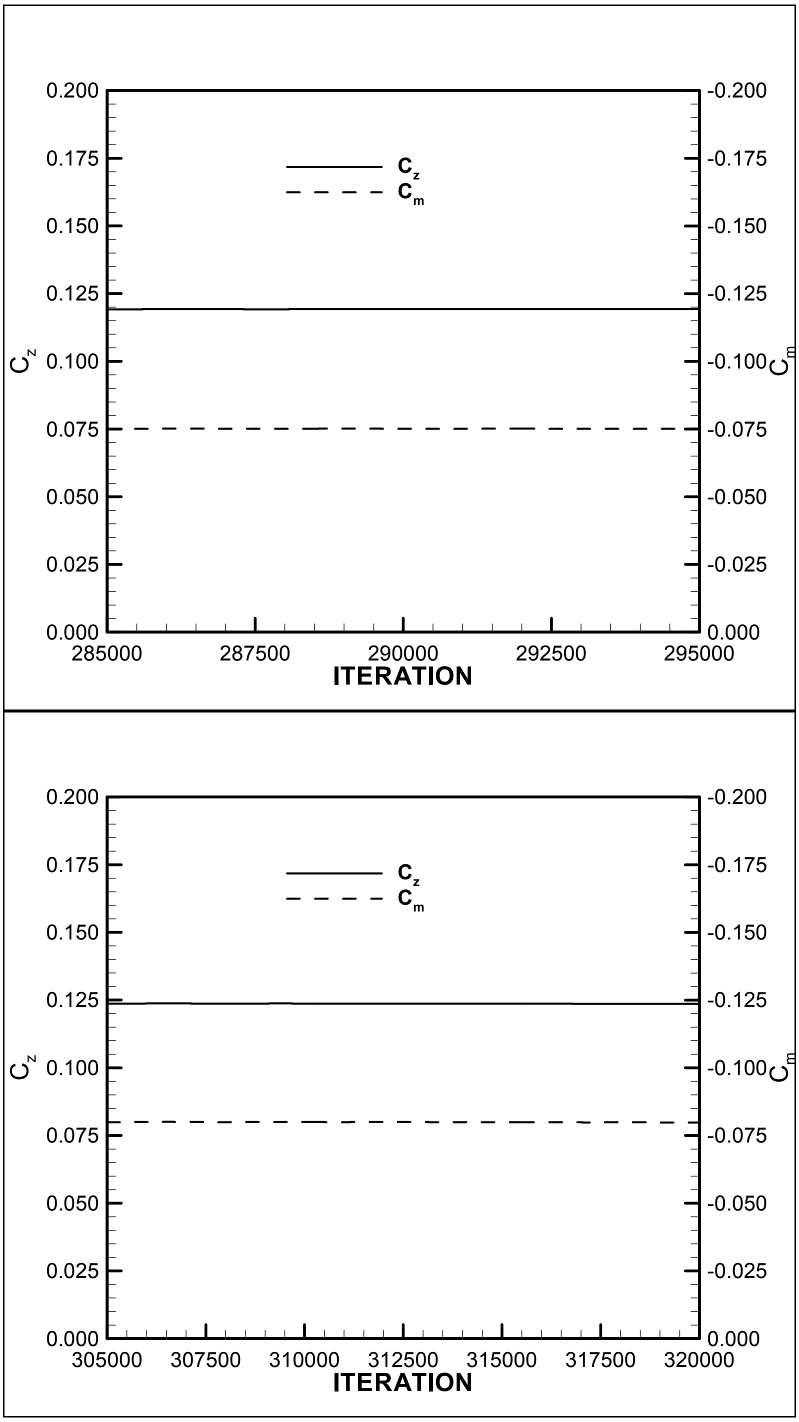

Fig. 4.76 N-S Nonuniform Inlet Velocity Profile Solution for M=0.7, β =53° and shift=0.0 and shift=0.25

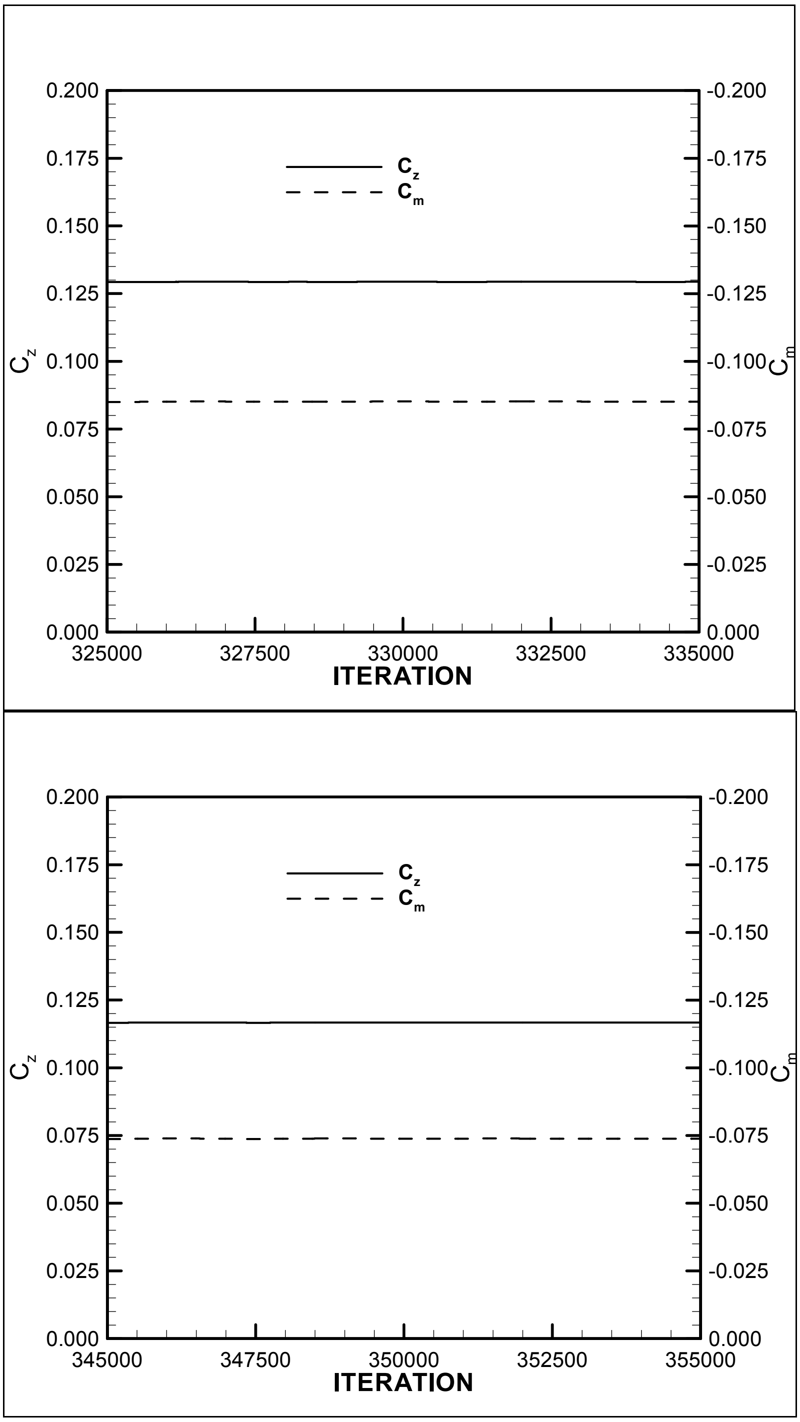

Fig. 4.77 N-S Nonuniform Inlet Velocity Profile Solution for M=0.7, β =53° and shift=0.50 and shift=0.75

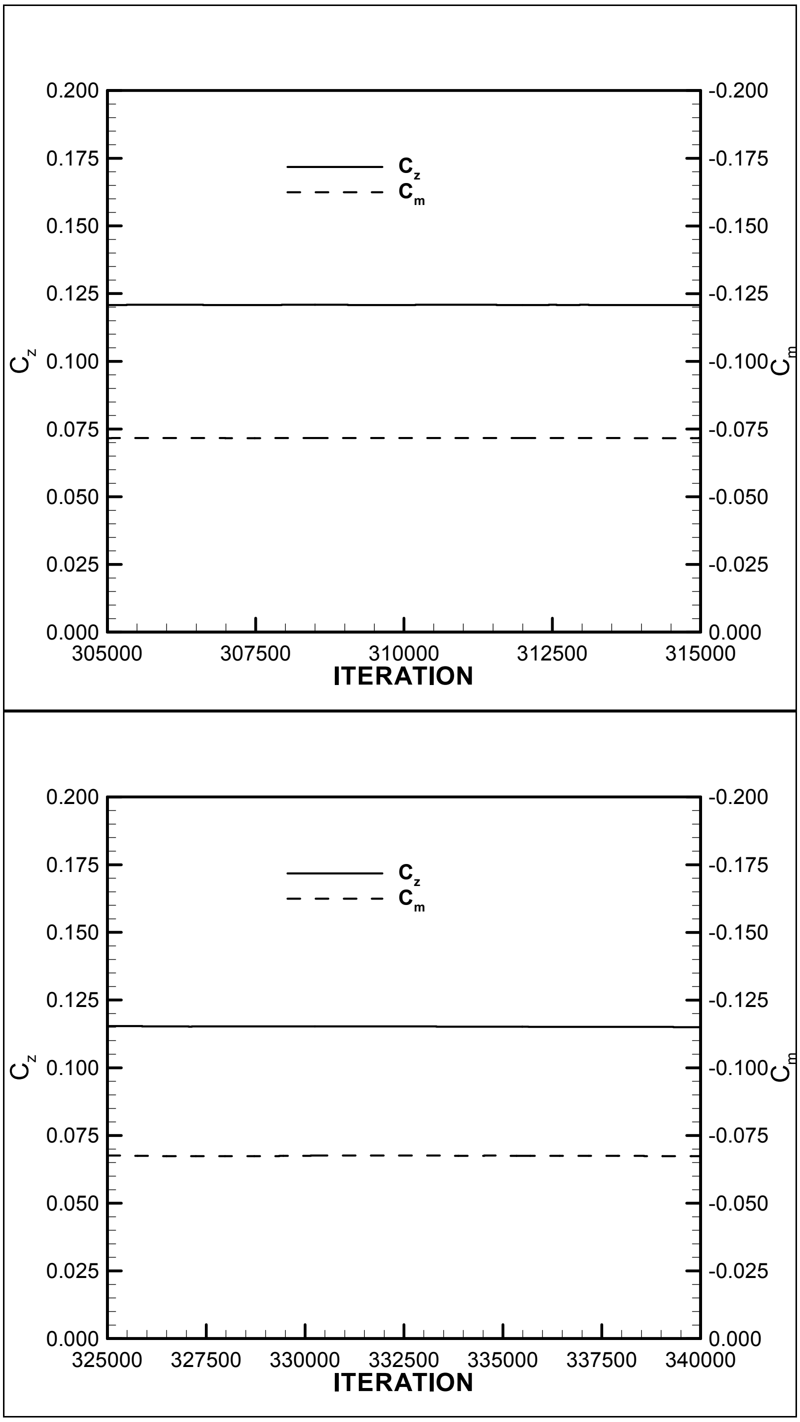

Fig. 4.78 N-S Nonuniform Inlet Velocity Profile Solution for M=0.7, β =55° and shift=0.0 and shift=0.25

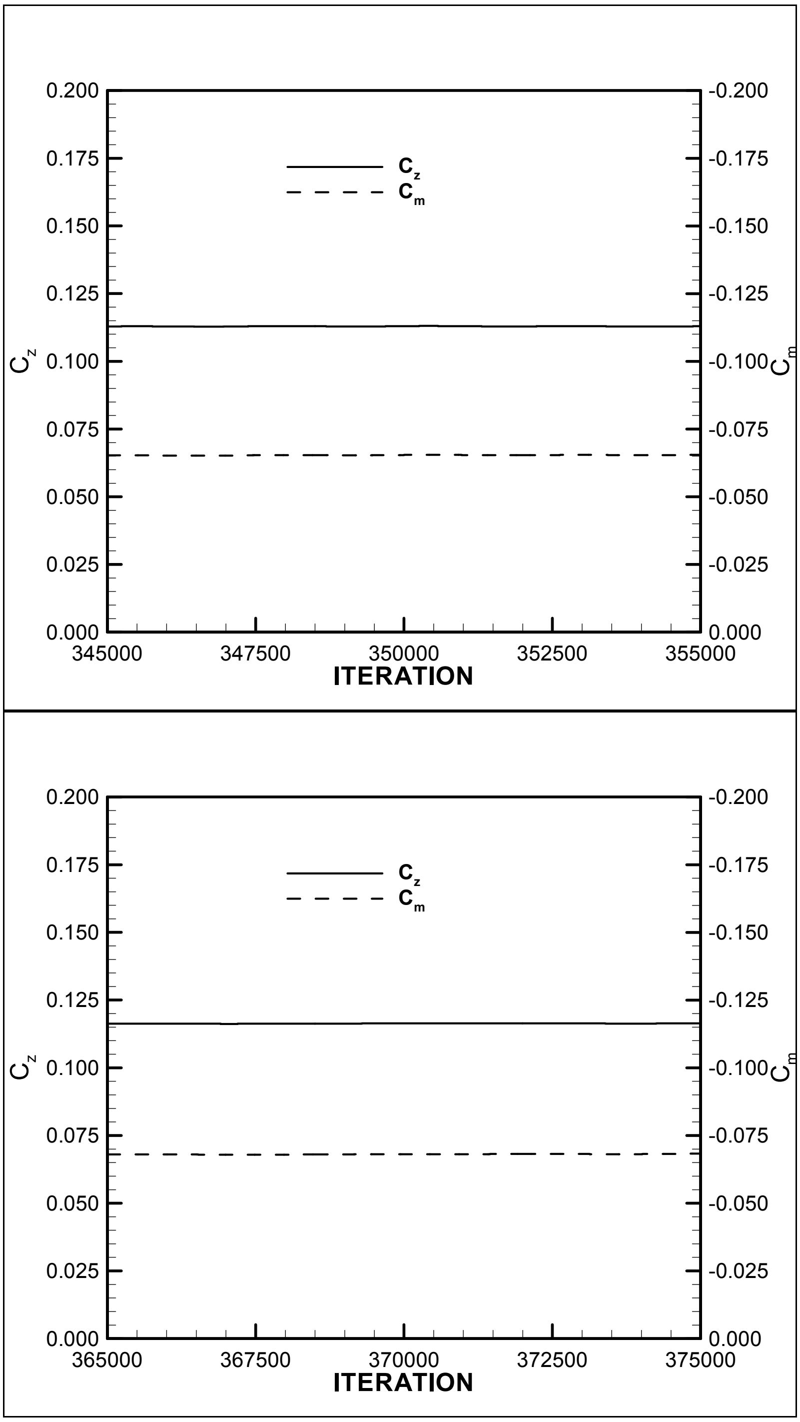

Fig. 4.79 N-S Nonuniform Inlet Velocity Profile Solution for M=0.7, β =55° and shift=0.50 and shift=0.75

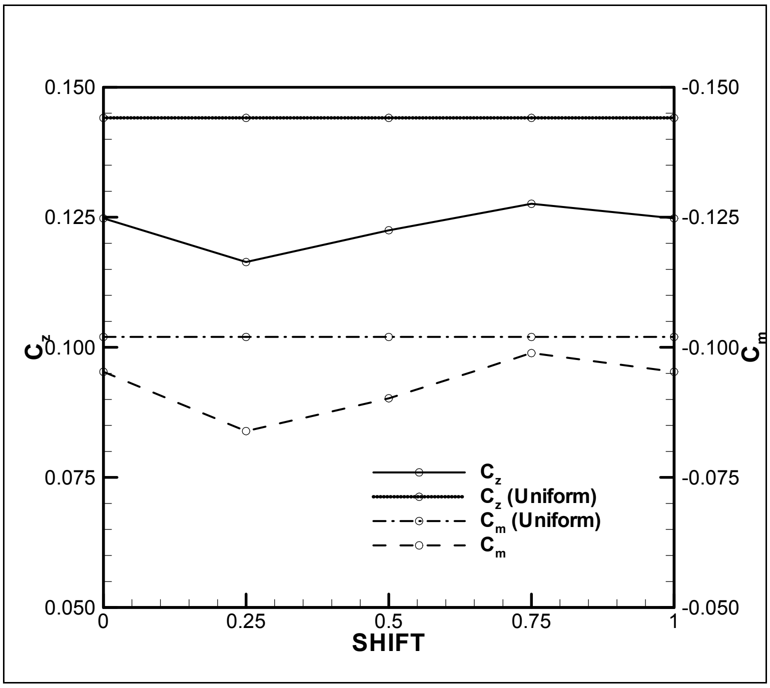

Fig. 4.80 Comparison of N-S Nonuniform Inlet Velocity Profile Solution with the uniform solution for M=0.7, β =49° and all shifts

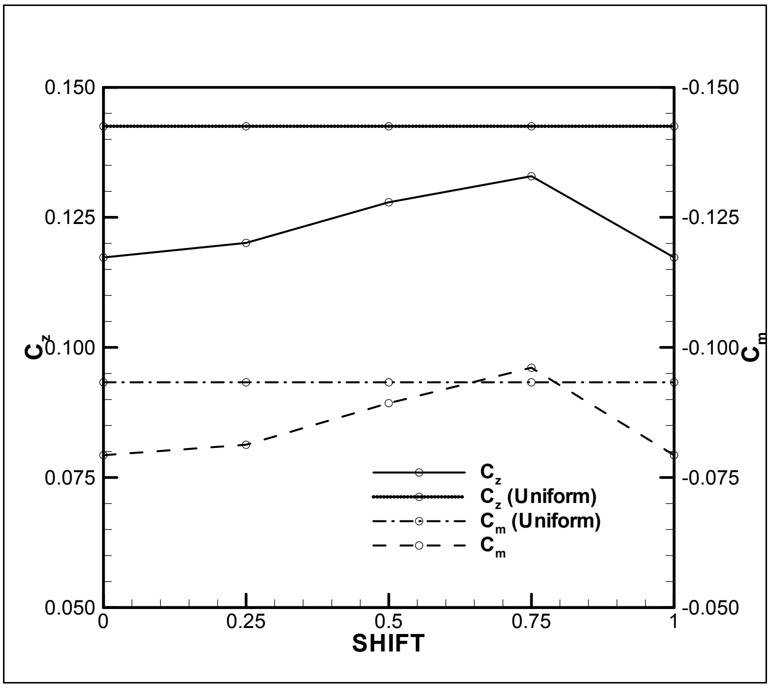

Fig. 4.81 Comparison of N-S Nonuniform Inlet Velocity Profile Solution with the uniform solution for M=0.7, β =51° and all shifts

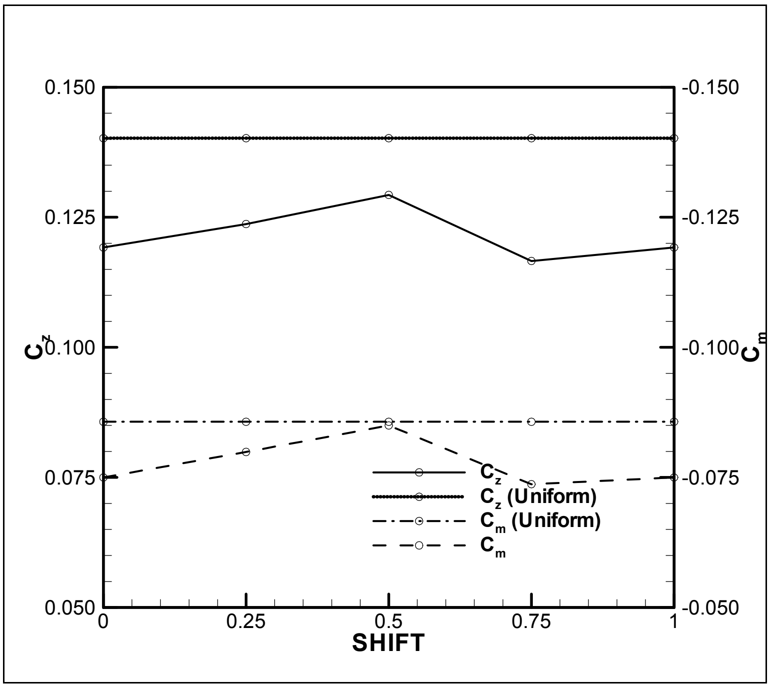

Fig. 4.82 Comparison of N-S Nonuniform Inlet Velocity Profile Solution with the uniform solution for M=0.7, β=53° and all shifts

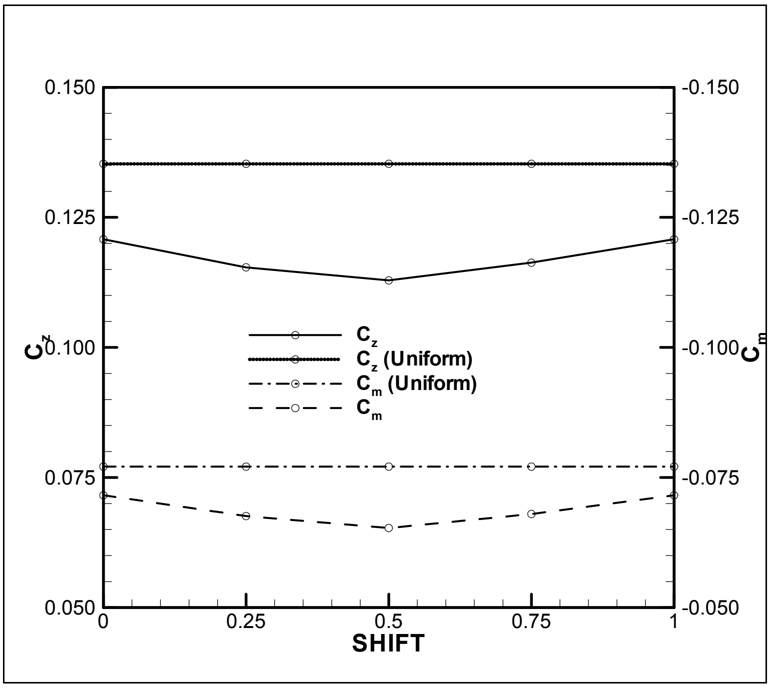

Fig. 4.83 Comparison of N-S Nonuniform Inlet Velocity Profile Solution with the uniform solution for M=0.7, β=55° and all shifts

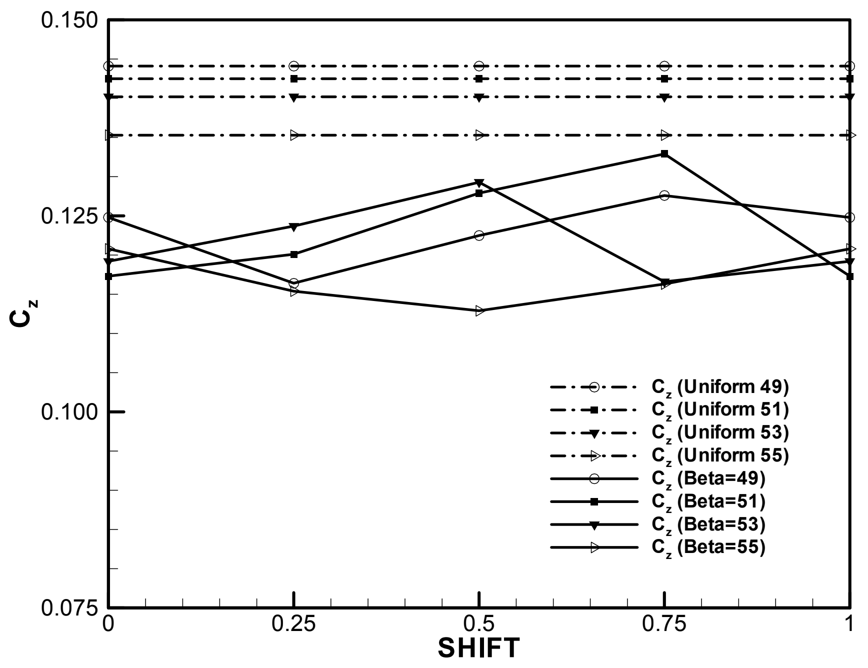

Fig. 4.84 Comparison of N-S Nonuniform Inlet Velocity Profile Solution with the uniform solution for M=0.7, all β s and all shifts

All above figures show that C_z and C_m values converged at least for the last 10000 iterations. For different shifts, converged value is different and this is good evidence for our theory.

Fig. 4.84 shows that there is an optimum value for each inlet angle that corresponds to a shift value. For example, when wake position or shift is on 0.75 location, β angle 51° has its maximum C_z value. Similarly for different shift locations there is different β angles that has the maximum C_z value.

Following figures also presents the surface pressure values compared with the experimental and N-S uniform solution. Similar disscussions can be done for that plots also.

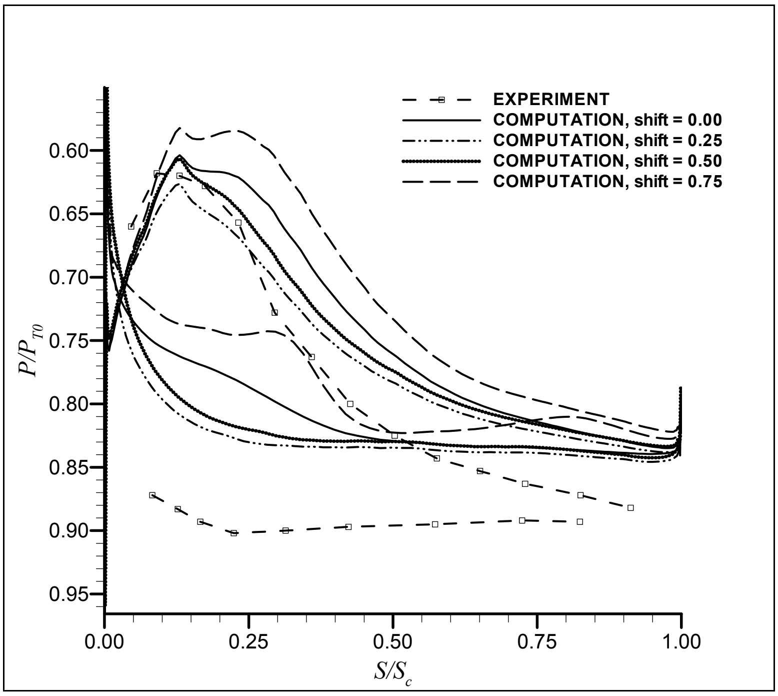

Fig. 4.85 N-S Solution comparison of surface pressures for M=0.7, β =49° and all shifts

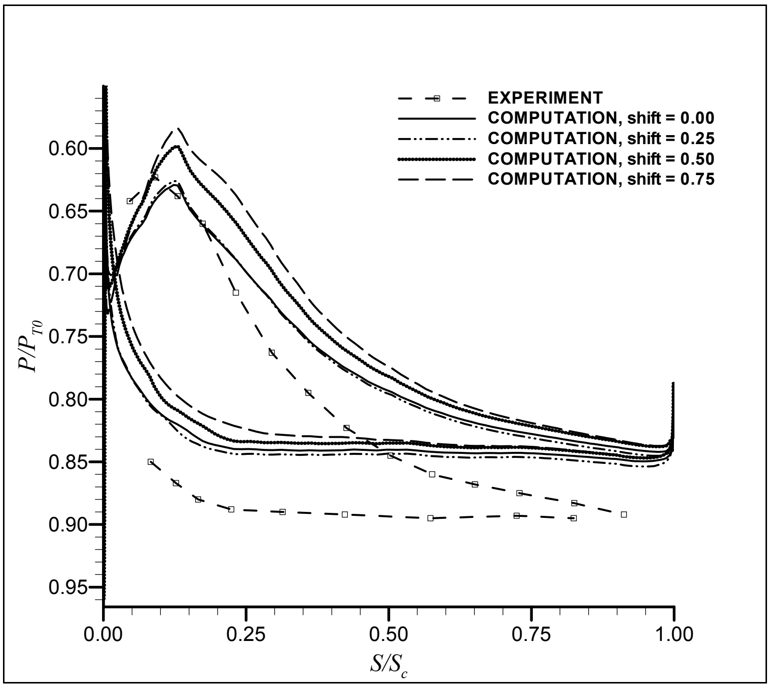

Fig. 4.86 N-S Solution comparison of surface pressures for M=0.7, β =51° and all shifts

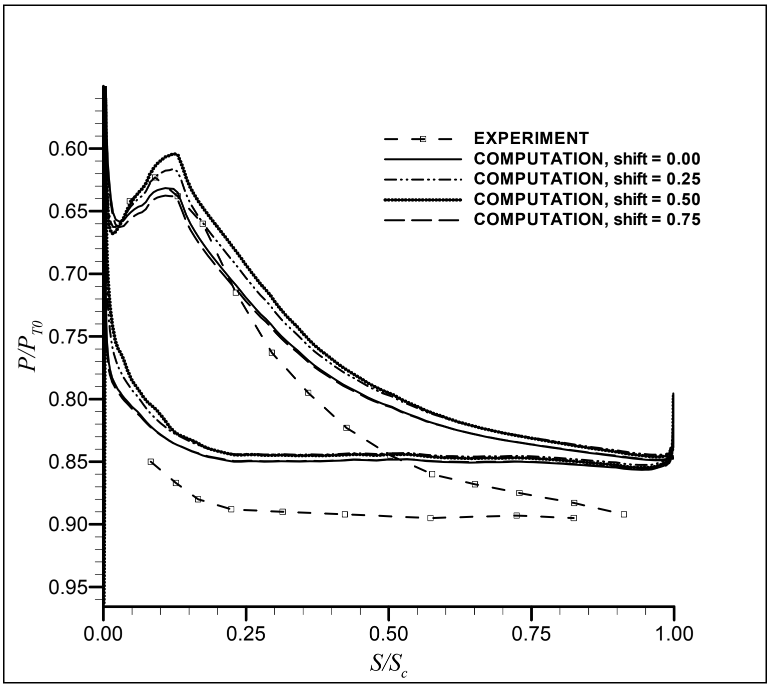

Fig. 4.87 N-S Solution comparison of surface pressures for M=0.7, β =53° and all shifts

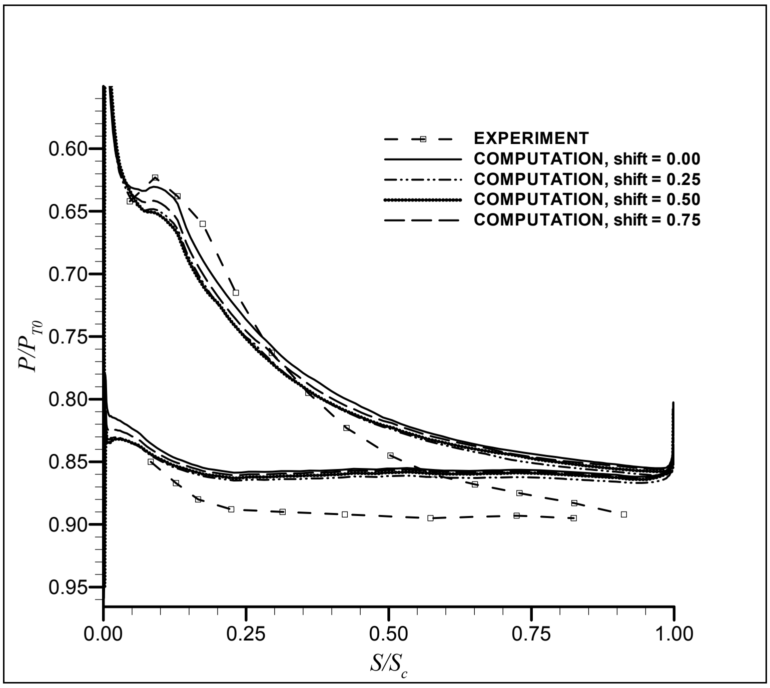

Fig. 4.88 N-S Solution comparison of surface pressures for M=0.7, β =55° and all shifts

CHAPTER V

UNSTEADY ANALYSES

In this chapter, unsteady analyses of the nonlinear inlet velocity profile cases are presented. Constant time step is used. The inlet velocity profile (or wake) shifts upwards at each time step (iteration) continuously. Period is defined as the time required for the rotor blade to go from one rotor blade to other and the period of this motion is selected as T=0.1 and T=1.0 based on the following assumptions and calculations:

Nondimensional time ($\bar{t}$) and period ($\bar{T}$) in PML3D is defined as follows:

$$\bar{t} = \frac{t}{L / a_\infty} \quad \text{for our case } L = c \tag{5.1}$$

$$\bar{T} = \frac{T}{c / a_\infty} \tag{5.2}$$

Assuming 10,000 m flight altitude yields $a_\infty = 299.5$ m/s, and approximately taken the chord value $c = 0.1$ m also yields the spacing $b = 0.0295$ m. By engineering approximations, radius of the engine has been selected as 0.75 m and RPM as 10,000 or 1047.2 rad/s. The tangential velocity is at the end 785 m/s which is the multiplication of radius with the RPM.

From the above definition of one period:

$$T = \frac{b}{V} = \frac{0.0295m}{785m/s} = 3.76 \times 10^{-5}s \tag{5.3}$$

$$\overline{T} = \frac{T}{c/a_\infty} = \frac{3.76 \times 10^{-5}}{0.1/299.5} = 0.1126 \approx 0.1$$

Therefore, nondimensional period of the calculations has selected 0.1 initially, but later in order to compare the different periods 10 times greater period which is T=1.0 has been selected and the results are obtained.

5.1. Unsteady Navier Stokes Solution:

5.1.1. Grid:

The same H-O-H type grid which was also used for the steady Navier Stokes Solutions with nonuniform inlet velocity profile cases is used.

5.1.2. Boundary Conditions:

For the center O-Grid at L=LMAX top and Bottom surfaces are periodic. Matched Surface Boundary Conditions are applied at the common boundaries with the front and rear blocks. At L=1, the surface boundary conditions are applied. J=1 and J=JMAX boundaries coincides (the wake behind the T.E.) and the periodic boundary conditions are applied at those boundaries.

For the front grid at J=1 a special unsteady boundary condition for CA115 stator cascade in rotor wake problem is specified. The nonuniform inlet velocity profile described in the steady Navier Stokes solutions chapter (Section 4.3) shifts upwards continuously at each time step. Full mshift is completed in a given period of time. At J=JMAX, Matched surface boundary conditions are applied with the central O-Block. L=1 (bottom surface) and L=LMAX (top surface) are periodic with each other.

For the rear grid at J=1 Matched surface boundary conditions are applied with the central O-Block. J=JMAX is the flow out plane pressure fixed extrapolation type boundary conditions are used. L=1 (bottom surface) and L=LMAX (top surface) are periodic with each other.

5.1.2.1. Calculation of exit to inlet static pressure ratio:

For the J=JMAX flow out plane pressure fixed extrapolation type boundary conditions are applied. $\frac{P_2}{P_1}$ values which are same as the $\frac{P_2}{P_1}$ values of the corresponding steady nonuniform Navier Stokes cases for shift=0.00 are used. These values are summarized in Table 5.1 below.

Table 5.1 Exit to inlet static pressure ratios for Unsteady Navier Stokes nonuniform inlet profile solution

Mach number	β angle	$\frac{P_2}{P_1}$
0.7	49°	1.187
0.7	51°	1.196
0.7	53°	1.205
0.7	55°	1.213

5.1.3. Results

In this section convergence in form of force and moment coefficients C_z and C_m vs iteration plots of the H-O-H grid, M=0.7, and β=49°, 51°, 53°, 55° unsteady N-S solutions are presented in Figs. from 5.1 to 5.3 initially for nondimensional period 0.1. In Figs. From 5.4 to 5.7 again convergence histories of the H-O-H grid, M=0.7, and

β =49°, 51°, 53°, 55° unsteady N-S solutions are presented but these results are obtained with the nondimensional period 1.0.

In the following figures both pressure and mach contours for periods 0.1 and 1.0 are presented.

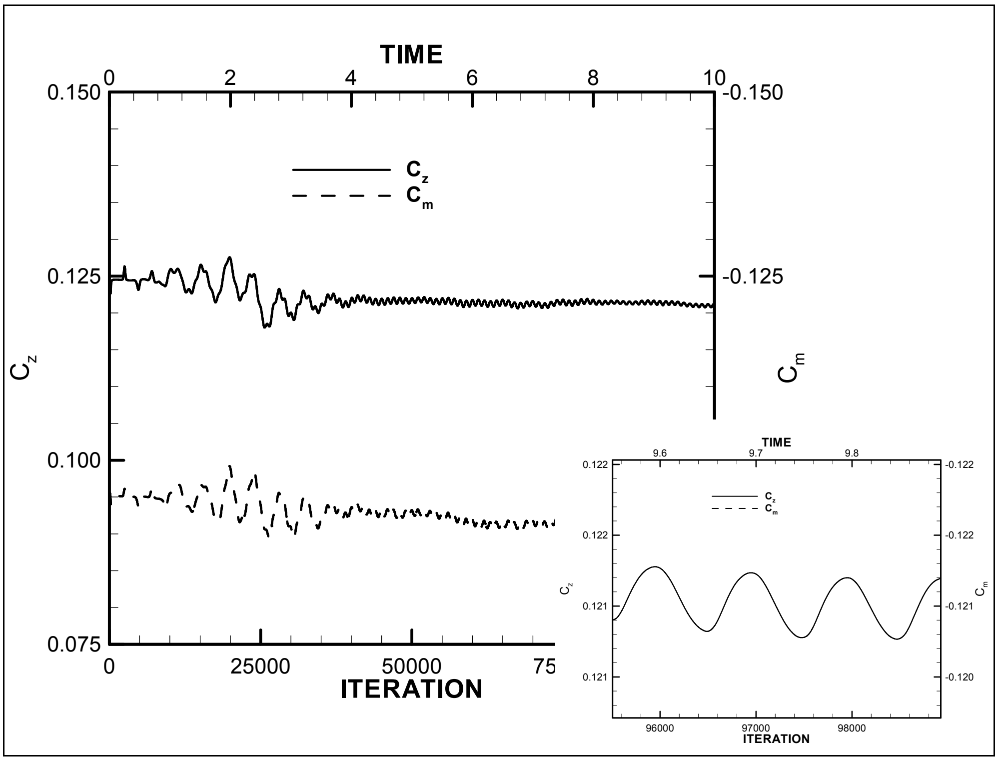

Fig. 5.1 N-S Nonuniform Inlet Velocity Profile Solution for M=0.7, β =49° and periodic wake shifting for period=0.1

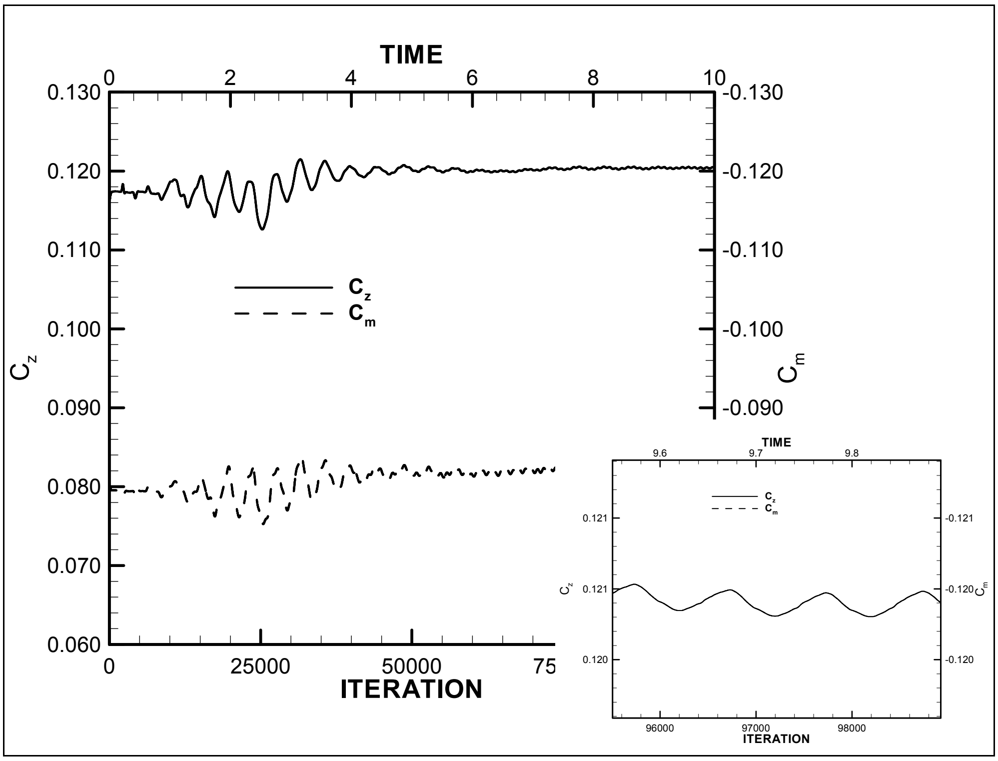

Fig. 5.2 N-S Nonuniform Inlet Velocity Profile Solution for M=0.7, β =51° and periodic wake shifting for period=0.1

In Figs. 5.1 and 5.2 it is obvious that there is oscillations in the force and momet coefficients. But the amplitude of the oscillation is so small that we can conclude that effect of rotor wake in the stator inlet flow for period 0.1 is negligible. As can be seen from the small figure at the bottom of the Figs. 5.1-5.3 the period is achieved in 1000 iterations which is exactly what is expected at the beginnig because the time step employed in this analysis has been 0.0001 and a period 0.1 is obtained in 1000 iterations.

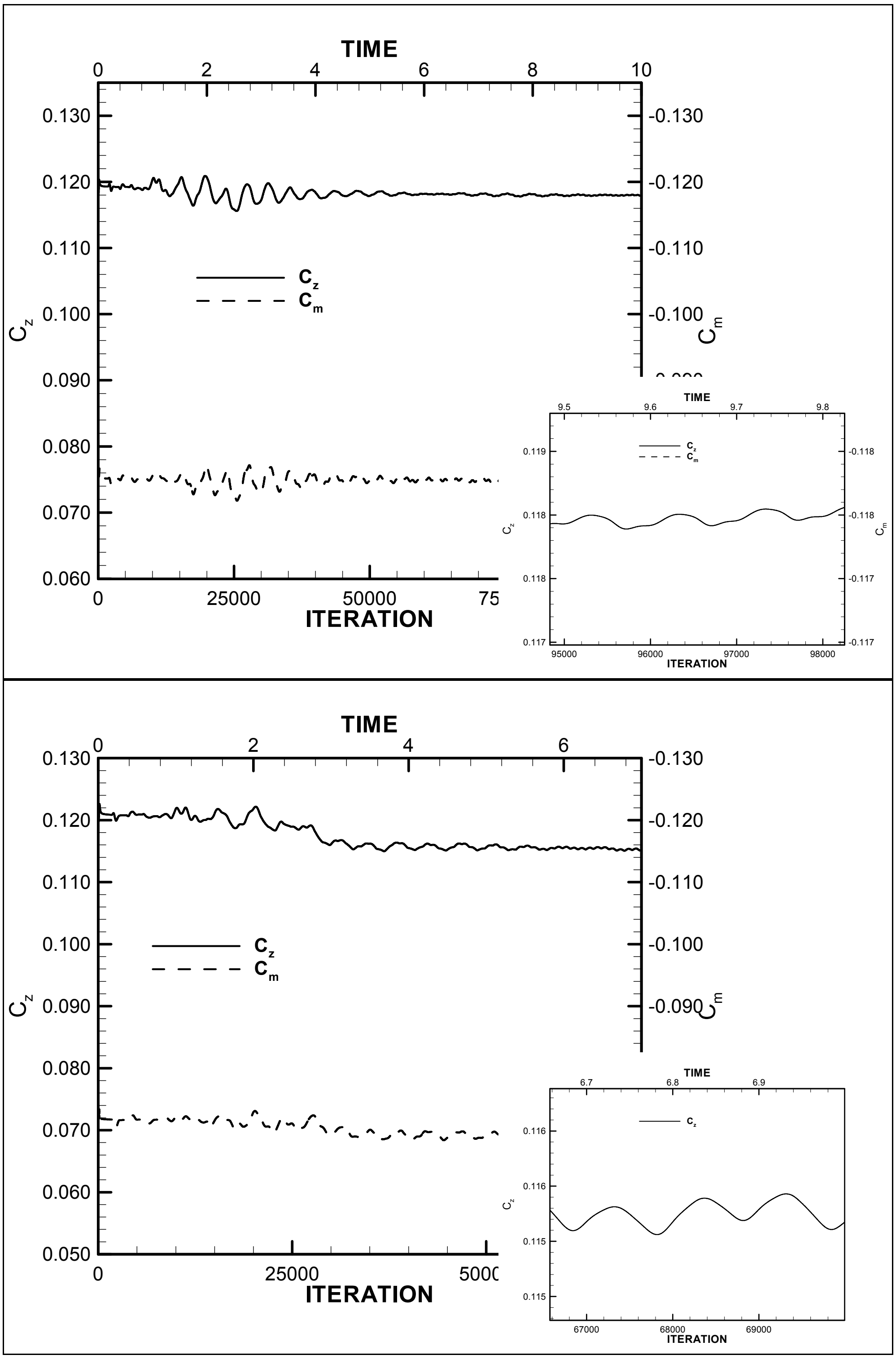

Fig. 5.3 N-S Nonuniform Inlet Velocity Profile Solution for M=0.7, β =53°(top) and 55° (bottom) and periodic wake shifting for period=0.1

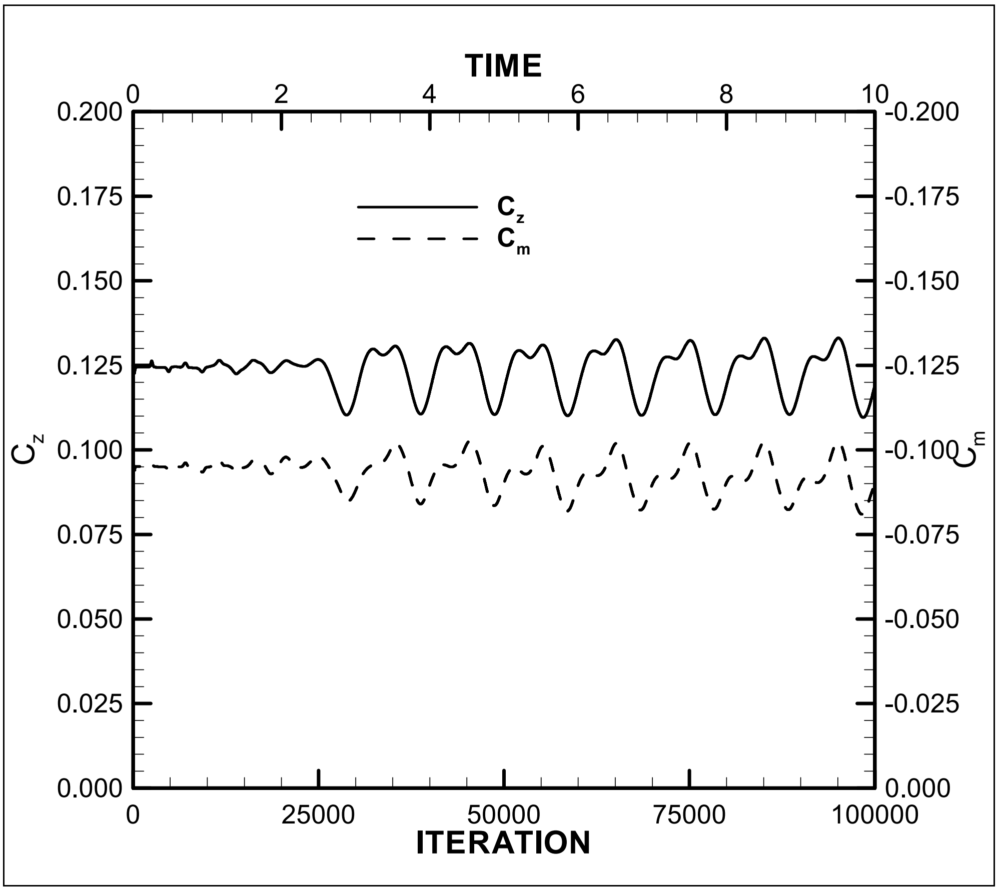

Fig. 5.4 N-S Nonuniform Inlet Velocity Profile Solution for M=0.7, β =49° and periodic wake shifting for period=1.0

In the Figs from 5.4 to 5.7 periodicity of the rotor wake has increased 10 times. Similar results presented in the section 4.3 have been expected due to large period time introduced in that analysis.

Results in the Figs from 5.4 to 5.7 shows that the amplitude has increased more than 10 times increase with an increase of 10 times in the period. It can be concluded that, the oscillation amplitude of the force and moment results are greatly dependent on the period of the wake introduced.

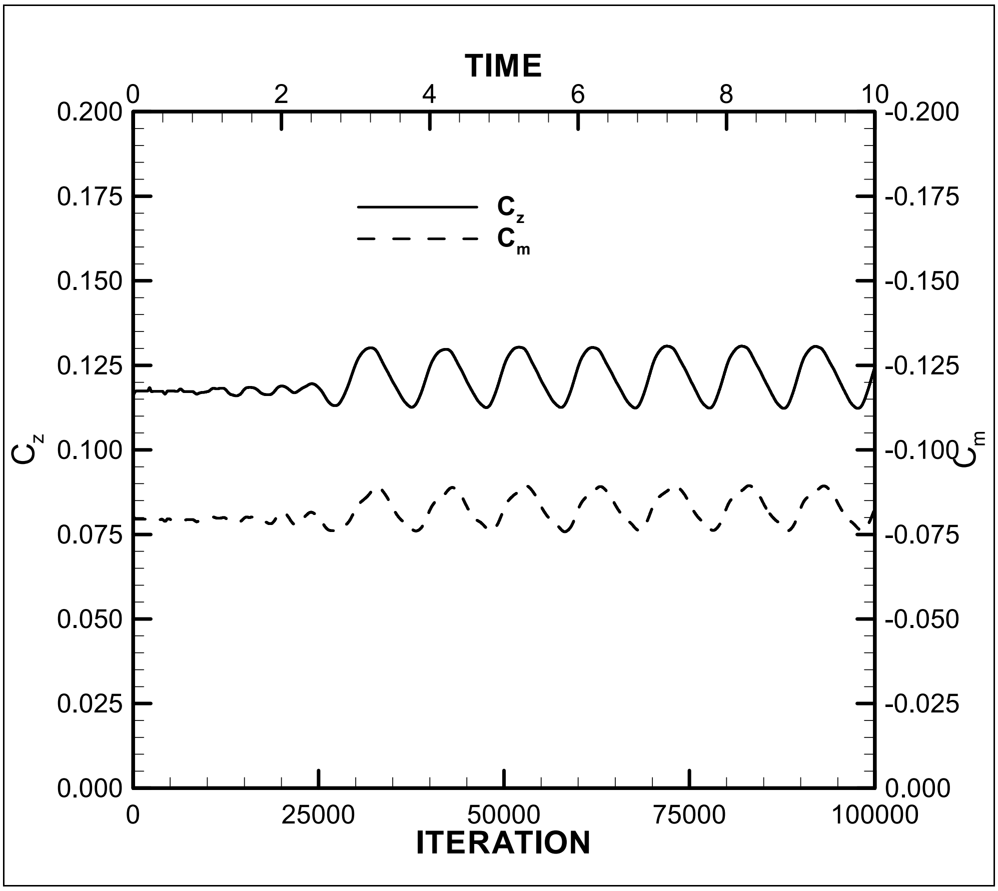

Fig. 5.5 N-S Nonuniform Inlet Velocity Profile Solution for M=0.7, β=51° and periodic wake shifting for period=1.0

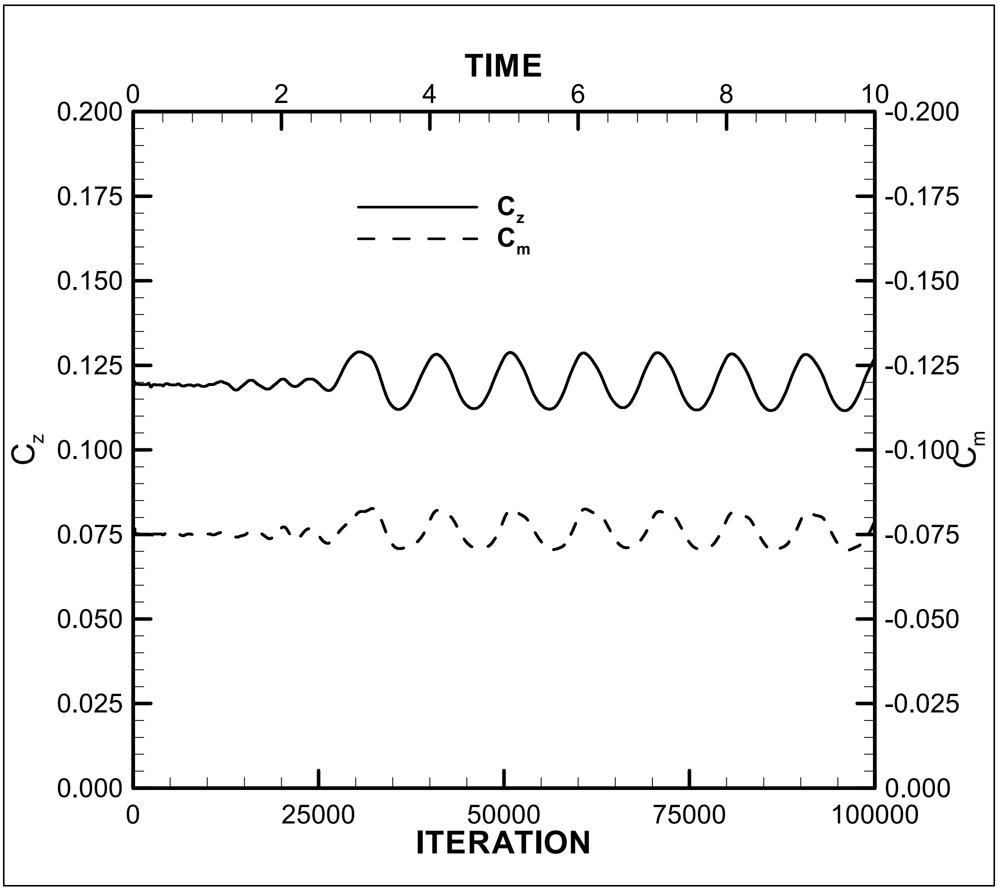

Fig. 5.6 N-S Nonuniform Inlet Velocity Profile Solution for M=0.7, β =53° and periodic wake shifting for period=1.0

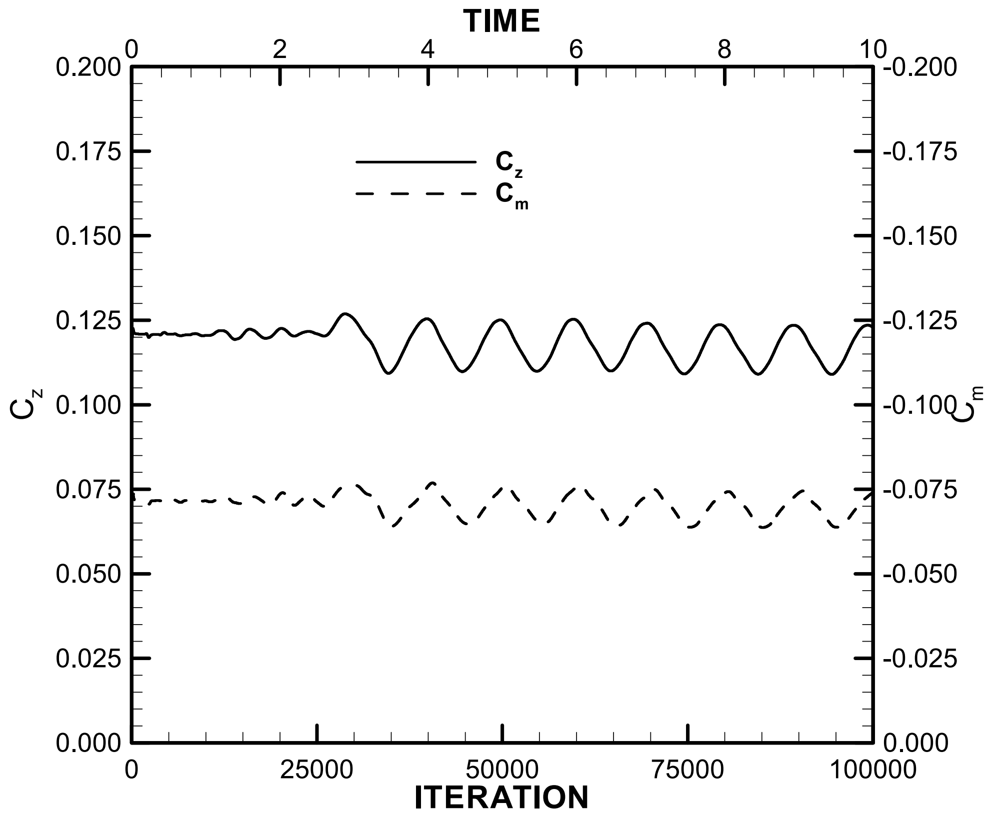

Fig. 5.7 N-S Nonuniform Inlet Velocity Profile Solution for M=0.7, β =55° and periodic wake shifting for period=1.0

In the following figures pressure and mach contours are presented for both periods that have been considered.

Effect of the rotor wake at the stator inlet flow can be seen more directly in the larger period results (for period = 1.0). Periodic changes in the contours especially at the front block can be seen easily also.

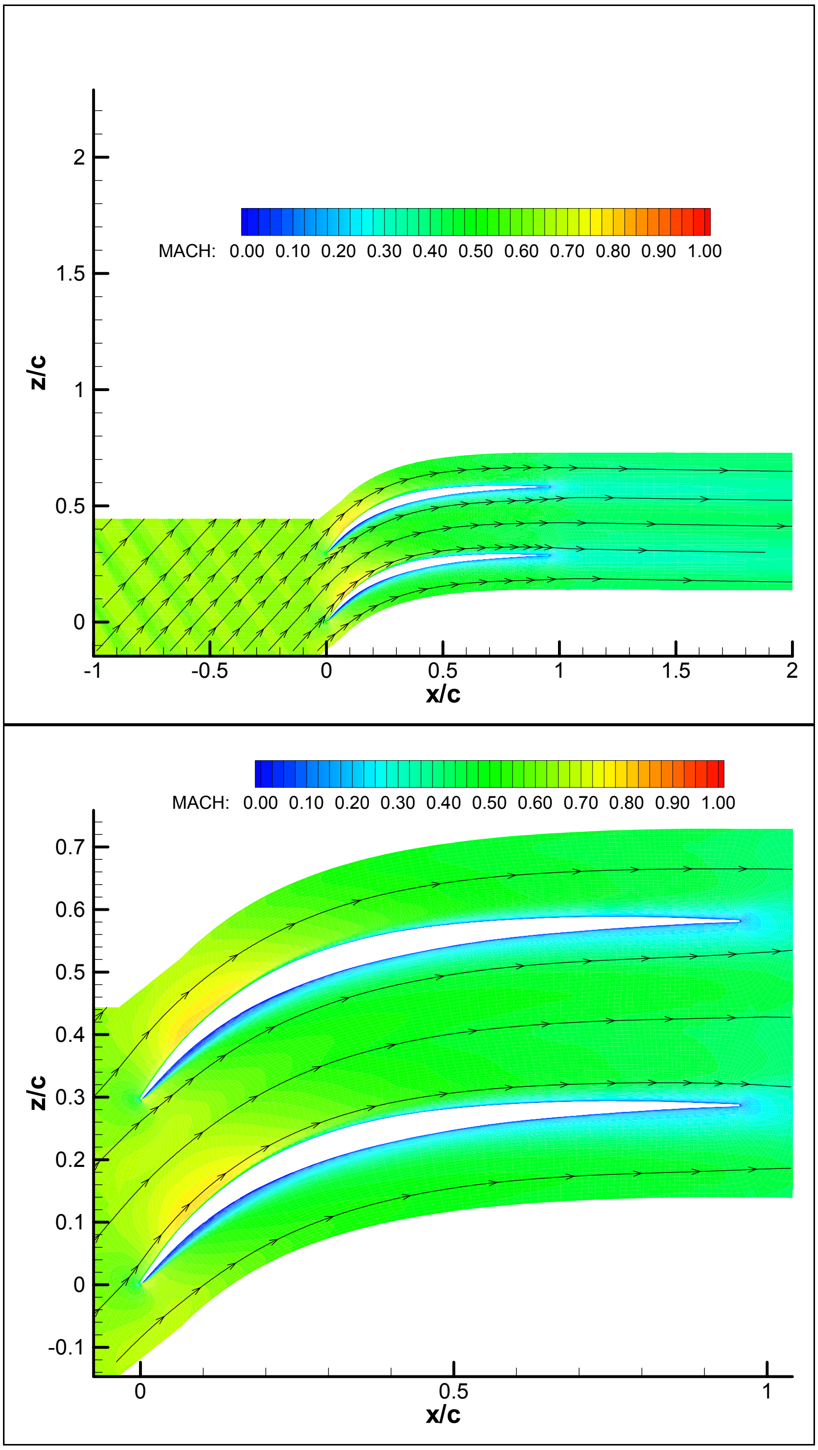

Fig. 5.8 N-S Nonuniform Inlet Velocity Profile Solution Mach Contours for M=0.7, β=49° and period=0.1

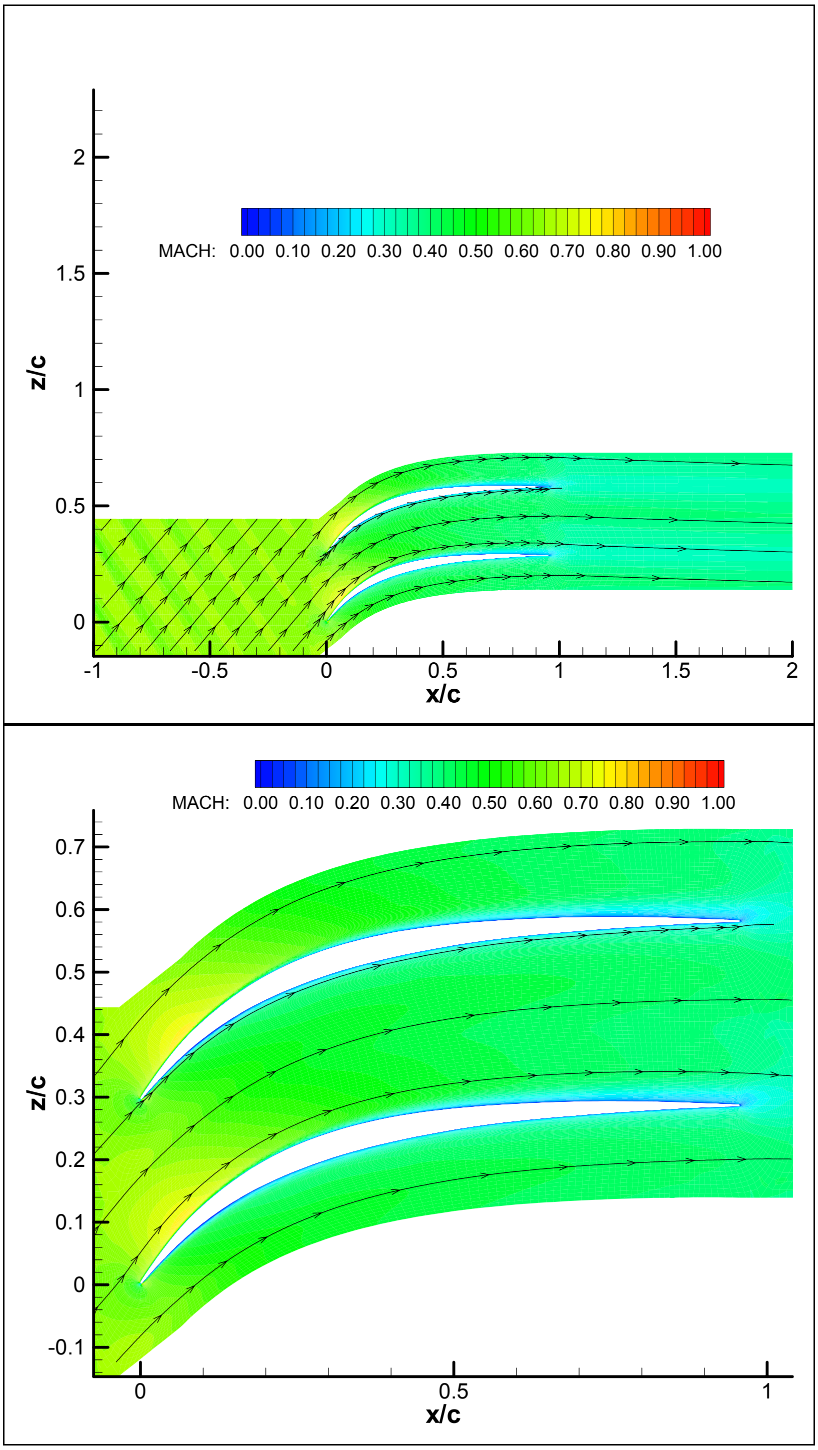

Fig. 5.9 N-S Nonuniform Inlet Velocity Profile Solution Mach Contours for M=0.7, β=51° and period=0.1

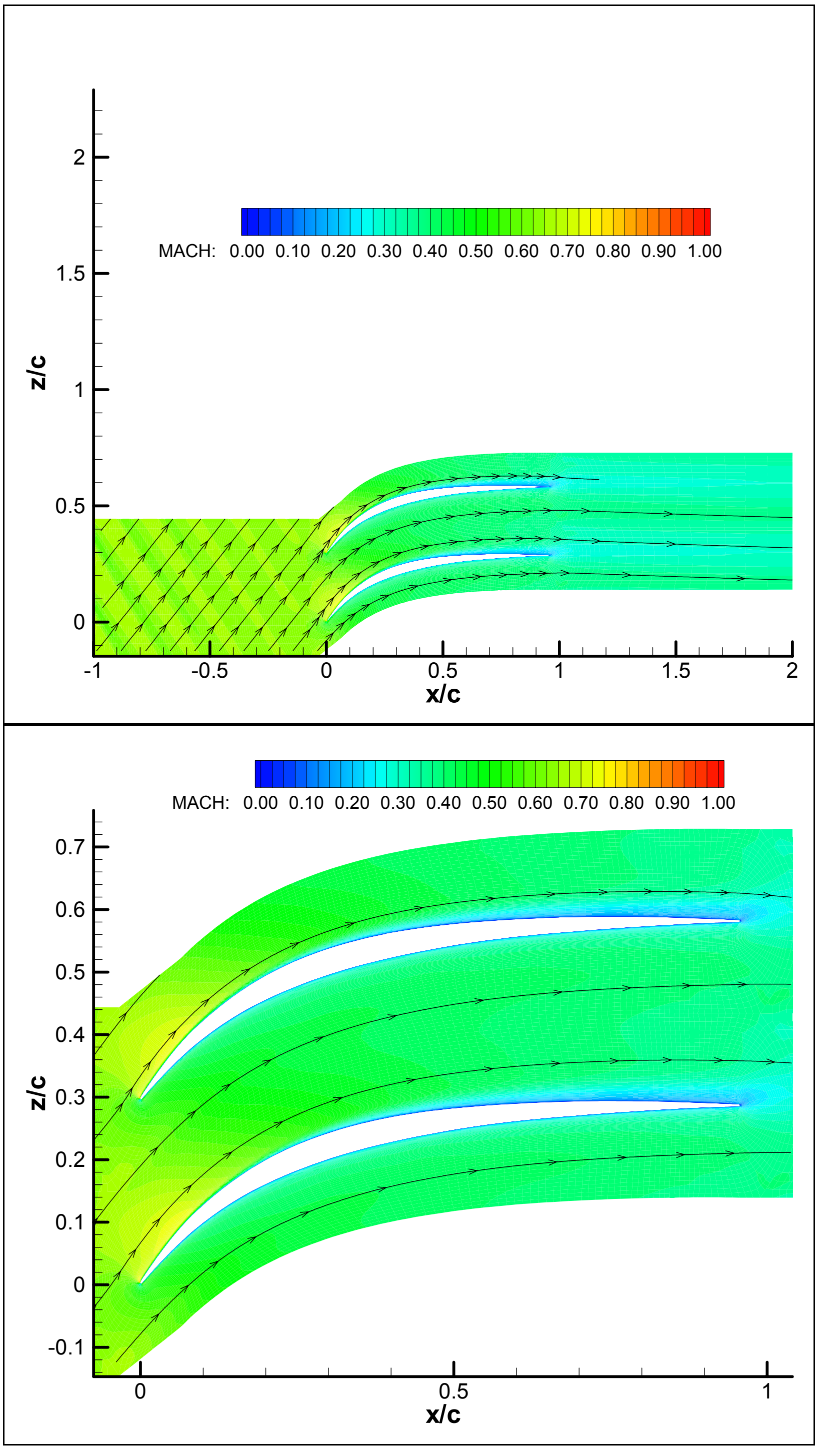

Fig. 5.10 N-S Nonuniform Inlet Velocity Profile Solution Mach Contours for M=0.7, β=53° and period=0.1

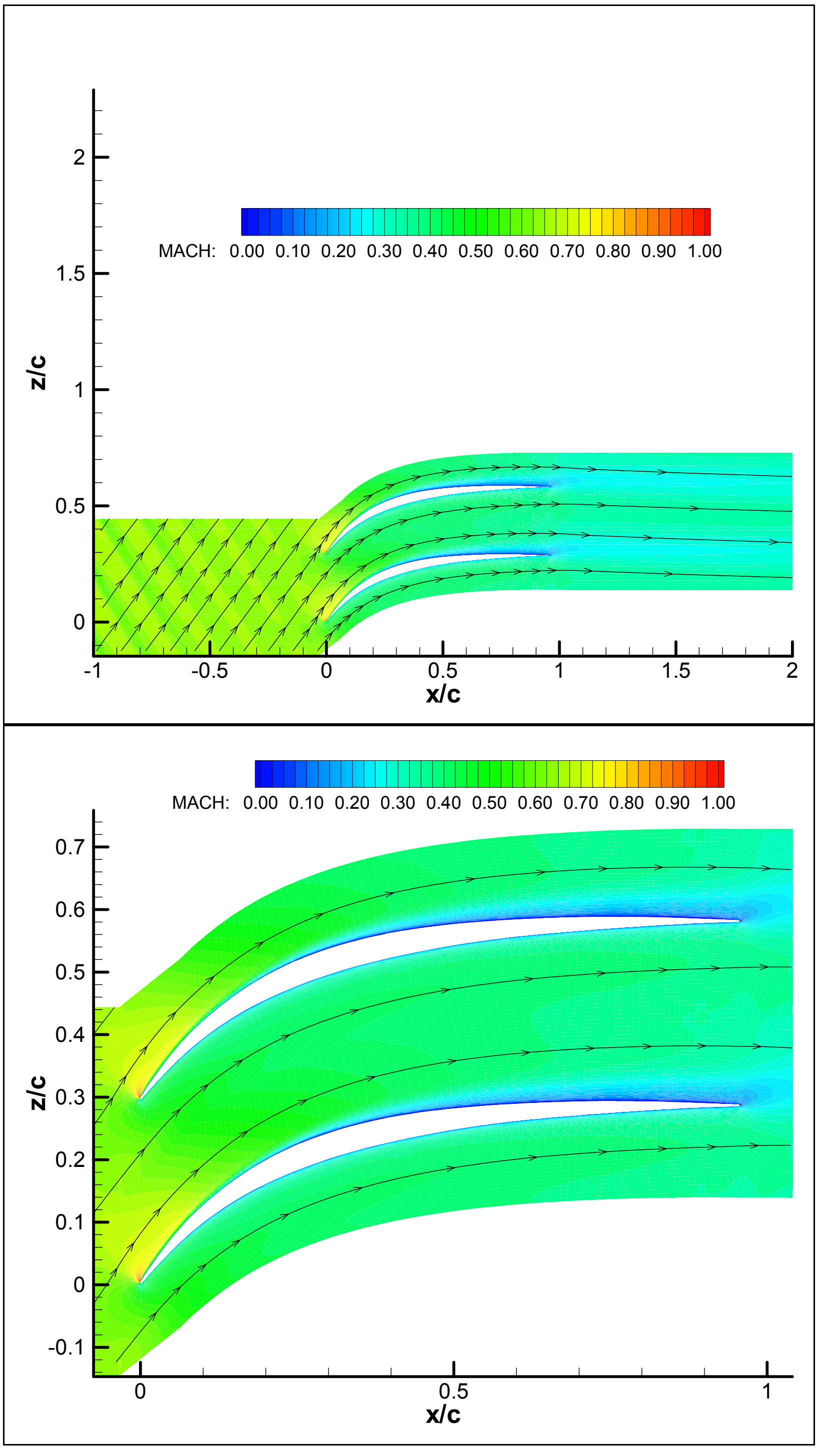

Fig. 5.11 N-S Nonuniform Inlet Velocity Profile Solution Mach Contours for M=0.7, β=55° and period=0.1

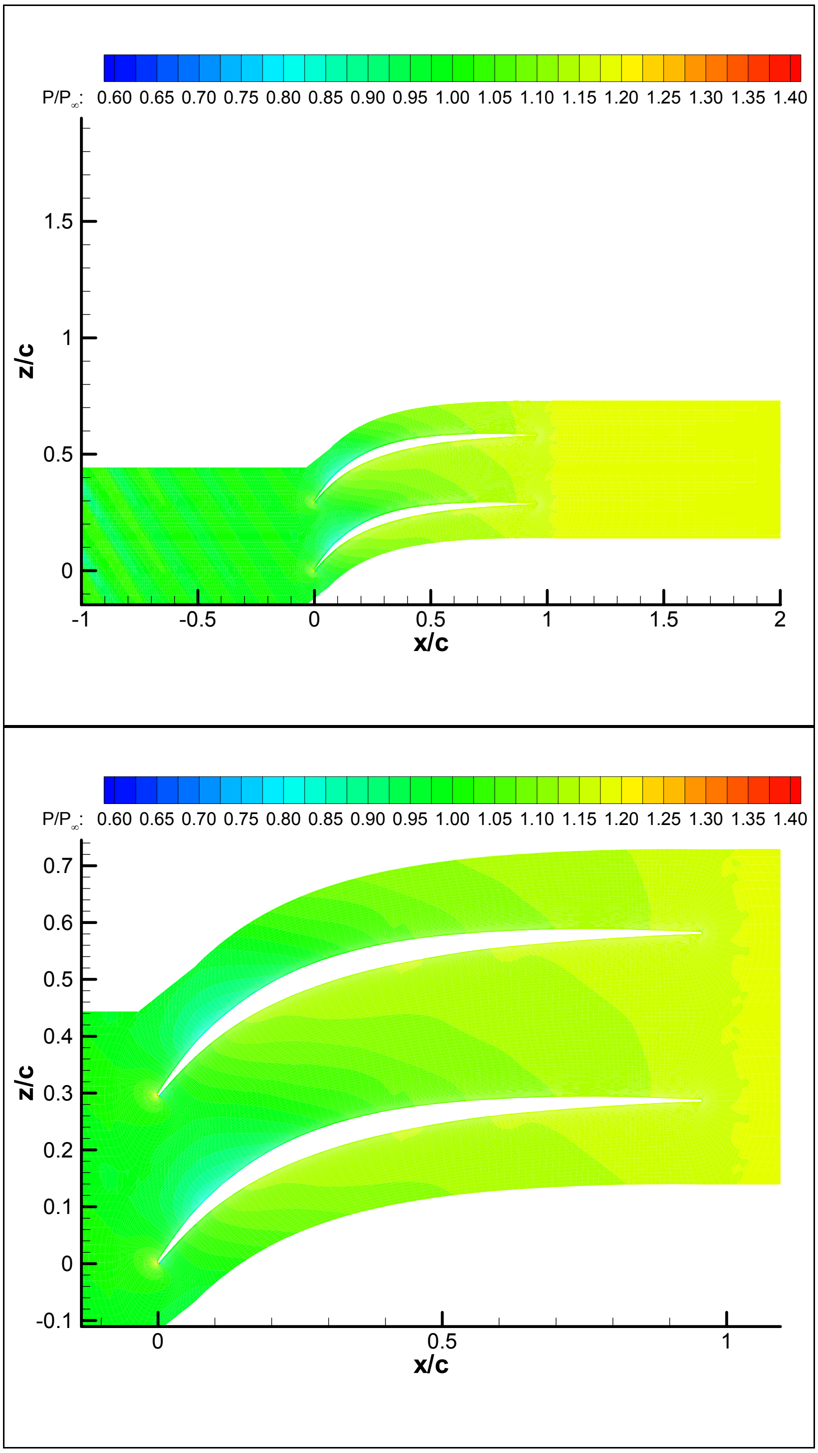

Fig. 5.12 N-S Nonuniform Inlet Velocity Profile Solution Pressure Contours for M=0.7, β=49° and period=0.1

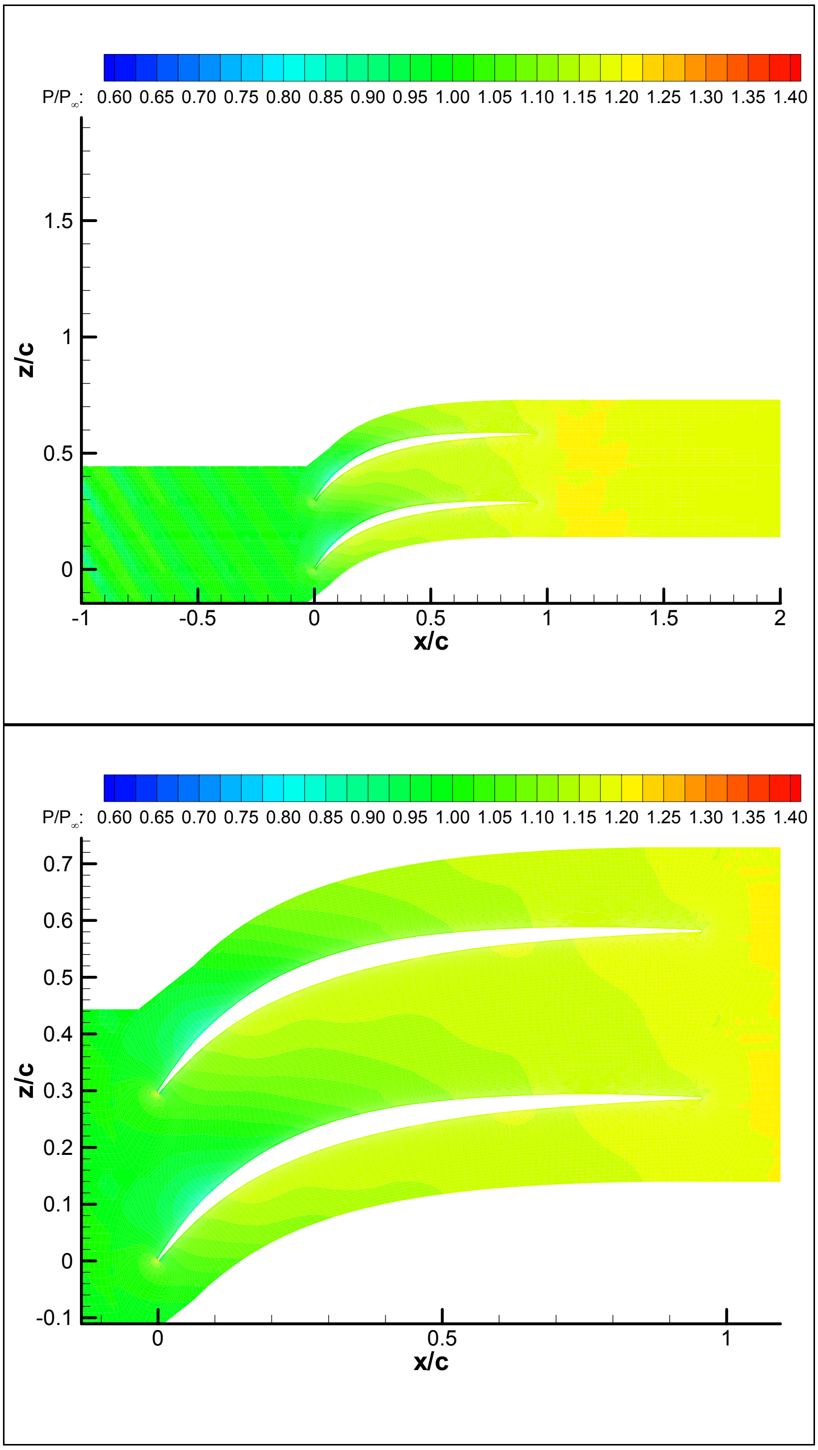

Fig. 5.13 N-S Nonuniform Inlet Velocity Profile Solution Pressure Contours for M=0.7, β=51° and period=0.1

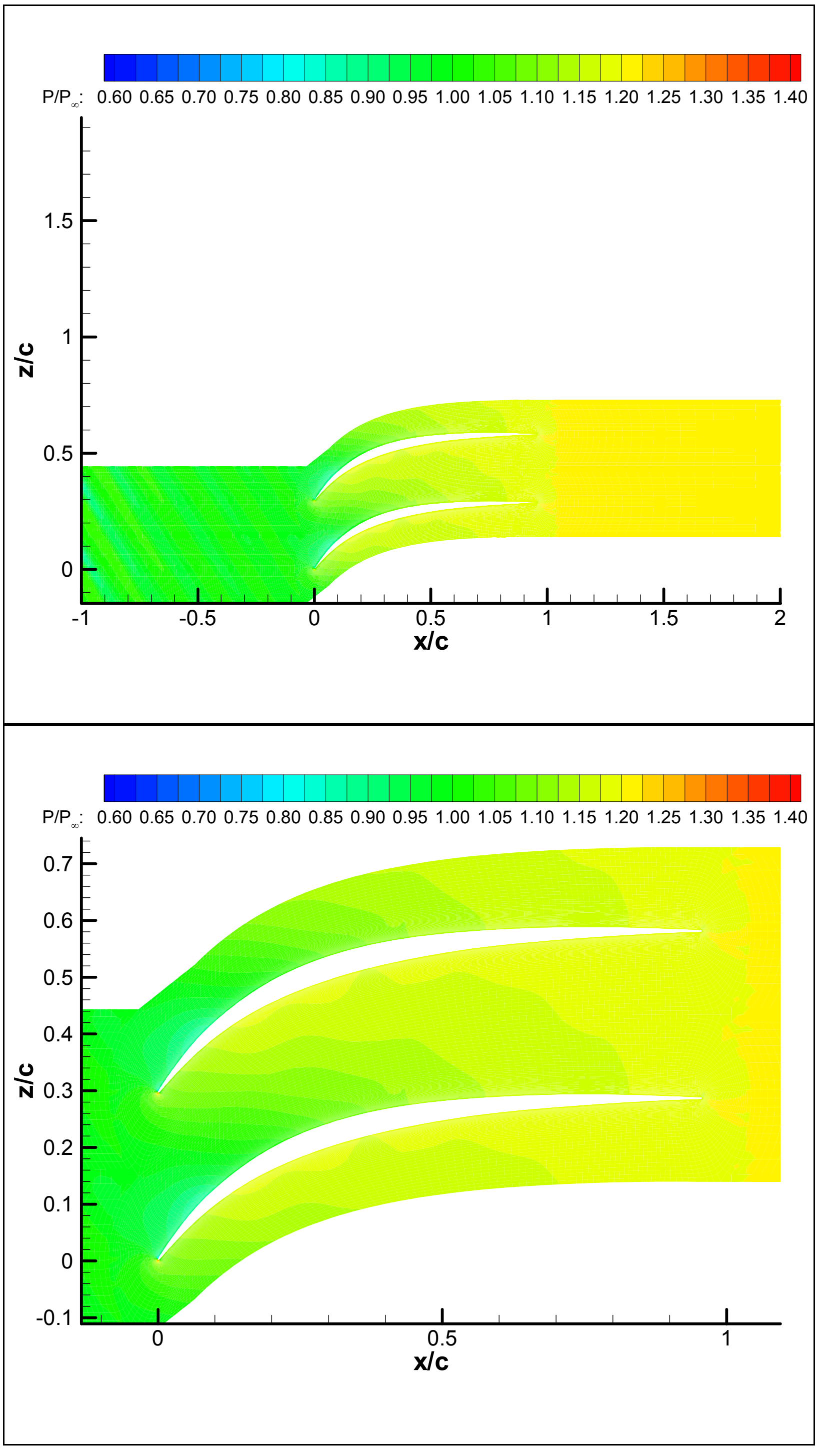

Fig. 5.14 N-S Nonuniform Inlet Velocity Profile Solution Pressure Contours for M=0.7, β=53° and period=0.1

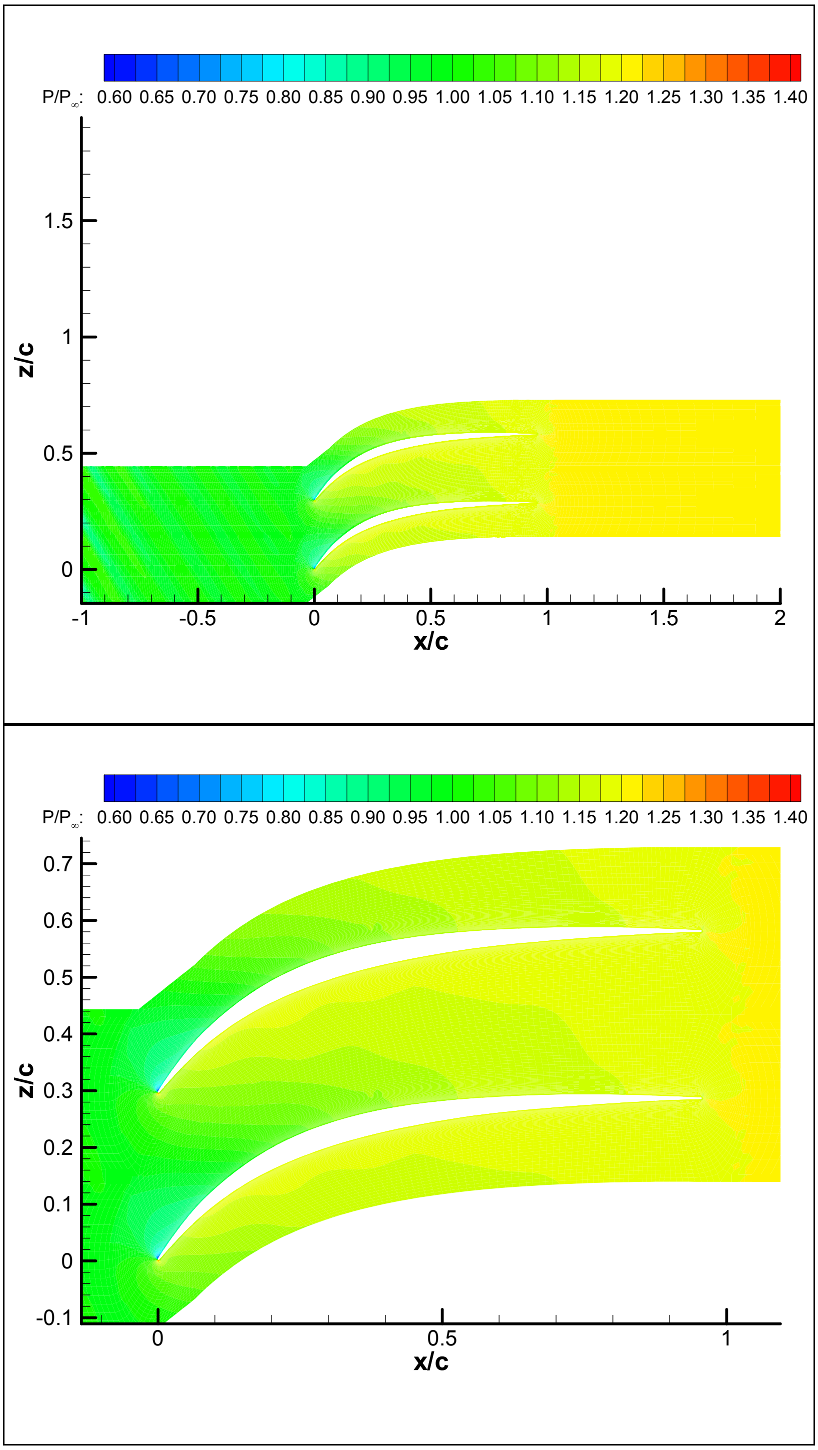

Fig. 5.15 N-S Nonuniform Inlet Velocity Profile Solution Pressure Contours for M=0.7, β=55° and period=0.1

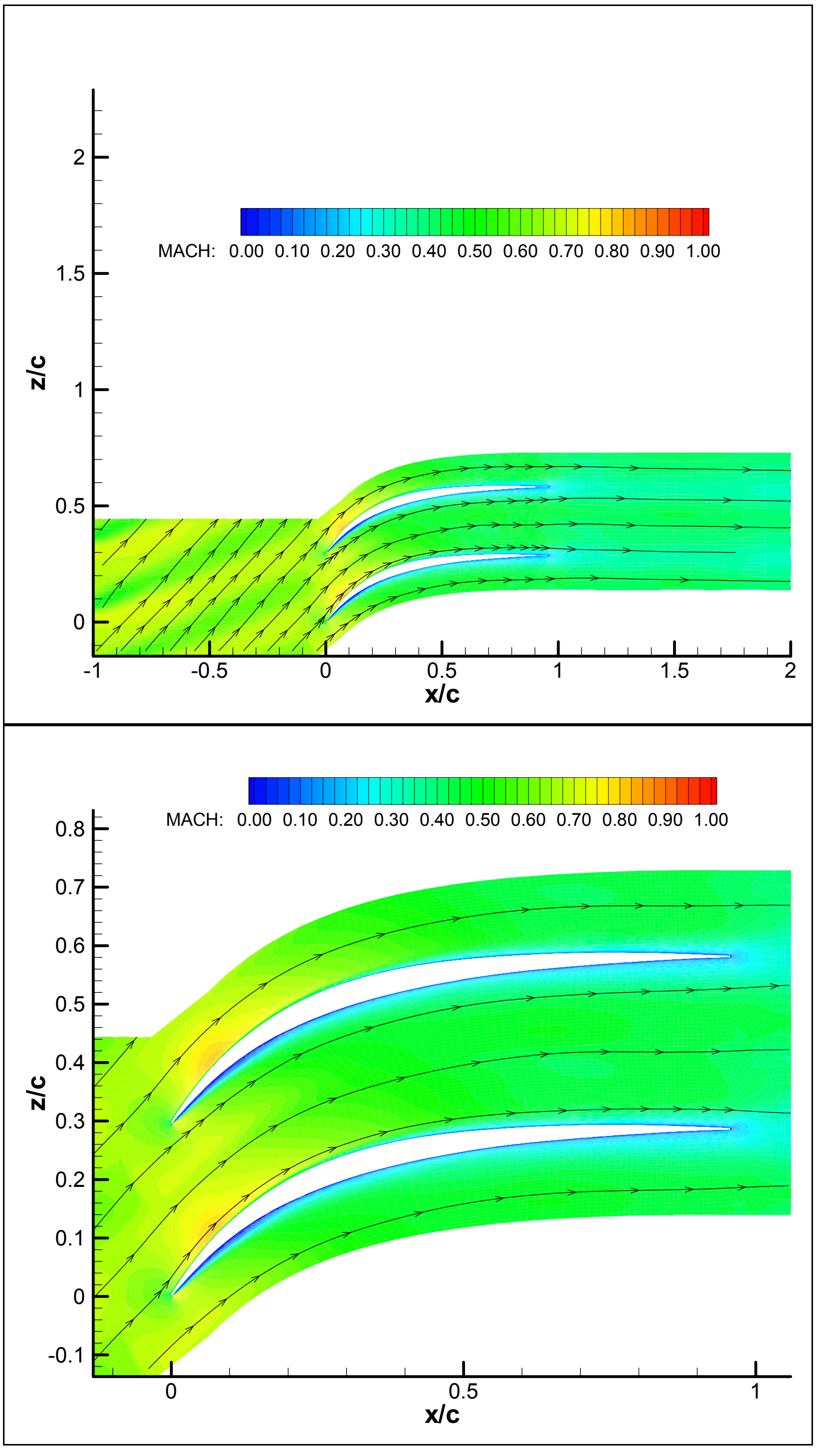

Fig. 5.16 N-S Nonuniform Inlet Velocity Profile Solution Mach Contours for M=0.7, β=49° and period=1.0

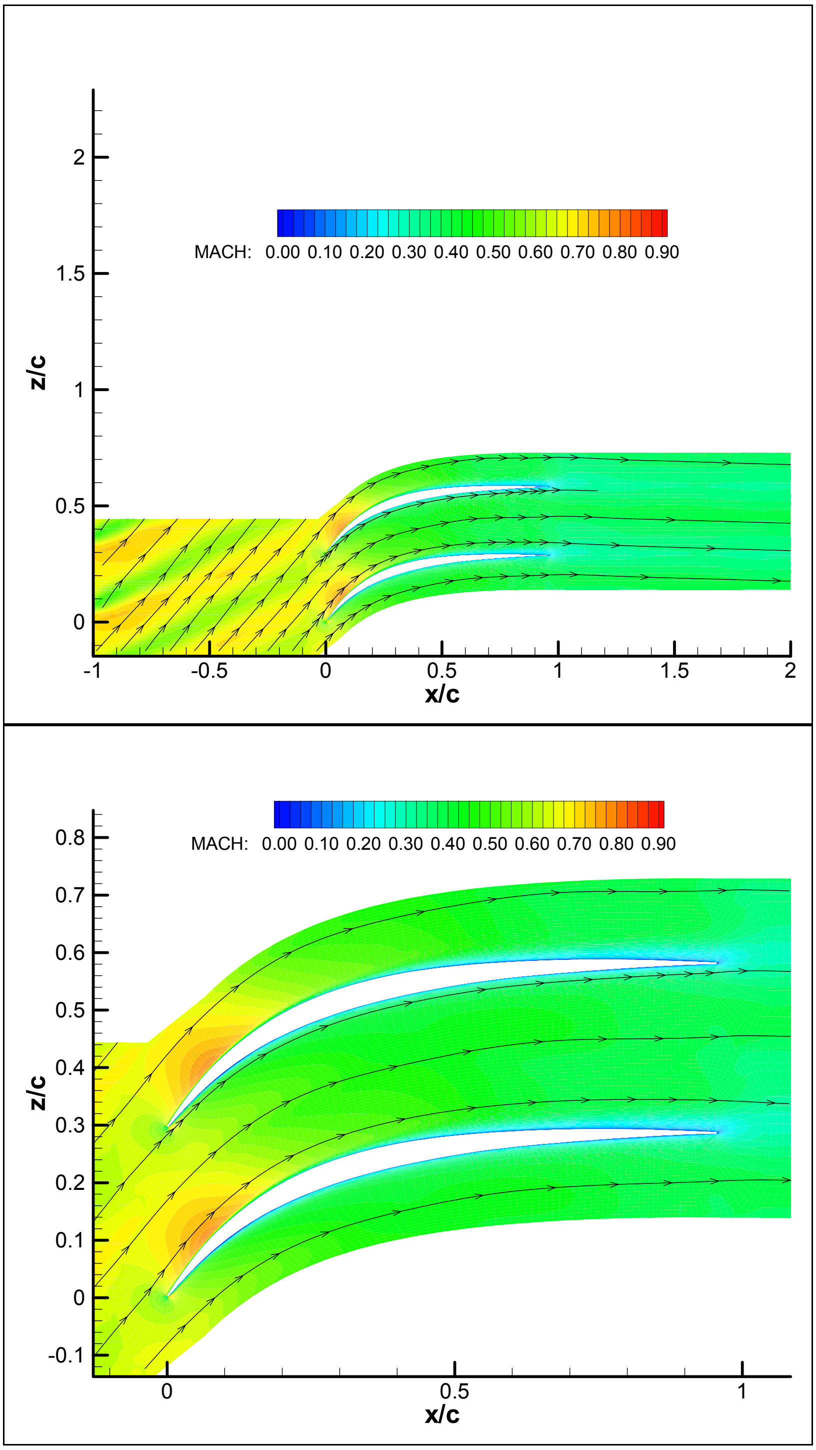

Fig. 5.17 N-S Nonuniform Inlet Velocity Profile Solution Mach Contours for M=0.7, β=51° and period=1.0

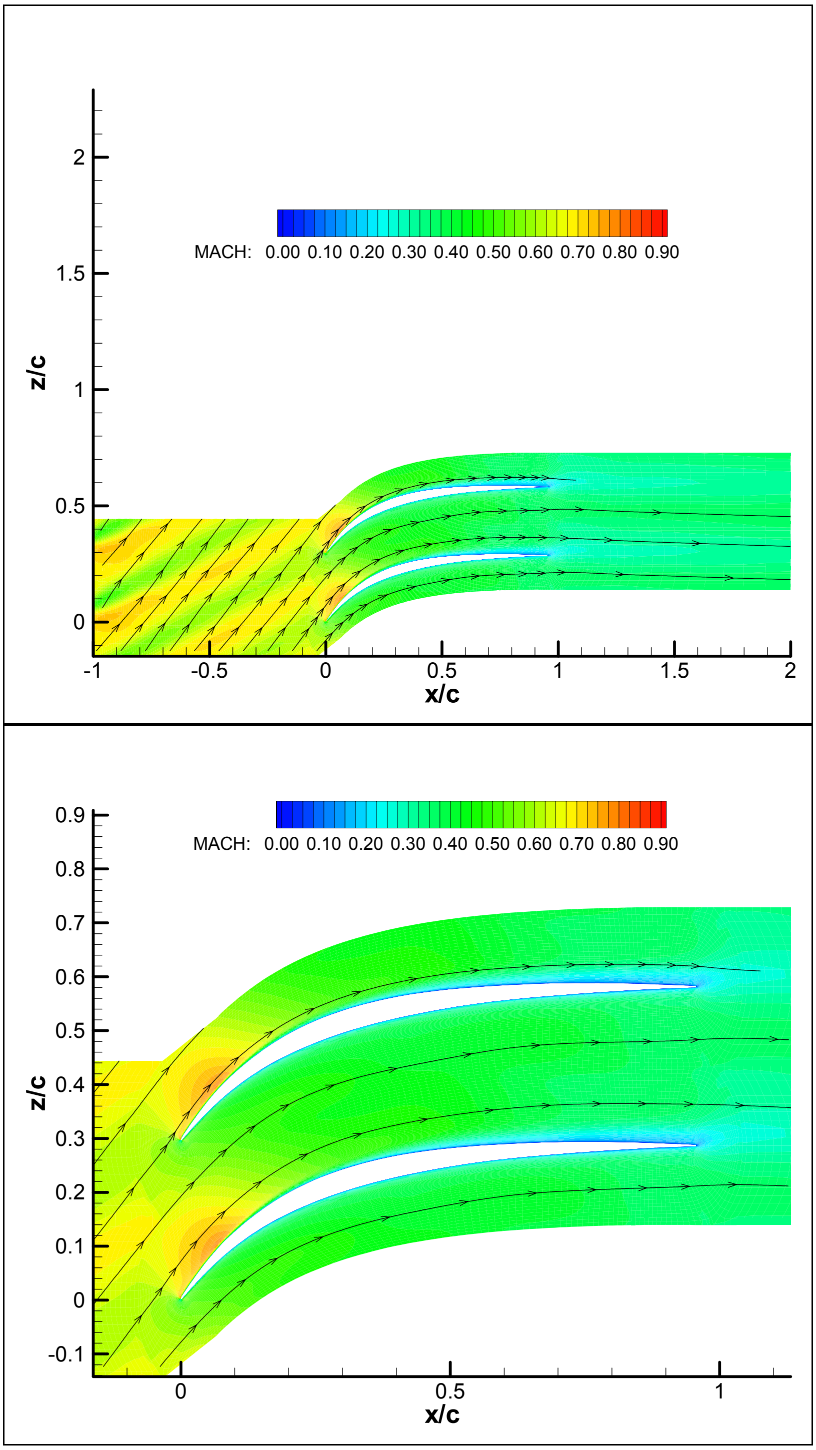

Fig. 5.18 N-S Nonuniform Inlet Velocity Profile Solution Mach Contours for M=0.7, β=53° and period=1.0

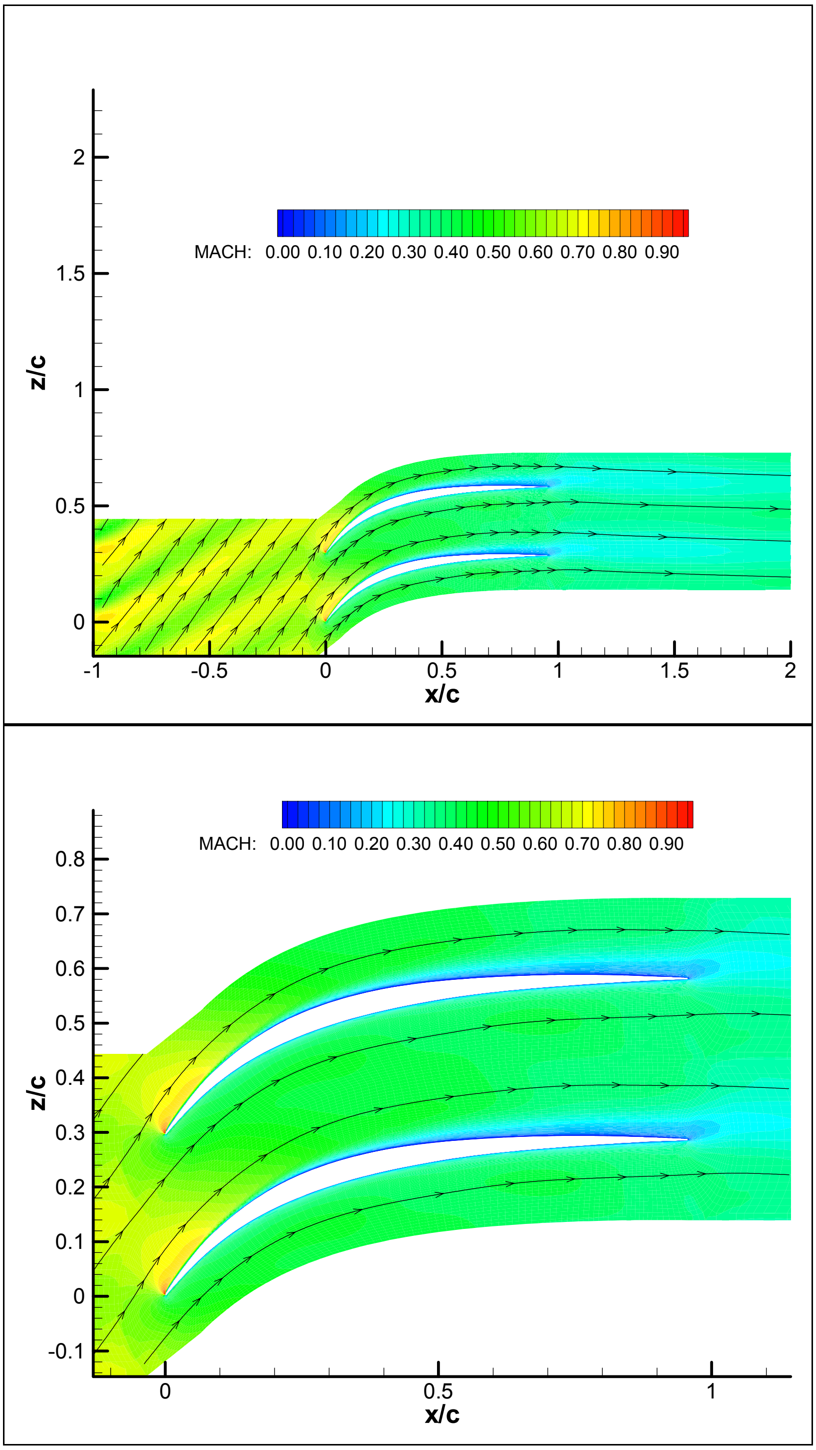

Fig. 5.19 N-S Nonuniform Inlet Velocity Profile Solution Mach Contours for M=0.7, β=55° and period=1.0

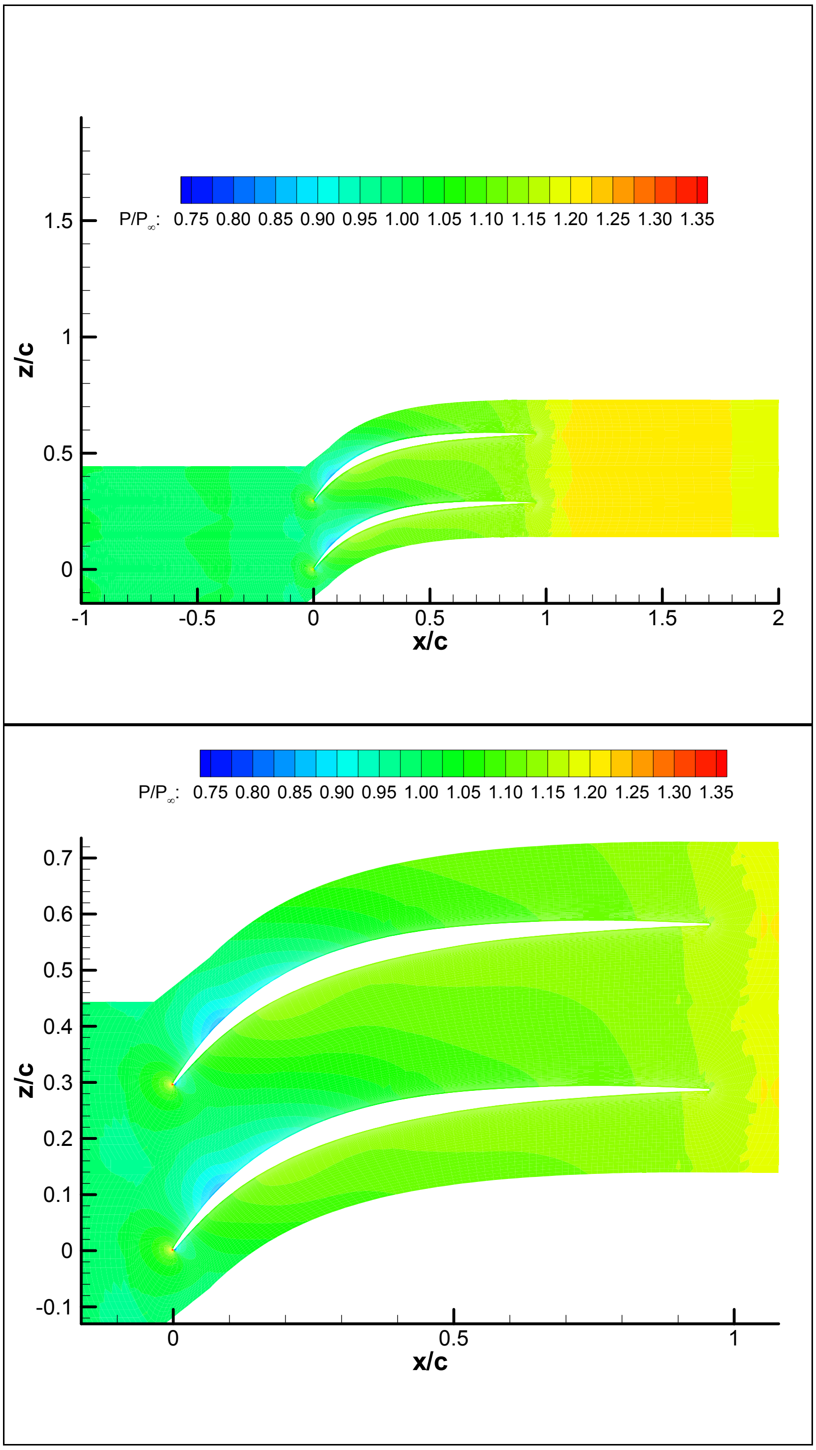

Fig. 5.20 N-S Nonuniform Inlet Velocity Profile Solution Pressure Contours for M=0.7, β=49° and period=1.0

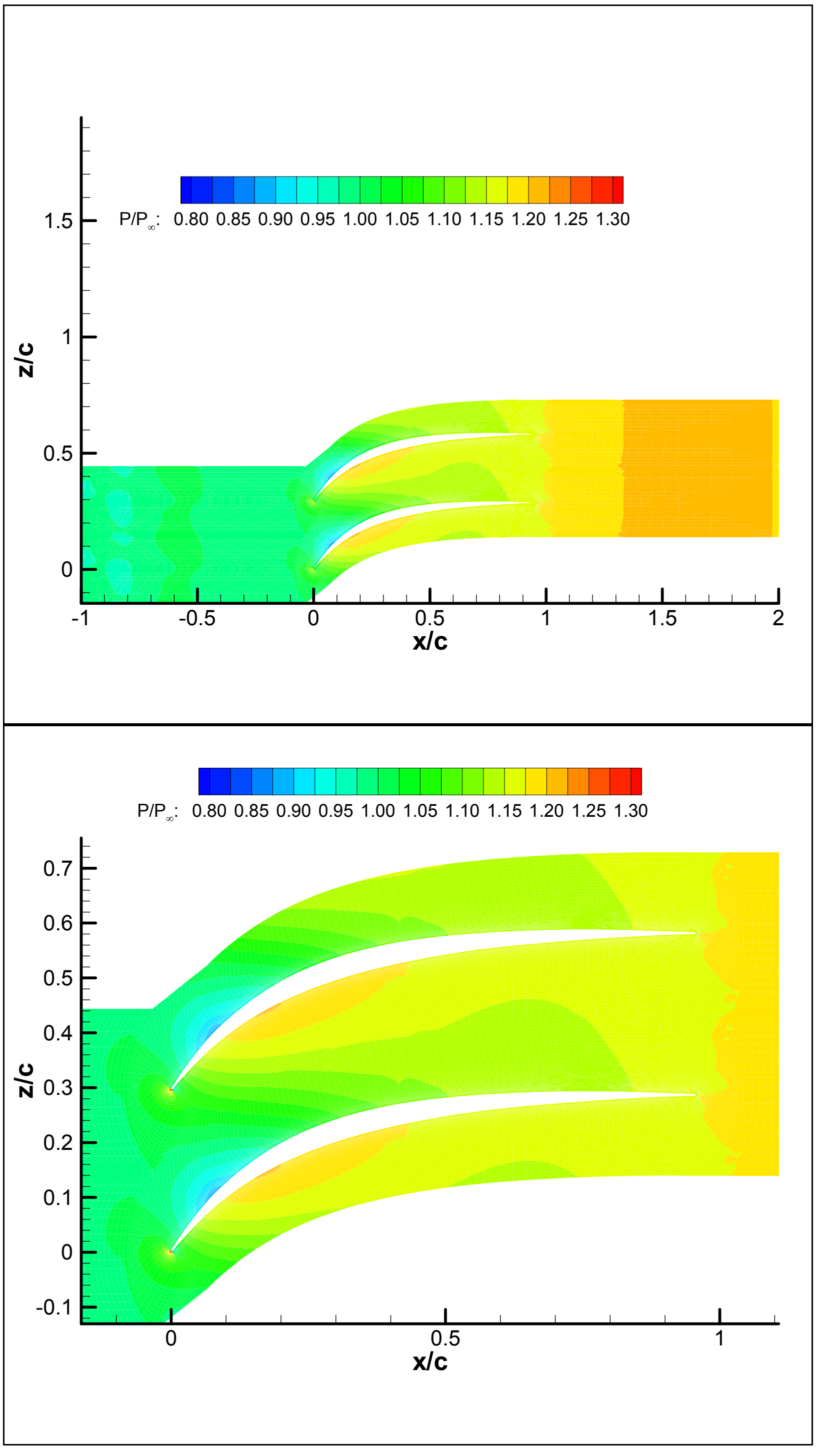

Fig. 5.21 N-S Nonuniform Inlet Velocity Profile Solution Pressure Contours for M=0.7, β=51° and period=1.0

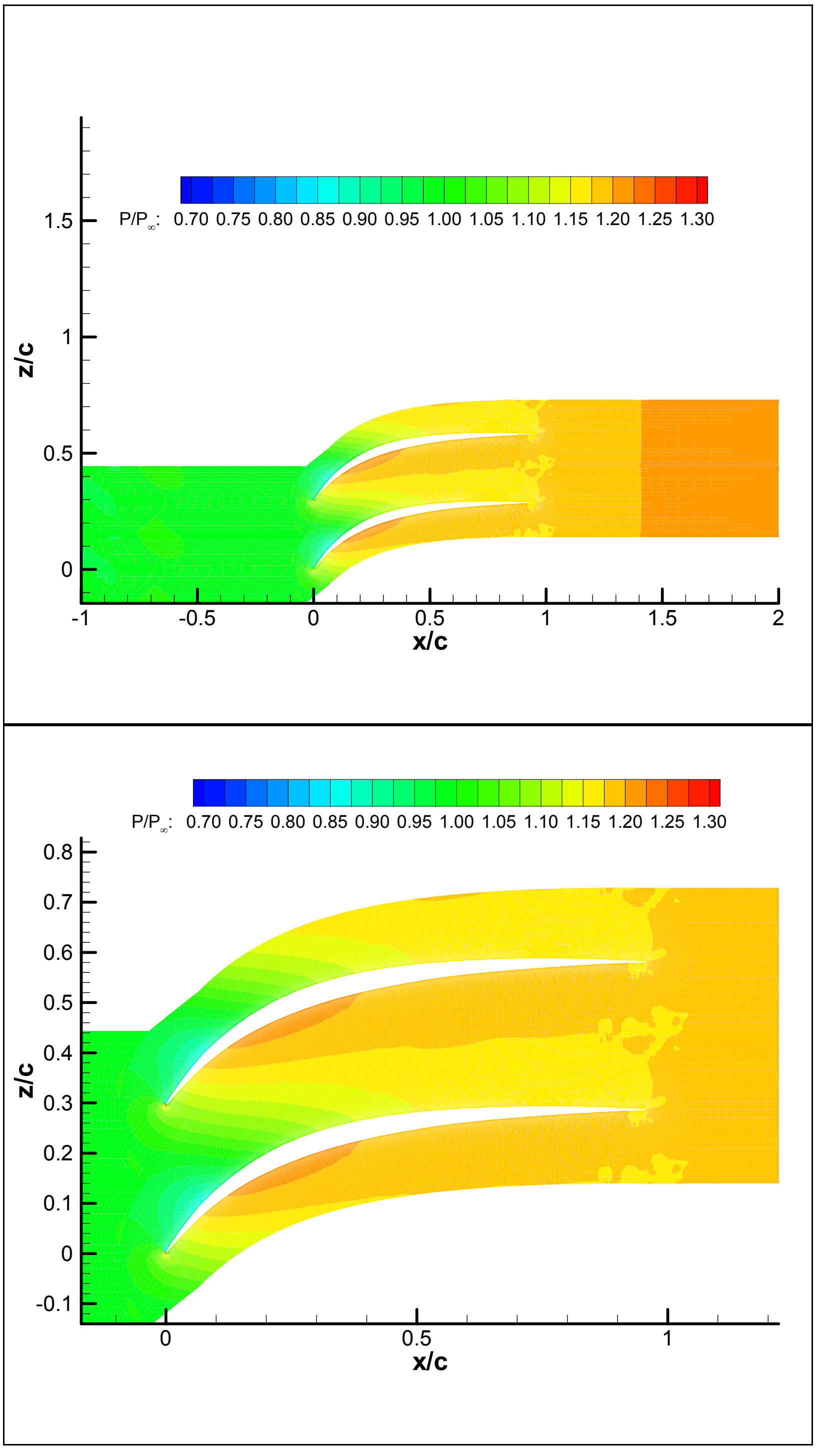

Fig. 5.22 N-S Nonuniform Inlet Velocity Profile Solution Pressure Contours for M=0.7, β=53° and period=1.0

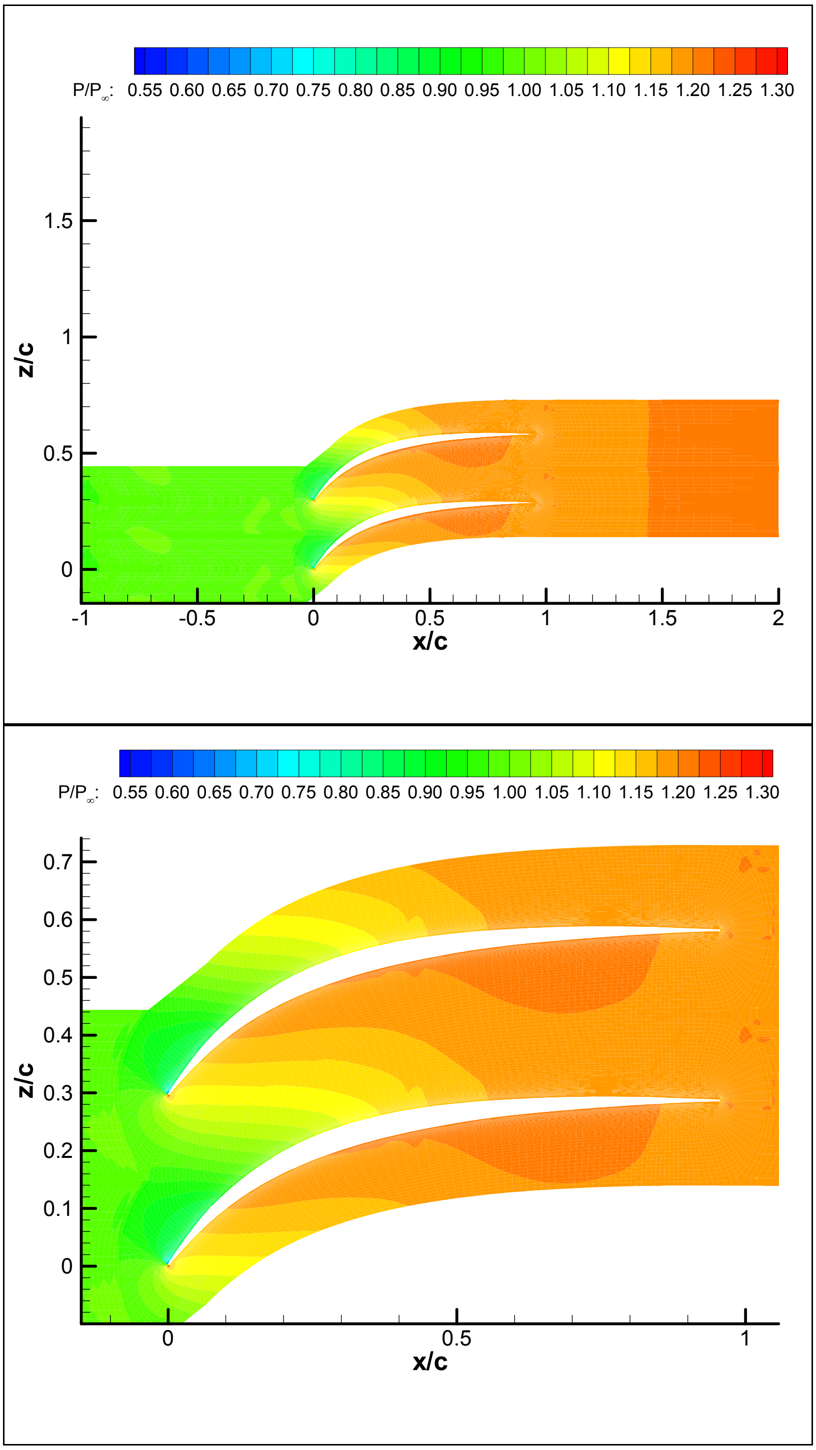

Fig. 5.23 N-S Nonuniform Inlet Velocity Profile Solution Pressure Contours for M=0.7, β=55° and period=1.0

CHAPTER VI

CONCLUSION

In this thesis, numerical solutions of a 2D stator compressor cascade at a given inlet Mach number (0.7) and four values of incidence (49°, 51°, 53° and 55°) has been obtained. Reynolds averaged, thin layer, compressible Navier Stokes equations are solved. Different grid types have been generated. Finite differencing approach and LU - ADI splitting technique are used. Three block parallel Euler and Navier Stokes solutions are compared with the experimental results. Baldwin-Lomax turbulence model is used in the turbulent predictions and boundary layer comparisons and numerical results are in good agreement with the experiment.

On the last part of the study, a wake in the inlet flow has been introduced in the steady and unsteady analyses. The influence of this wake and the wake location in the inlet flow, to the total force and pressure is presented. The results have been showed that there is a relationship between the wake position, wake motion period and the incidence value of the case.

A parallel multi-block Navier-Stokes flow solver has been modified and tested against experimental data. The code has been verified using 2D test cases for CA115 compressor stators.

As conclusion, computer codes which solve the Reynolds-averaged Navier-Stokes equations are now used by many manufacturers and researchers to design turbomachines, but there is no consensus about which grids and which turbulence models are good enough to provide a reliable basis for design decisions. Mixing-length turbulence models are unsuitable for turbomachines with their complex endwall flows; some kind of turbulent transport model is essential. No turbulence model was found which always gave good loss predictions.

Future work can be concentrated on modifying this study such as introduction of movable grid in pitching motion and changing wake position. Improvements to the turbulence models can be also taken into account in the future studies.

REFERENCES

[1] Lee B. H. K., *"Self-sustained shock oscillations on airfoils at transonic speeds"*, Progress in Aerospace Sciences Journal, Vol. 37, pp. 147-196, 2001.

[2] Kerrebrock J. L., Mikolajczak A. A., *"Intra-stator transport of rotor wakes and its effect on compressor performance"*, Journal of Engineering for Power, Vol. 92, pp. 359-368, 1970.

[3] Rai, Man Mohan, *"Unsteady Three-dimensional Navier-Stokes Simulation of Turbine Rotor-Stator Interaction"*, AIAA Paper, 87-2, San Diego, CA, 1987

[4] Erdos, J. I., Alzner, E., and McNally, W., *"Numerical Solution of Periodic Transonic Flow through a Fan Stage"*, AIAA Journal, Vol. 15, No. 11, pp. 1559-1568, 1977

[5] Şen T. S., *"Development of a Three Dimensional Multiblock Parallel Navier Stokes Solve*r", Ph.D. Thesis, METU, Dept. Of Aeronautical Engineering, November 2001.

[6] Beam R. M., Warming R. F., *"An Implicit Factored Scheme for the Compressible Navier-Stokes Equations"* AIAA Journal, 16, 393, April 1978.

[7] Obayashi S., Kuhawara K., *“LU Factorization of an Implicit Scheme for the Compressible Navier Stokes Equations”*, AIAA paper 84-1670, Snowmass, Colorado, June, 1984.

[8] Beam R. M., Warming R. F., *“An Implicit Factored Scheme for the Compressible Navier-Stokes Equations”* AIAA Journal, 16, 393, April 1978.

[9] Fujii K., *“Practical Applications of New LU-ADI Scheme for the Three Dimensional Navier-Stokes Computation of Transonic Viscous Flows”*, AIAA 24th Aerospace Sciences Meeting, Reno, Nevada, January 1986.

[10] Steger J. L., Warming R. F., *“Flux Vector Splitting of the Inviscid Gas Dynamics Equations with Application to Finite Difference Methods”*, Journal of Computational Physics, Vol. 40, pp. 263-293, 1981.

[11] Obayashi S., Matsushima K., Fujii K., Kuwahara K., *“Improvements in Efficiency and Reliability for Navier Stokes Equations Using the LU-ADI Factorization Algorithm"*, AIAA paper 86-0338, Reno, Nevada, January, 1986.

[12] Baldwin B. S., Lomax H., *“Thin Layer Approximation and Algebraic Model for Separated Turbulent Flows”*, AIAA 16th Aerospace Meeting, Huntsville, Alabama, January 1978.

[13] Meauze G., Hoorelbeke J., and Gaillard R., *“Test Case E/CA-3 High Subsonic Compressor Cascade 115”,* in AGARD Advisory Report No. 275, Test Cases for Computation of Internal Flows in Aero Engine Components

[14] *“CFD Validation for Propulsion System Components La Validation CFD des Organes des Propulseurs”* in AGARD Advisory Report No. 355, May 1998; 96p.

APPENDIX A

BOUNDARY CONDITION SUBROUTINES

subroutine BC_Manager:

- Opens boundary condition data files for each block namely *bcdata.xxx*, and calls related boundary condition subroutines.

- FORTRAN format of read sequence is defined as:
  FORMAT(A7,9I5,4F8.4)

- Seven-character length variable, CTYPE, defines the related boundary condition subroutine,

Table A.1 Boundary condition routines and "CTYPE" names

CTYPE (A7)	SUBROUTINE	DESCRIPTION
2DSP_BC	Sideplane_bc	Used for two dimensional applications
EXTR_BC	Extrapolation_bc	Inflow and/or outflow plane extrapolation
FFCC_BC	Farfield_bc	Farfield circulation correction to reduce outer domain
FIXV_BC	Fixed_Velocity_bc	Fixed pressure and/or velocity applications
FORMOM	Formom	C_L, C_D, force and moment coefficients

PARA_BC	Matched_Surface_bc	Matched block faces for parallel calculations
PARA_BC	UnMatched_Surface_bc	Unmatched block faces for parallel calculations
PRDC_BC	Periodic_bc	Repetitive, periodic or wake-cut boundaries
SING_BC	Singularity_bc	Singular line correction
SPIN_BC	Spining_Body_bc	Rotating/spinning surface calculation
SURF_BC	Surface_bc	Surface boundary conditions
SYMM_BC	Symmetric_bc	Mirror-symmetry boundary
MTBL_BC	Turbulence_bc	Turbulence boundary conditions
INWK_BC	Inlet_Wake_bc	Special Steady Boundary Condition for CA 115 Stator Cascade in Rotor Wake Problem
UIWK_BC	Unsteady_Inlet_Wake_bc	Special Unsteady Boundary Condition for CA 115 Stator Cascade in Rotor Wake Problem

- In all boundary condition routines, there are seven common parameters. First parameter, namely "ISURF", defines constant surface where the selected boundary condition applied. Other six parameters define starting and ending indices of each direction.

Table A.2 Definition of common parameters

ISURF	-1 0 1	for j-constant plane for k-constant plane For l-constant plane

subroutine Extrapolation_bc:

- Extrapolates all outflow variables from previous points.

- For subsonic case, energy is calculated from all other extrapolated variables.

- The parameters are defined in *bcdata.xxx* files as,

EXTR_BC ISURF JJ1 JJ2 KK1 KK2 LL1 LL2 PRA

PRA	Local to freestream pressure ratio at the extrapolation plane, P/Pinf

subroutine Farfield_bc:

- Farfield circulation correction based on potential vortex is added to reduce dependency of solution to the outer boundary distance to the surface.

- This correction is valid only for two dimensional applications, or three dimensional problems with the assumption of no change in spanwise direction (which lies in k-direction).

- The parameters are defined in *bcdata.xxx* files as,

FFCC_BC ISURF JJ1 JJ2 KK1 KK2 LL1 LL2

subroutine Fixed_Velocity_bc:

- Fixes the velocities and pressure on desired boundary.
- If any contravariant velocity component is given as 99.0, then it is calculated automatically similar to surface boundary.
- The parameters are defined in *bcdata.xxx* files as,

FIXV_BC ISURF IP JJ1 JJ2 KK1 KK2 LL1 LL2 QN QT1 QT2 PRATIO

IP	Switch for the calculation of pressure
	"0" if pressure is obtained using e, V and ρ of adjacent points
	"1" if pressure is calculated as, P=PRATIOxPINF
QN	Normal contravariant velocity to the surface
QT1	Tangential contravariant velocity to the surface
QT2	Other tangential contravariant velocity to the surface
PRATIO	Ratio of local pressure to freestream pressure. (P/P_∞)
RRATIO	Ratio of local density to freestream density. (ρ/ρ_∞)

subroutine Formom:

- Used for calculation of force and moment coefficients.
- Pressure, base, and viscous drag coefficients can be calculated.
- The parameters are defined in *bcdata.xxx* files as,

FORMOM ISURF IP JJ1 JJ2 KK1 KK2 LL1 LL2 X0 Y0 Z0

X0	X coordinate of reference point 0
Y0	Y coordinate of reference point 0

Z0	Z coordinate of reference point 0
SREF	Reference area

subroutine Matched_Surface_bc:

- Used for parallel multi block applications.
- Transfers information between two adjacent blocks.
- The parameters are defined in *bcdata.xxx* files as,

PARA_BC ISURF IDIR FACEID JJ1 JJ2 KK1 KK2 LL1 LL2

IDIR	Parameter for sweep direction. "-1" for JLK ordered grid; "+1" for JKL ordered grid
FACEID	Face ID number which is used for opening face data files of adjacent surface

subroutine Mutur:

- Calculates turbulent kinematic viscosity term using Baldwin-Lomax turbulence model.

subroutine Periodic_bc:

- Calculates the flow variables at periodic, repeated, or wake-cut type boundaries.

- Turbine cascade problem has periodic type boundary conditions.

- Wake-cut boundaries are widely used in airfoil, and wing problems.

- The parameters are defined in *bcdata.xxx* files as,

PRDC_BC ISURF ITYPE JJ1 JJ2 KK1 KK2 LL1 LL2 IEND

ITYPE	-1 for "O" and "H" type grids, 0 or 1 for "C" type grid (see Figure A.1).
IEND	Always 0 for "O" and "H" type grids For "C" type grids, it takes the maximum index number of the cut in that direction (see Figure A.1)

ISURF	**ITYPE**	
	0	**1**
j (-1)	k	l
k (0)	l	j
l (1)	j	k

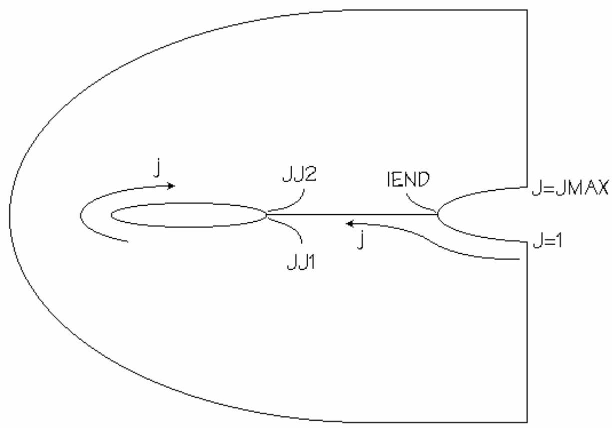

Fig. A.1 Representation of indices around two surfaces

subroutine Sideplane_bc:

- Used for solving two dimensional problems with three dimensional algorithm.

- Three planes in third dimension are required. The mid-plane is the solution plane. The values of inner and outer planes are set exactly to that of mid-plane.

- The parameters are defined in *bcdata.xxx* files as,

2DSP_BC ISURF JJ1 JJ2 KK1 KK2 LL1 LL2

subroutine Singularity_bc:

- Calculates the flow variables at singularity.

- Takes average of values from neighbor points.

- The parameters are defined in *bcdata.xxx* files as,

SING_BC IDIR IVAL JJ1 JJ2 KK1 KK2 LL1 LL2 IAXS

IDIR	Shows the direction where singularity exists. -1, 0, or 1 for J, K, or L direction respectively
IVAL	Defines the sweep direction. It takes -1 or +1 values.
IAXS	If the flow is Axisymmetric, it is equal to 1; otherwise 0.

subroutine Surface_bc:

- Calculates the flow variables on the solid wall.

- For inviscid problems, surface flow tangency condition is imposed. Normal contravariant velocity is set to zero. Tangential contravariant velocities are extrapolated using first two mesh points away from the wall.

- For viscous problems, no slip condition is applied. All velocity components set to zero.

- Surface pressure is obtained from normal momentum equation.

- The parameters are defined in *bcdata.xxx* files as,

  SURF_BC ISURF JJ1 JJ2 KK1 KK2 LL1 LL2

subroutine Symmetric_bc:

- Calculates flow variables on the planes where the mirror symmetry exists.

- Tangential contravariant velocities are set to zero and the normal gradient of perpendicular contravariant velocity is also zero.

- The parameters are defined in "bcdata.xx" files as,

  SYMM_BC ISURF JJ1 JJ2 KK1 KK2 LL1 LL2

subroutine UnMatched_Surface_bc:

- Used for parallel multi block applications for unmatching grids at the adjacent faces.

- Transfers information between two adjacent blocks.

- The parameters are defined in *bcdata.xxx* files as,

PARA_BC ISURF IDIR FACEID JJ1 JJ2 KK1 KK2 LL1 LL2

IDIR	Always equal to “2”
FACEID	Face ID number which is used for opening face data files of adjacent surface

subroutine Turbulence_bc:

- Calculates turbulence on the solid surfaces, at the inlet, and calls Baldwin Lomax model for wake regions.

- The parameters are defined in "bcdata.xx" files as,

MTBL_BC ISURF JJ1 JJ2 KK1 KK2 LL1 LL2 MDEGANI X Y Z XY Q TURMU

For this boundary condition only, ISURF calls different turbulence subroutines:

if MDEGANI=0 do not apply Degani Schiff modification

subroutine Inlet_Wake_bc:

- This subroutine is a special boundary condition for CA 115 Stator Cascade in Rotor Wake Problem. The wake is described in Ref. [14].

- Profile of the wake can be shifted upwards if desired.

- The parameters are defined in "bcdata.xx" files as,

INWK_BC .. .. SHIFT .. .. X Y Z .. Q

Note that SHIFT is a number between 0.0 and 1.0. For example, if shift=0.5 this means profile is shifted 50% upwards of the pitch of the upstream blade in tangential direction.

subroutine Unsteady_Inlet_Wake_bc:

- This subroutine is a special boundary condition for Unsteady CA 115 Stator Cascade in Rotor Wake Problem.

- Wake is shifted in upwards tangential direction and completes one cycle at a given period of time.

- Calculates the shift value at each time step and calls Inlet_Wake_BC subroutine for that shift value.

- The parameters are defined in "bcdata.xx" files as,

UIWK_BC .. .. TIME PERIOD .. .. .. X Y Z .. Q

APPENDIX B

INPUTS AND BOUNDARY CONDITIONS

The input and boundary condition files of PML3D flow solver is described in this section. For both analyses those have been explained in Chapters 4 and 5, input and boundary condition files are different. In order to guide future investigations these files are also included within this section.

For a single block computation the input files are:

input The main flowfield and flow solver parameters are specified.

bcdata.001 Boundary conditions are specified.

BLOCK.001 The grid file

For an N block multi block computation the input files are

input The main flowfield and flow solver parameters are specified.

bcdata.001 bcdata.02 ...... bcdata.00N Boundary conditions.

BLOCK.001 BLOCK.002...... BLOCK.00N The grid files

Output files are:

qfile.001, qfile.002, ... qfile.00N These are solution files. They can be used to extract data for plotting or continuing the iterations

errors The residual histories (L2 and Max) for all the blocks are available in this file for plotting.

resid.001, resid.002, ... resid.00N residual histories of the corresponding blocks these files also includes the J,K,L location of the max error whis is a helpful information if there is a problem at a certain location.

computer screen During the iterations residuals are printed on the screen. When the iterations are finished CPU time information is also printed on the screen. For each case a table will be available for comparison of the CPU time with different computer environment.

B.1. I/O Files for Euler Solution with Uniform Inlet Velocity Profile:

Input File of both H-Grid and H-O-H Grid:

A sample input file of the H-grid, M=0.7 and β=49° for initializing flow field and variables is given below. Input file for H-O-H grid is similar.

```
&INPUT                     PR=0.72,          INVISC=0,
  NMAX=5000,               CNBR=10,          LAMIN=0,
  UINF=0.4592,             SMU=3.0,          IREAD=0,
  VINF=0.0,                SMR=3.0,          NWR=10,
  WINF=0.5283,             DT=0.0,           NOUT=250,
  RMUE=1.0,                ISTD=1,           IBLM=1,
  RE=1.0e6,                SSP=100,        &END
```

Boundary Condition File for H-Grid:

The boundary condition file (bcdata.001) for the PML3D flow solver is shown below:

```
EXTR_BC   -1  140  139    1    3    1   70    0    0   1.257
2DSP_BC    0    2  139    1    2    1   70
2DSP_BC    0    2  139    3    2    1   70
PRDC_BC    1   -1    2   19    1    3    1   70    0
PRDC_BC    1   -1  121  139    1    3    1   70    0
SURF_BC    1   20  120    1    3    1    2
SURF_BC    1   20  120    1    3   70   69
```

Boundary Condition Files for H-O-H Grid:

The boundary condition files are shown below:

CENTRAL O-GRID (bcdata.001):

```
2DSP_BC    0    1  249    1    2    1   29
2DSP_BC    0    1  249    3    2    1   29
PRDC_BC   -1   -1    1  249    1    3    1   29    0
PRDC_BC    1    0  115  135    1    3   29   28  239
SURF_BC    1    1  249    1    3    1    2
PARA_BC    1    1    2  115  135    1    3   29   28
PARA_BC    1    1    3  249  239    1    3   29   28
PARA_BC    1    1    5   11    1    1    3   29   28
```

FRONT GRID (bcdata.002):

```
2DSP_BC    0    2   25    1    2    1   21
2DSP_BC    0    2   25    3    2    1   21
PRDC_BC    1   -1    2   24    1    3    1   21    0
PARA_BC   -1   -1    1   25   24    1    3    1   21
```

REAR GRID (bcdata.003):

```
EXTR_BC   -1   25   24    1    3    1   21    0    0   1.257
2DSP_BC    0    2   24    1    2    1   21
2DSP_BC    0    2   24    3    2    1   21
PRDC_BC    1   -1    2   25    1    3    1   21    0
PARA_BC   -1   -1    4    1    2    1    3   21   11
PARA_BC   -1   -1    6    1    2    1    3   11    1
```

B.2. I/O Files for Navier Stokes Solution with Uniform Inlet Velocity Profile:

Input File (for β=49°):

```
&INPUT                               DT=0.0,
  NMAX=10000,                        ISTD=1,
  UINF=0.4592,                       SSP=500,
  VINF=0.0,                          INVISC=1,
  WINF=0.5283,                       LAMIN=1,
  RMUE=1.0,                          IREAD=1,
  RE=1.0e6,                          NWR=10,
  PR=0.72,                           NOUT=250,
  CNBR=10.0,                         IBLM=1,
  SMU=3.0,                         &END
  SMR=3.0,
```

Boundary Condition Files:

Sample boundary condition files are shown below (for β=49°):

CENTRAL O-GRID (bcdata.001):

```
2DSP_BC    0    1  249    1    2    1   78
2DSP_BC    0    1  249    3    2    1   78
PRDC_BC   -1   -1    1  249    1    3    1   78    0
PRDC_BC    1    0  115  135    1    3   78   77  239
SURF_BC    1    1  249    1    3    1    2
PARA_BC    1    1    2  115  135    1    3   78   77
PARA_BC    1    1    3  249  239    1    3   78   77
PARA_BC    1    1    5   11    1    1    3   78   77
MTBL_BC    0    2  248    2    2    2   76
MTBL_BC    4    8    2    2    2   33   76
MTBL_BC    4  242  248    2    2   33   76
```

FRONT GRID (bcdata.002):

```
2DSP_BC    0    2   25    1    2    1   21
2DSP_BC    0    2   25    3    2    1   21
PRDC_BC    1   -1    2   24    1    3    1   21    0
PARA_BC   -1   -1    1   25   24    1    3    1   21
```

REAR GRID (bcdata.003):

```
EXTR_BC   -1   25   24    1    3    1   21    0    0   1.255
2DSP_BC    0    2   24    1    2    1   21
2DSP_BC    0    2   24    3    2    1   21
PRDC_BC    1   -1    2   25    1    3    1   21    0
PARA_BC   -1   -1    4    1    2    1    3   21   11
PARA_BC   -1   -1    6    1    2    1    3   11    1
```

B.3. I/O Files for Navier Stokes Solution with Nonuniform Inlet Velocity Profile:

Input File:

A sample input file of M=0.7, β =49° and shift=0.0 for initializing flow field and variables is given below.

```
&INPUT                                DT=0.000165,
  NMAX=20000,                         ISTD=0,
  UINF=0.4592,                        SSP=500,
  VINF=0.0,                           INVISC=1,
  WINF=0.5283,                        LAMIN=1,
  RMUE=1.0,                           IREAD=1,
  RE=1.0e6,                           NWR=10,
  PR=0.72,                            NOUT=250,
  CNBR=0.0,                           IBLM=1,
  SMU=3.0,                          &END
  SMR=3.0,
```

Boundary Condition Files:

Sample boundary condition files are shown below (for β=49° shift=0.0):

CENTRAL O-GRID (**bcdata.001**):

```
2DSP_BC    0    1  249    1    2    1   78
2DSP_BC    0    1  249    3    2    1   78
```

```
PRDC_BC   -1   -1    1  249    1    3    1   78    0
PRDC_BC    1    0  115  135    1    3   78   77  239
SURF_BC    1    1  249    1    3    1    2
PARA_BC    1    1    2  115  135    1    3   78   77
PARA_BC    1    1    3  249  239    1    3   78   77
PARA_BC    1    1    5   11    1    1    3   78   77
MTBL_BC    0    2  248    2    2    2   76
MTBL_BC    4    8    2    2    2   33   76
MTBL_BC    4  242  248    2    2   33   76
FORMOMC    1    1  249    1    3    1    2    0    0   0.000   0.000
0.000   1.000
```

FRONT GRID (**bcdata.002**):

```
2DSP_BC    0    2  100    1    2    1   21
2DSP_BC    0    2  100    3    2    1   21
PRDC_BC    1   -1    2   99    1    3    1   21    0
PARA_BC   -1   -1    1  100   99    1    3    1   21
INWK_BC                                                  0.000
MTBL_BC    5                                           250.000    1   21
```

REAR GRID (**bcdata.003**):

```
EXTR_BC   -1   25   24    1    3    1   21    0    0   1.187
2DSP_BC    0    2   24    1    2    1   21
2DSP_BC    0    2   24    3    2    1   21
PRDC_BC    1   -1    2   25    1    3    1   21    0
PARA_BC   -1   -1    4    1    2    1    3   21   11
PARA_BC   -1   -1    6    1    2    1    3   11    1
cTBL_BC    5                                                250.000
```

B.4. I/O Files for Unsteady Navier Stokes Solution with Nonuniform Inlet Velocity Profile:

Input File:

A sample input file of M=0.7, and β=49° for initializing flow field and variables is given below.

```
&INPUT                     PR=0.72,              INVISC=1,
  NMAX=70000,              CNBR=0.0,             LAMIN=1,
  UINF=0.4592,             SMU=3.0,              IREAD=1,
  VINF=0.0,                SMR=3.0,              NWR=10,
  WINF=0.5283,             DT=0.0001,            NOUT=250,
  RMUE=1.0,                ISTD=0,               IBLM=1,
  RE=1.0e6,                SSP=500,            &END
```

Boundary Condition Files:

Sample boundary condition files are shown below (for β=49°):

CENTRAL O-GRID (**bcdata.001**):

```
2DSP_BC    0    1  249    1    2    1   78
2DSP_BC    0    1  249    3    2    1   78
PRDC_BC   -1   -1    1  249    1    3    1   78    0
PRDC_BC    1    0  115  135    1    3   78   77  239
SURF_BC    1    1  249    1    3    1    2
PARA_BC    1    1    2  115  135    1    3   78   77
PARA_BC    1    1    3  249  239    1    3   78   77
PARA_BC    1    1    5   11    1    1    3   78   77
MTBL_BC    0    2  248    2    2    2   76    0
MTBL_BC    4    8    2    2    2   33   76
MTBL_BC    4  242  248    2    2   33   76
FORMOMC    1    1  249    1    3    1    2    0    0   0.000   0.000
0.000   1.000
```

FRONT GRID (**bcdata.002**):

```
2DSP_BC    0    2  100    1    2    1   21
2DSP_BC    0    2  100    3    2    1   21
PRDC_BC    1   -1    2   99    1    3    1   21    0
PARA_BC   -1   -1    1  100   99    1    3    1   21
cNWK_BC                                                 0.000
UIWK_BC                                                 5.000   0.100
MTBL_BC    5                                          250.000
cTBL_BC    4    1   99    2    2    2   20
```

REAR GRID (**bcdata.003**):

```
EXTR_BC   -1   25   24    1    3    1   21    0    0   1.187
2DSP_BC    0    2   24    1    2    1   21
2DSP_BC    0    2   24    3    2    1   21
PRDC_BC    1   -1    2   25    1    3    1   21    0
PARA_BC   -1   -1    4    1    2    1    3   21   11
PARA_BC   -1   -1    6    1    2    1    3   11    1
cTBL_BC    5                                          250.000
cTBL_BC    4    1   24    2    2    2   20
```

APPENDIX C

COMPUTATIONAL REQUIREMENTS

In this study different configured computers have been employed. A comparison of CPU times for that computers are presented in the following table.

Euler Solution with Uniform Inlet Velocity Profile:

Computations are performed on a Pentium 3, 450 Mhz computer with 256 MB RAM. For the 5000 iteration as example for M=0.7 and β=49° CPU time usage is as follows:

Table C.1 Computer Usage for H-O-H grids

		GRID	RAM (MB)	CPU (%)
H-O-H GRID	Pml3d.exe (BLOCK-1)	249*3*29 = 21,663	16.144	85-95 (90)
	Pml3d.exe (BLOCK-2)	25*3*21 = 1,575	4.268	2-5 (3)
	Pml3d.exe (BLOCK-3)	25*3*21 = 1,575	4.264	3-5 (4)
	MPIRun.exe		6.360	
	TOTAL	24,813	31.036	97

<u>M=0.7 and β=49°:</u>

USER: 40.68 min
SYSTEM: 0.24 min
I/O: 5.15 min
TOTAL: 46.07 min

Navier Stokes Solution with Uniform Inlet Velocity Profile:

Computations are performed on a Pentium 3, 450 Mhz computer with 256 MB RAM.

M=0.7 and β=49° :

Table C.2 N-S Computer Usage for H-O-H grids

ITER	CNBR	SSP	P_2/P_1	NOTES
5001-5250	1.0	500	1.2463	USER: 5.4min SYSTEM: 0.03min I/O: 0.43min TOTAL: 5.86min
5251-5750	0.5	500	1.2463	USER: 10.72min SYSTEM: 0.05min I/O: 0.48min TOTAL: 11.25min
5751-10000	0.25	500	1.2463	USER: 90.94min SYSTEM: 0.29min I/O: 3.60min TOTAL: 94.83min
10001-15000	1.00	500	1.2463	USER: 109.71min SYSTEM: 0.35min I/O: 4.67min TOTAL: 114.73min
15001-40000	5.00	500	1.2463	USER: 539.98min SYSTEM: 1.68min I/O: 0min TOTAL: 877.25min
40001-70000	5.00	500	1.2463	USER: 1.36min SYSTEM: 432.09min I/O: 0min TOTAL: 997.78min
70001-90000	5.00	500	1.250	USER: 45626min SYSTEM: 1.71min I/O: 70.85min TOTAL: 528.82min
90001-100000	10.00	500	1.255	USER: 221.09min SYSTEM: 0.72min I/O: 20.92min TOTAL: 242.73min

Navier Stokes Solution with Nonuniform Inlet Velocity Profile:

Computations are performed on a Centrino, 1.4 Ghz computer with 256 MB RAM.

<u>M=0.7 and β=49° :</u>

Table C.3 Computer Usage for H-O-H grids for M=0.7, β=49°, shift=0.0:

ITER	CNBR	SSP	P_2/P_1	NOTES
320001-340000	2.5	500	1.187	User time: 109.11min. System time: 0.33min. I/O time: 9.33min. Total time: 118.77min.
340001-360000	2.5	500	1.187	User time: 109.87min. System time: 0.32min. I/O time: 9.41min. Total time: 119.59min.

Table C.4 Computer Usage for H-O-H grids for M=0.7, β=49°, shift=0.25:

ITER	CNBR	SSP	P_2/P_1	NOTES
290001-310000	2.5	500	1.192	User time: 109.72 min. System time: 0.34 min. I/O time: 10.39 min. Total time: 120.45 min.
310001-325000	2.5	500	1.192	User time: 82.67min. System time: 0.24 min. I/O time: 9.93 min. Total time: 92.84 min.

Table C.5 Computer Usage for H-O-H grids for M=0.7, β=49°, shift=0.50:

ITER	CNBR	SSP	P_2/P_1	NOTES
300001-320000	2.5	500	1.186	User time: 109.81 min. System time: 0.33 min. I/O time: 11.16 min. Total time: 121.30 min.
320001-335000	5.0	500	1.186	User time: 81.91 min. System time: 0.26 min. I/O time: 7.34 min. Total time: 89.50 min.

Table C.6 Computer Usage for H-O-H grids for M=0.7, β=49°, shift=0.75:

ITER	CNBR	SSP	P_2/P_1	NOTES
340001-360000	2.5	500	1.187	User time: 109.94 min. System time: 0.34 min. I/O time: 9.96 min. Total time: 120.24 min.
360001-375000	5.0	500	1.187	User time: 81.98 min. System time: 0.26 min. I/O time: 7.34 min. Total time: 89.58 min.

Unsteady Navier Stokes Solution with Nonuniform Inlet Velocity Profile:

Computations are performed on a Centrino, 1.4 Ghz computer with 256 MB RAM.

<u>M=0.7 and β=49° :</u>

Table C.7 Unsteady N-S Computer Usage for H-O-H grids:

ITER	CNBR	SSP	P_2/P_1	NOTES
1-100000	2.1635	500	1.187	User time: 546.88 min. System time: 1.59 min. I/O time: 49.79 min. Total time: 598.26 min.

Comparison of CPU times for 10,000 iterations in different configured computers:

P3, 450 Mhz, 256 MB RAM	242.73 min
P4, 1.8 Ghz, 512 MB RAM	107.10 min
Centrino, 1.4 Ghz, 256 MB RAM	59.18 min